DEEP SEISMIC SOUNDING IN SOUTHERN MANITOBA AND SASKATCHEWAN

A THESIS
PRESENTED TO
THE UNIVERSITY OF MANITOBA

IN PARTIAL FULFILLMENT OF
THE REQUIREMENTS FOR THE DEGREE
MASTER OF SCIENCE

BY
WANDA-LEE DE LANDRO
FEBUARY 1981

DEEP SEISMIC SOUNDING IN SOUTHERN MANITOBA AND SASKATCHEWAN

BY

WANDA-LEE DE LANDRO

A thesis submitted to the Faculty of Graduate Studies of
the University of Manitoba in partial fulfillment of the requirements
of the degree of

MASTER OF SCIENCE

ABSTRACT

A CO-CRUST seismic refraction survey was done in July 1977 in southern Manitoba and Saskatchewan to determine the structure of the Churchill- Superior boundary. Data from two reversed refraction profiles, one north/south in the Superior Province and one east/west across the boundary of the Superior and Churchill Provinces were obtained.

Preliminary interpretation of the data by Green et al. (1980) suggested that the crust beneath the north/south profile is similar to previously published crustal models for the Superior Province, while that of the east/west is typical of Churchillian crust of eastern Alberta and Saskatchewan.

In this thesis, with the aid of such data processing and interpretation methods as bandpass and polarisation filtering, Herglotz inversion, ray tracing and WKBJ synthetic seismogram modelling, a detailed analysis and interpretation of the data was performed. The results indicate that for the north-south profile, the crust is divided into four laterally homogeneous layers, with velocity gradients both within and between layers. The crust under the east-west profile contains fault structures,

layers of decreasing velocity and lateral velocity changes. From this study, the boundary is a region of finite lateral extent, marked by upper crustal discontinuities and lower crustal velocity changes.

ACKNOWLEDGEMENTS

The author wishes to express her thanks and appreciation to Dr. Wooil Moon for his advice and careful supervision of this work.

Special thanks to Dr. Allan Green for his initial encouragement and continued interest in my work. The writer also acknowledges Dr. D. H. Hall and the members of the Earth Sciences Department, the University of Manitoba for their contributions towards making this study possible.

Above all thanks to my family without whose constant support none of this would have been possible.

TABLE OF CONTENTS

LIST OF FIGURES

LIST OF TABLES

Chapter I

INTRODUCTION

In July 1977, the Consortium for Canadian Crustal Studies (COCRUST) currently composed of geophysicists from the Earth Physics Branch and the Universities of Manitoba, Alberta, Western Ontario, Toronto and Saskatchewan; conducted it's first corporative seismic survey in southwestern Manitoba. The objective of the survey was to obtain information on the nature of the boundary between the Churchill and Superior Provinces of the Canadian Precambrian Shield beneath the Phanerozoic cover.

This boundary is associated with at least two economically important types of deposits. In the outcrop area to the north, copper - nickel ore is mined from the Thompson Nickel Belt near the boundary. In southern Manitoba, there is an accumulation of oil and gas in the Phanerozoic sedimentary rocks overlying the boundary. Better understanding of the structural and stratigraphic relationships within the transition area will aid in exploration activities in the region and will also give insight into the tectonic processes which might have occurred in the early history of the Earth.

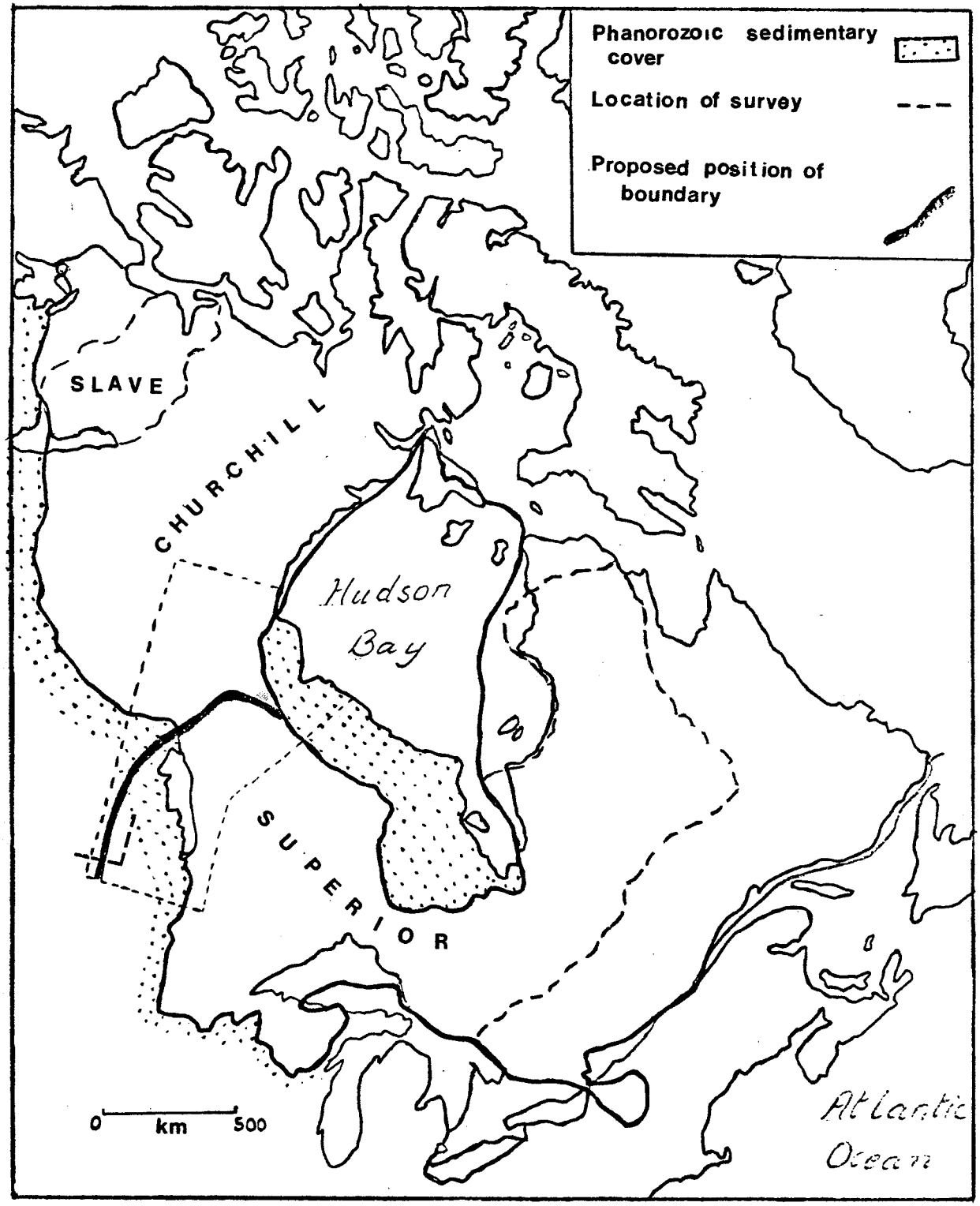

Figure 1.1 - The Churchill and Superior Provinces of the Canadian Shield

Similar seismic work have been done in areas farther east, in the Superior Province, by Hall and Hajnal (1969). Numerous geophysical and geological studies have been carried out in the boundary area to the north. However prior to this seismic experiment little seismic work has been done in extending the boundary into southern Manitoba.

A preliminary analysis of the data gathered from this survey was done by Green et al. (1980), in addition seismic modelling based on velocity - depth models derived by Green was carried out by Lewanski (1979) and Lau (1979).

In this thesis, an attempt will be made to interpret the same set of refraction data using Herglotz type inversion, WKBJ synthetic seismogram modelling and ray tracing in order to obtain a more accurate picture of the seismic and tectonic nature of the boundary zone.

The general geology of the survey area may be summarised as follows :

In the province of Manitoba the Canadian Shield lies exposed as shown in Figure 1.1 . To the northeast and southwest it is buried under the Paleozioc cover of the Hudson Bay Lowlands and the Interior Plains respectively. The Shield area in Manitoba is divided into two major geologic provinces the Churchill Province in the northwest and the Superior Province in the southeast. It is the

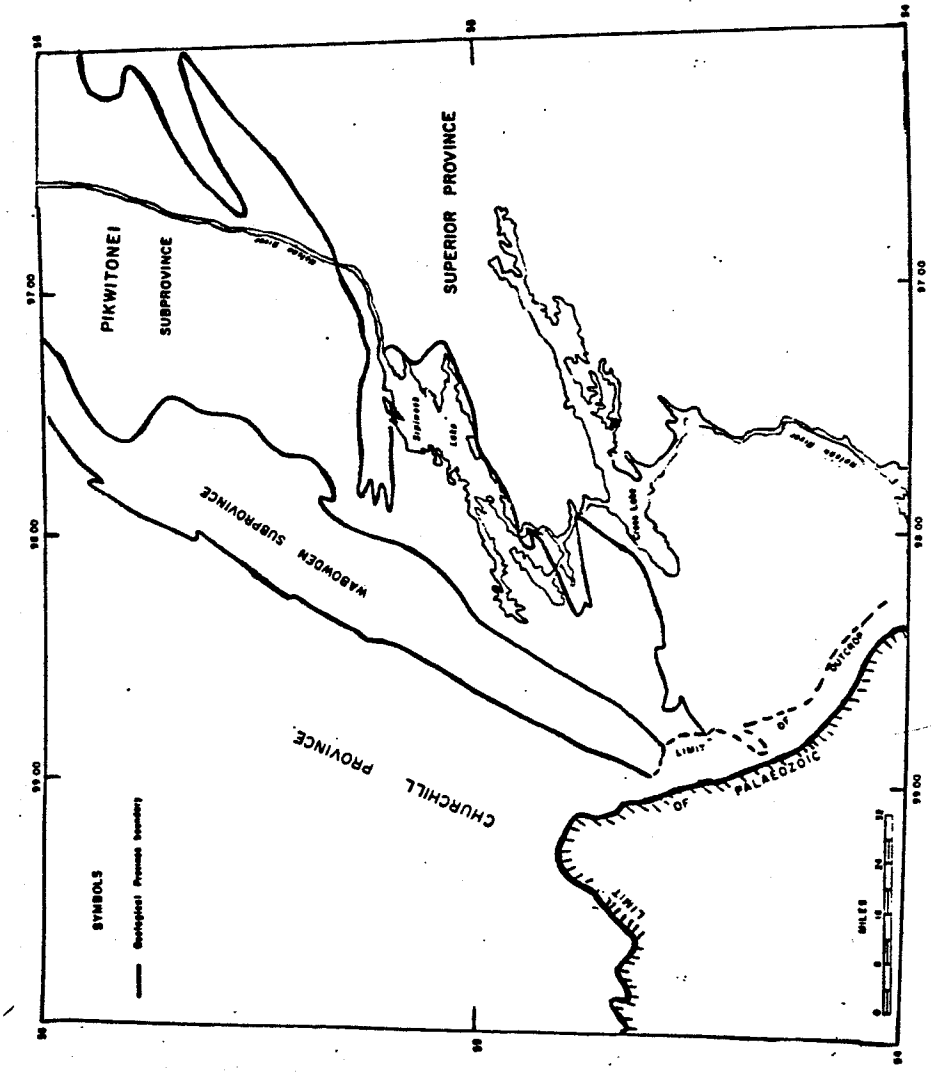

Figure 1.2 - Boundary area in northern Manitoba.

boundary between these two provinces which is of concern in this thesis.

There are several theories as to the origin of the boundary between the Churchill and Superior Provinces. One hypothesis championed by Gibb (1975) proposes a collision type formation. He suggested that the Slave and Superior protocontinents were separated by Aphebian seas and continental fragments which at that time constituted the Churchill Province. Subsequent convergence of the two protocontinents led to the Hudsonian Orogeny, the formation of the Churchill Province and coalition of the the Churchill and Superior Provinces.

In the north where the boundary is exposed, the regional geology has been studied extensively. In the vicinity of the boundary, the area can be conveniently divided into blocks of similar geological trend viz., the Superior Block, the Pikwitonei Subprovince, the Wabowden Subprovince and the Churchill Block (see Figure 1.2) .

In the northwest, the Superior Block is composed of layered felsic gneisses, amphibolite and foliated granitoid masses. To the south, there are easterly trending Archean greenstone belts, cross -cut by east northeasterly trending faults. The adjacent Pikwitonei Subprovince is underlain by granulite facies gneisses and minor amounts of amphibolites. The Wabowden Subprovince which is also referred to as the

Thompson Nickel Belt and the Thompson - Moak Nickel Belt is composed of predominantly migmatic and layered, cataclastic felsic gneisses. Graywackes and shale - derived gneisses underly the Churchill Block in the region adjacent to the boundary area.

The character and position of the Churchill - Superior boundary is another area of controversy. Believed by some to be a sharp contact, it has been variously positioned between the Churchill and Superior Blocks. Bell (1971) suggested the contact between the Pikwitonei and Wabowden Subprovinces is to be considered as the Churchill - Superior boundary. Review of the the geological relationships in the region by Weber and Scoates (1978) has led to a relocation of the boundary contact. Weber and Scoates (1978) proposed that the Wabowden and Pikwitonei Subprovinces are sufficiently similar to the Archean terrain of the Superior Province to be considered part of the Superior Block. The Churchill - Superior boundary, by their reasoning, therefore lies at the contact between the Wabowden Subprovince and the Churchill Block.

A sharp contact between the two geologic provinces does not meet with unanimous approval. There are those who suggest that a gradational transition is more in keeping with the postulated mode of formation and the geological and geophysical findings. They propose that the boundary is a

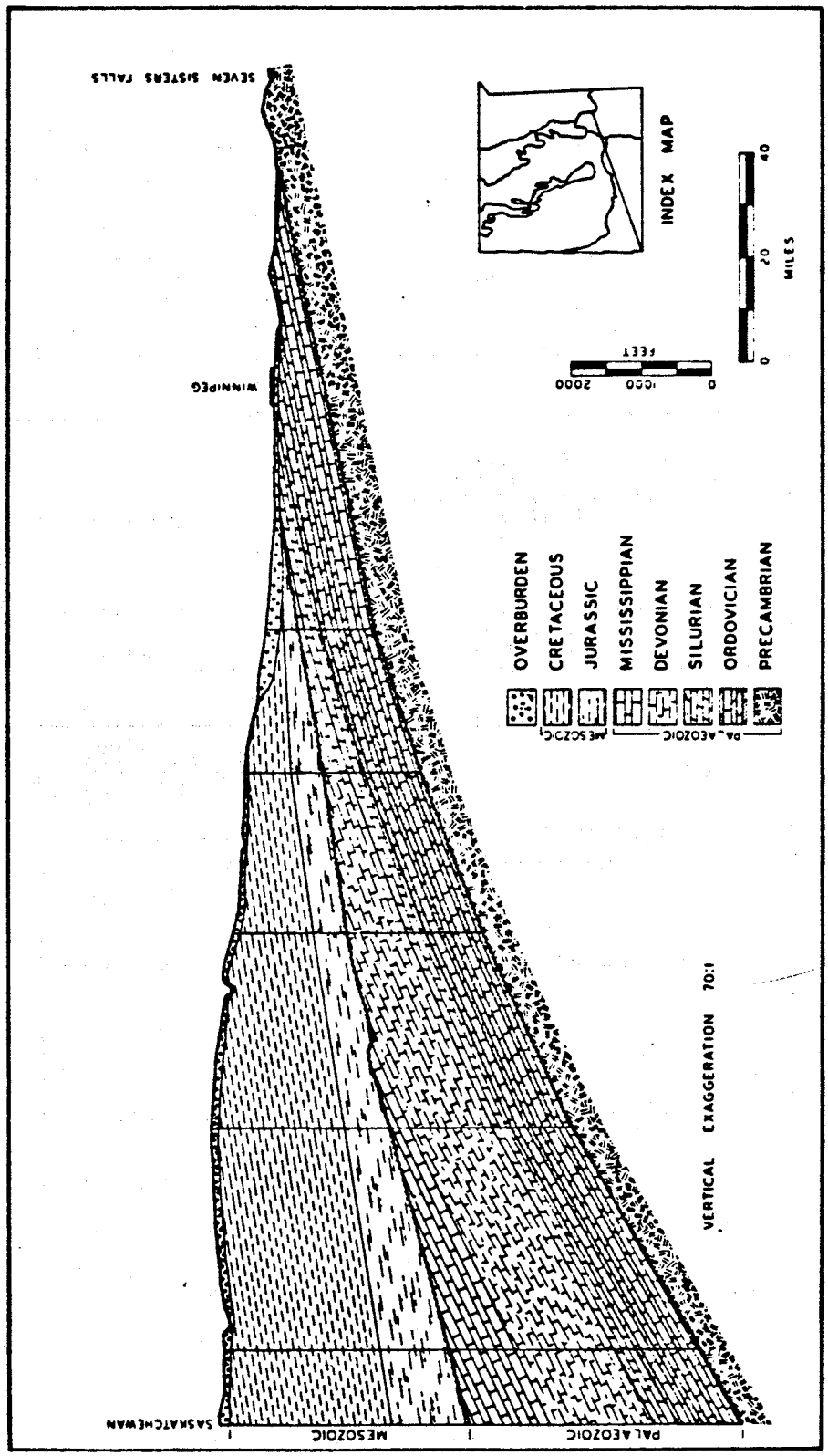

Figure 1.3 - Geological cross section of southwestern Manitoba (McCabe,1963).

ERA	PERIOD	BASIC LITHOLOGY
CENOZOIC	Quarternary	Soil alluvial deposits, sand dunes, bogs, glacial deposits
	Tertiary	Shale, sandstone, lignite
MESOZOIC	Cretaceous	Hard grey siliceous shale, bentonite beds, non-calcareous shale, calcareous shale, limestone beds, sand, shale, sandstone, clay and lignite
	Jurrasic	Varicoloured shale, limestone, gypsum, anhydrite, dolomite
	Triassic	Not reported in Manitoba
PALEOZOIC	Permian Pennsylvanian	
	Mississippian	Dolomite, anhydrite, limestone, shale
	Devonian	Limestone,anhydrite, dolomite, halite, shale
	Silurian	Dolomite
	Ordovician	Dolomite, calcareous shale, limestone
	Cambrian	Glauconitic sandstone
Precambrian		

Table 1.1 - Basic lithology of southwestern Manitoba (Mc Cabe, 1963).

zone of finite lateral extent encompassing both the Wabowden and Pikwitonei Subprovinces.

Further south the boundary disappears under the Paleozoic cover of the Interior Plains. The geology of southwestern Manitoba can be divided into two parts, the Precambrian basement and the Phanerozoic sedimentary geology. The Phanerozoic sequence is thick and the maximum depth is approximately 2 kilometres. It is comprised of Ordovician, Silurian, Devonian, Mississippian, Jurassic and Cretaceous strata (see Figure 1.3). Table 1.1 gives the rock types associated with these sequences.

Little is known about the Precambrian rocks underlying the sedimentary cover. Correlation of diamond drill information and oilwell logs by Bodhan and Homeniuk (1970) have led to a division into seven broad categories of rocks. Figure 1.4 gives the basement geology as deduced by Bodhan and Homeniuk (1970).

The thick sedimentary cover prevents wide scale mapping of the basement geology in the south. In order to delineate the position of the boundary in this area geophysical methods were used. Green et al. (1979) obtained a tentative eastern and western limit for the boundary by correlating the trends in the magnetics and gravity established in the north with those in the south.

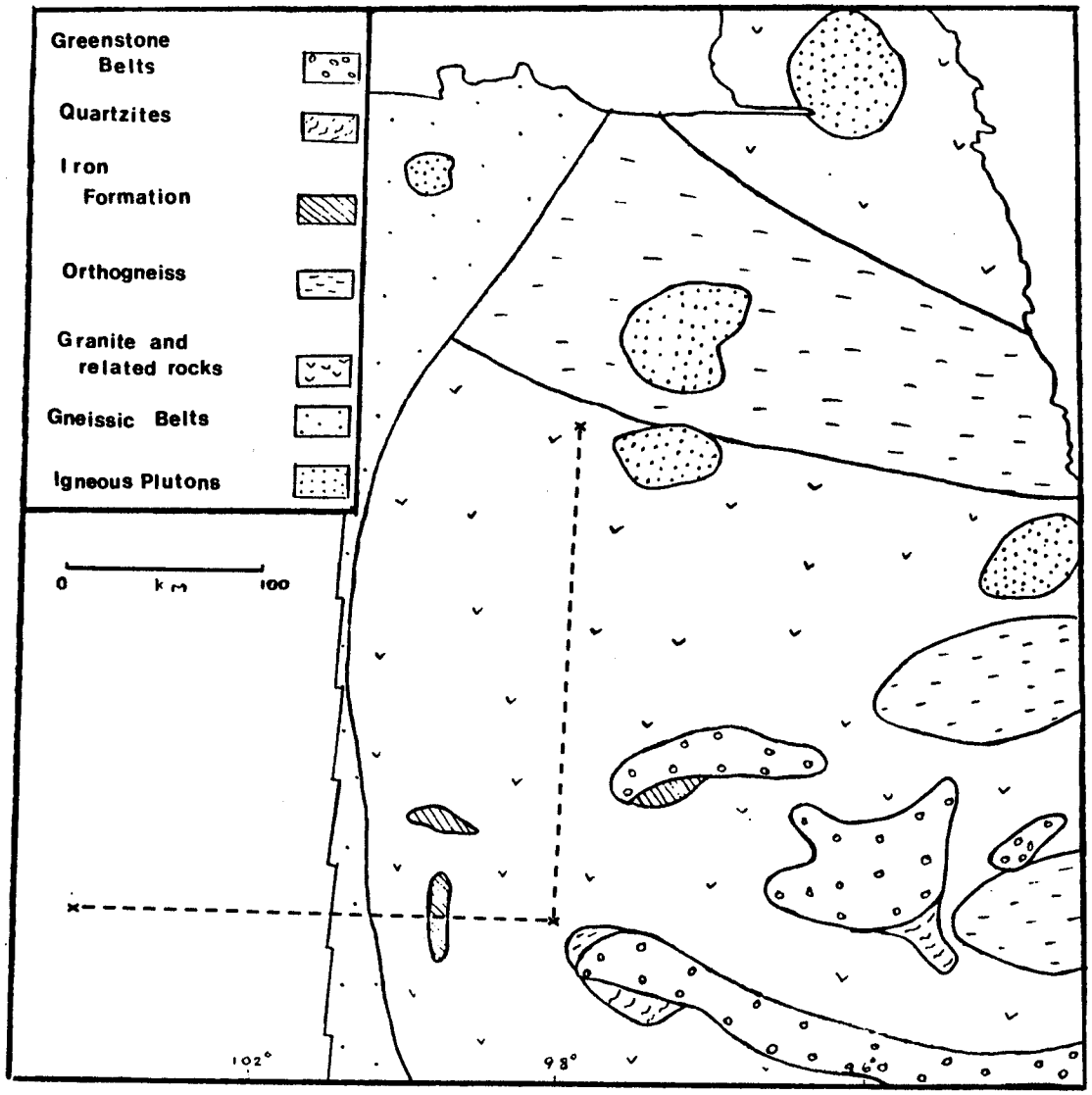

Figure 1.4 - Precambrian geology in southwestern Manitoba (Bod -han and Homeniuk, 1970), dotted lines indicate position of seismic profiles.

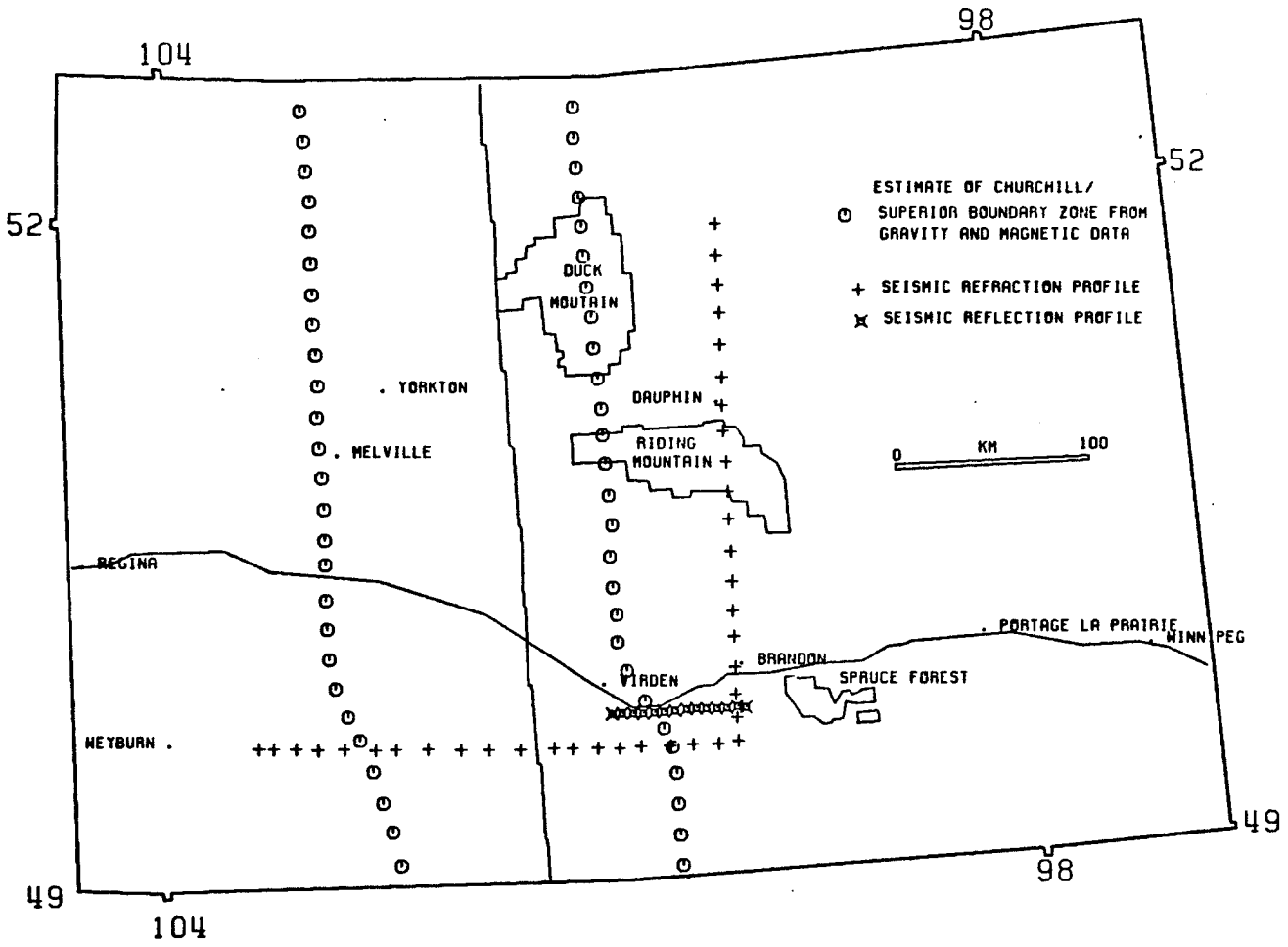

Figure 1.5 - Location of Seismic Survey.

With this postulated boundary position in mind, two seismic lines , a north - south and an east - west (see Figure 1.5), were shot in order to determine the change in crustal structure from the Superior to Churchill Province.

In the following chapters a brief description of the seismic survey procedure and a detailed interpretation of the data are given.

Chapter II

THE REFRACTION SURVEY

The refraction survey comprised of two 240 km reversed profiles; one in a north-south direction from latitude 49.6356 degrees to latitude 51.7983 degrees north and the other an east-west line from longitude 100.0066 degrees to 103.3251 degrees west (see Figure 1.5). In an attempt to obtain information on the gross velocity structure over an area that included several fault blocks, the north/south profile was located entirely in the Superior province. The east/west line traversed the Superior province, the boundary zone and the Churchill province. The depths to the crustal discontinuities should be obtained from analysis of the data obtained from this profile.

2.1 SEISMIC ENERGY SOURCE

A total of eight shots were detonated, with a small and a large shot at the end of each line. The charges were made up of 60% geogel. These were detonated in drillholes about 15 to 37 metres deep and 13 to 15 inches in diameter. The size of the charge for the smaller holes varied from 362

to 363 kilograms and that for the larger charges from 816 to 1119 kilograms. The significant range of sizes for the larger shots was a result of the sympathetic detonation of charges primed for a smaller shot when shot 3 was fired.

The total shot sizes, latitude, longitude and elevation of the shots are contained in Table 2.1 . The accuracy of latitude, longitude and elevation at these sites are approximately ± 0.0005 degrees, ± 0.0005 degrees and ± 8 metres respectively. All shots were fired sucessfully during relatively quiet periods of the day.

TABLE 1

Shot Parameters

Shot	Shot #	Charge Size (kg)	Latitude (degrees)	Longitude (degrees)	Elevation (m)
N Large	1	816	51.8216	99.9473	256
N Small	2	363	51.8217	99.9477	256
S Large	3	1119	49.6217	99.9716	472
S Small	4	362	49.6213	99.9716	472
E Large	5	816	49.6215	99.9716	472
E Small	6	363	49.6215	99.9726	472
W Large	7	816	49.6449	103.3380	472
W Small	8	363	49.6456	103.3376	472

2.2 THE RECEIVER ARRAY

The receivers used in this survey were supplied by the University of Toronto and the Earth Physics Branch,

Ottawa. A vertical 1Hz, north/south and east/west horizontal seismometers were set up at each of six sites by the Earth Physics Branch ; while the University of Toronto installed 1Hz radial horizontal seismometers at the remaining in-line recording sites and a vertical 1Hz instrument at a remote site about 0.6 kilometres away. With this arrangement, it was hoped that some information on the apparent velocity of P-waves could be obtained. The combined equipment allowed for recording at seventeen different positions along the line.

The receivers on the north/south profile were located beside minor gravel roads within 9 kilometres of the Manitoba Highway Number 10, its northern continuation, Highway Number 20 and a gravel road leading to Lake Winnipegosis. The east/west profile was set up along minor roads some 6 kilometres from Manitoba Highway Number 3 and its westerly extension into Saskatchewan Highway Number 13.

These recording sites did not deviate by more than $\pm$ 4 kilometres from a straight line. The latitude, longitude and elevation of the receivers are given in Table 2.2 (a) and (b). The accuracy of the absolute latitude, longitude and elevation are $\pm$ 0.0005 degrees, $\pm$ 0.0005 degrees and $\pm$ 8 metres respectively.

RECIEVER NUMBER	LATITUDE °N		LONGITUDE °W		ELEVATION (m)	
	LOCAL	REMOTE	LOCAL	REMOTE	LOCAL	REMOTE
10	49.6356		99.9848		472	
20	49.6947		99.9726		485	
30	49.7538		99.9848		405	
40	49.8091		99.9841		398	
50	49.9011		99.9807		413	
60	49.9750		99.9809		482	
70	50.0490	50.0540	99.9801	99.9801	503	512
80	50.1266	50.1318	99.9805	99.9805	503	556
90	50.1969	50.1968	99.9680	99.9680	564	564
100	50.2696	50.2639	99.9763	99.9763	590	590
110	50.3433	50.3372	99.9764	99.9764	599	599
120	50.4178	50.4128	99.9288	99.9288	609	619
130	50.4908	50.4857	99.9301	99.9301	649	658
140	50.5655	50.5710	99.9425	99.9425	613	617
150	50.6236	50.6188	99.9795	99.9773	628	622
160	50.6936	50.6905	99.9722	99.9775	617	617
165	50.7469	50.7464	99.9971	99.9881	686	686
170	50.7718	50.7715	99.9948	99.9872	657	657
180	50.8360	50.8387	100.0149	100.0133	620	620
190	50.8960	50.8972	100.0556	100.0591	678	678
195	50.9474	50.9480	100.0406	100.0406	652	652
205	51.0222	51.0277	100.0388	100.0388	326	323
210	51.0667	51.0722	100.0388	100.0388	311	309
220	51.1218	51.1166	100.0161	100.0153	291	291
230	51.2297	51.2351	99.9920	99.9920	276	276
240	51.2874	51.2874	99.9958	99.9946	267	267
250	51.3622	51.3677	99.9982	99.9982	267	267
260	51.4380		99.9927		262	
270	51.5078		99.9937		261	
290	51.6527		99.9328		262	
300	51.7390		99.9645		256	
310	51.7981		99.9658		256	

Table 2.2 (a) - Reciever Locations for the north-south profile line.

RECIEVER NUMBER	LATITUDE °N		LONGITUDE °W		ELEVATION (m)	
	LOCAL	REMOTE	LOCAL	REMOTE	LOCAL	REMOTE
10	49.6068		100.0066		469	
20	49.6061		100.0979		457	
30	49.6055		100.1881		442	
40	49.6042		100.3028		434	
50	49.6060		100.4153		431	
60	49.6063		100.5408		431	
70	49.6135	49.6138	100.6441	100.6530	433	433
80	49.6063	49.6063	100.7711	100.7711	434	433
90	49.6063	49.6063	100.9161	100.9075	436	436
100	49.6062	49.6062	101.0619	101.0537	457	465
110	49.6061	49.6061	101.1763	101.1687	485	485
120	49.6062	49.6062	101.3038	101.3124	507	510
130	49.6052	49.6052	101.4163	101.4086	538	538
140	49.6065	49.6065	101.5290	101.5205	556	561
145	49.6063	49.6063	101.5994	101.5994	579	579
150	49.6062	49.6062	101.6327	101.6245	587	587
155	49.6060	49.6060	101.7124	101.7039	591	591
160	49.6061	49.6061	101.7573	101.7500	603	613
170	49.6058	49.6058	101.8715	101.8631	617	617
180	49.6096	49.6096	101.9854	101.9854	626	626
190	49.6177	49.6177	102.0737	102.0737	632	632
200	49.6310	49.6310	102.2089	102.2089	632	632
210	49.6285	49.6385	102.3213	102.3213	625	625
220	49.6315	49.6315	102.4348	102.4348	625	625
230	49.6391	49.6191	102.5473	102.5389	609	609
240	49.6401	49.6387	102.6605	102.6537	602	602
250	49.6387		102.7961		613	
260	49.6387		102.9080		616	
270	49.6390		103.0111		617	
280	49.6384		103.1354		609	
290	49.6449		103.2479		606	
300	49.6418		103.3251		609	

Table 2.2 (b) - Reciever Locations for the east-west profile line.

2.3 FIELD PROCEDURE

The placing of receivers along roadways meant that a considerable amount of noise from vehicular traffic, farm equipment and some wind generated geophone motion would hamper the recording of the true signal. To avoid this problem, recording as done in the early morning and late evening, when these effects were less severe.

The seismometers were laid out on one half of the north/south profile and during separate time windows, the smaller shot was fired at the end closest to the spread and the larger shot was detonated at the farther end. The instruments were moved to the other half of the profile and the procedure was repeated. To tie up the signals recorded from both halves of the line, the central receiver was kept stationary during shooting. The whole procedure was repeated for the east/west profile.

The WWV radio time signal was used for comparing the shot and receiver chronometers. So synchronization between them was to better than 30 microseconds. The distances between shot points were approximately 245 kilometres for the north/south profile and about 242 kilometres for the east/west profile. The distances between adjacent receiver stations ranged between 2.4 and 16.2 kilometres, with an average value of 7.7 kilometres.

Chapter III

DIGITAL PROCESSING OF THE DATA

The raw data for each of the north, south, east, and west shots is presented as amplitude-corrected record sections of vertical local, horizontal and remote vertical component traces. Elevation corrections have also been applied to the data.

The raw data for each of the eight shots for the local vertical type receiver is shown in Figures 3.1 (a), (b), (c) and (d). The data quality varies from very good to poor. A considerable amount of noise at and before onset of the signal is visible on some of the traces, making it difficult to recognise the first breaks. Examples of traces where this situation occurs are traces 1011,2011,3011 and 4011, on the north shot. In other traces, for example 11041,12041, and 16041 from near the south shot point the energy was sufficiently large so as to overload the system, causing squaring off of the waveform. At some locations along the profile no signal was recieved due to malfunctioning of the particular channels so that records are missing.

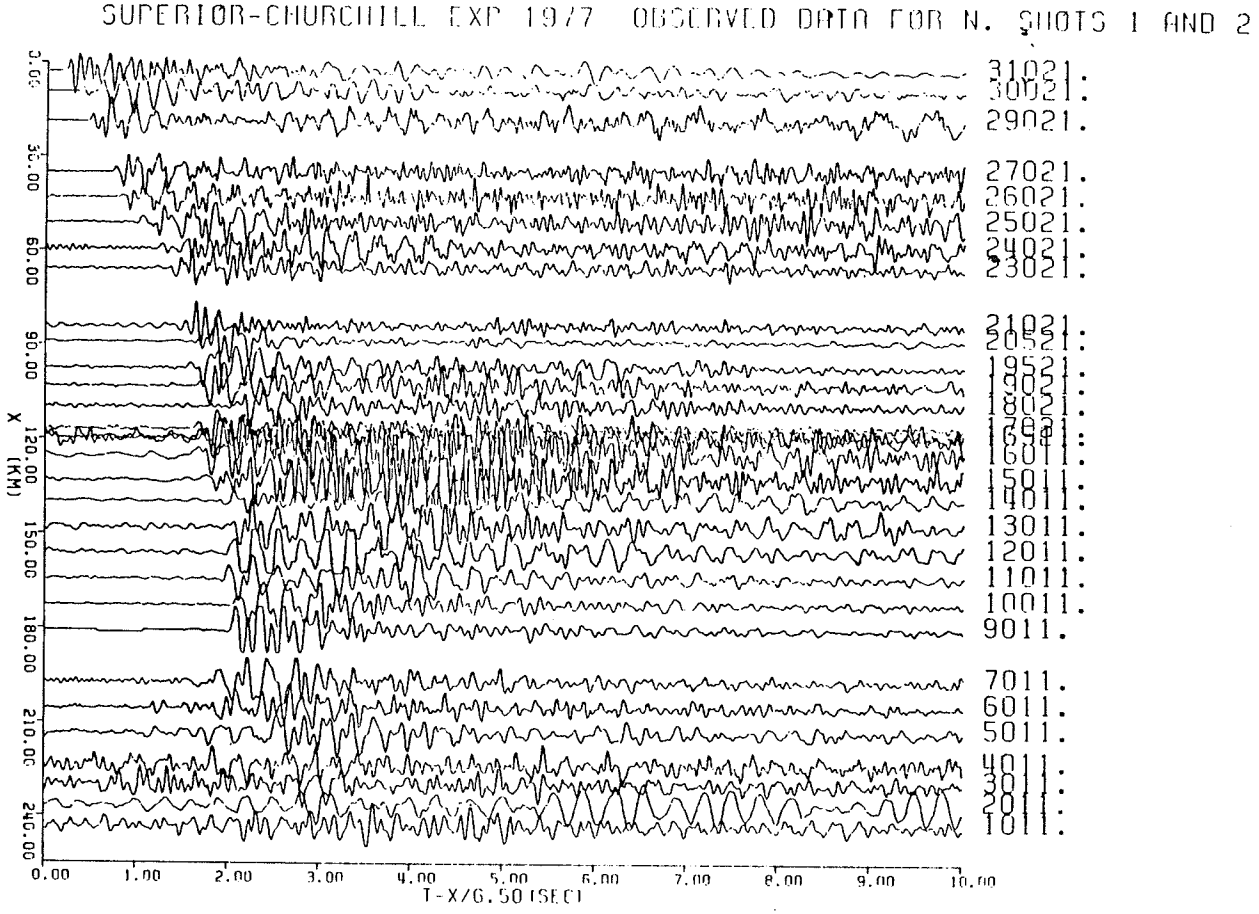

Figure 3.1 (a) - Record section for the north shot (local vertical).

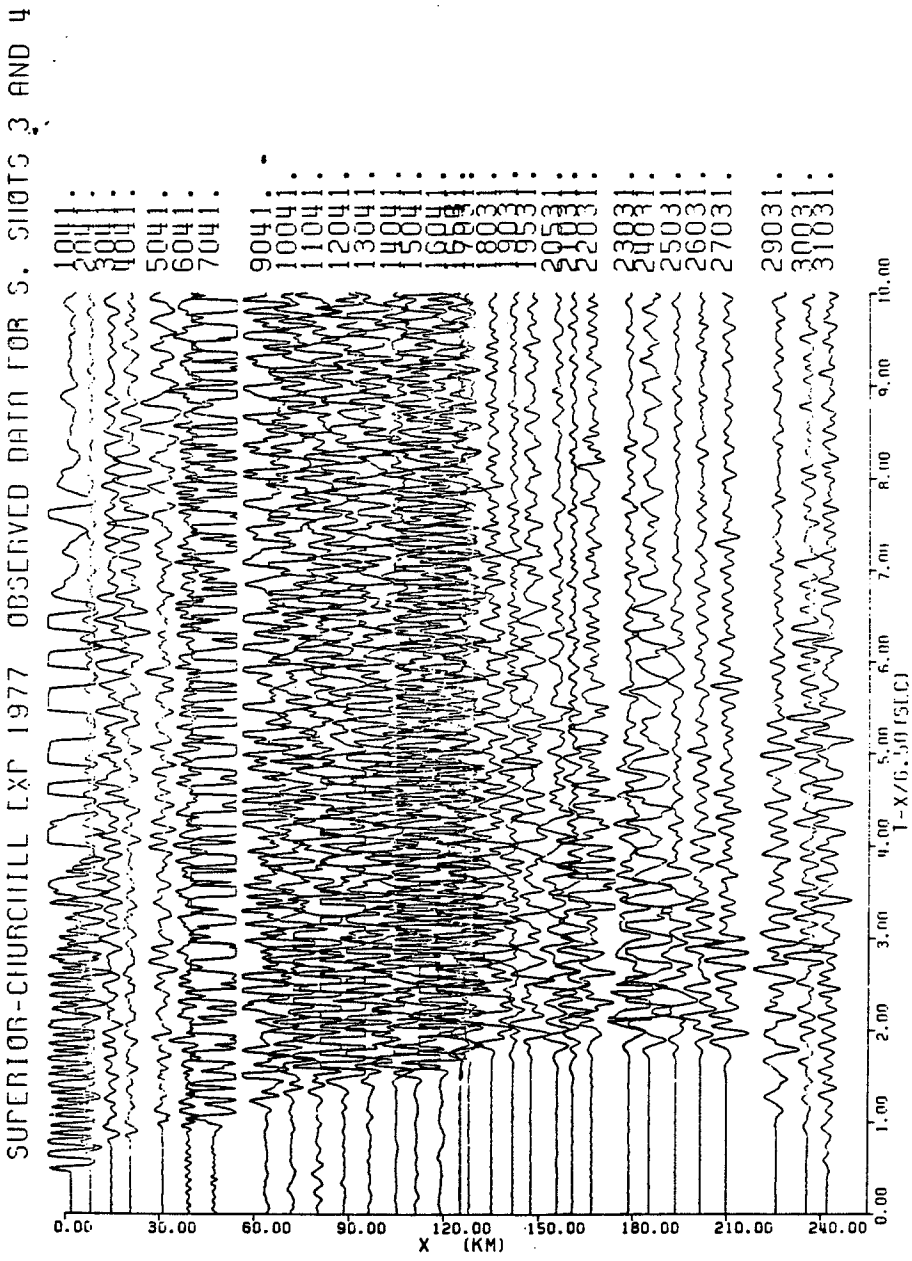

Figure 3.1 (b) - Record section for the south shot (local vertical).

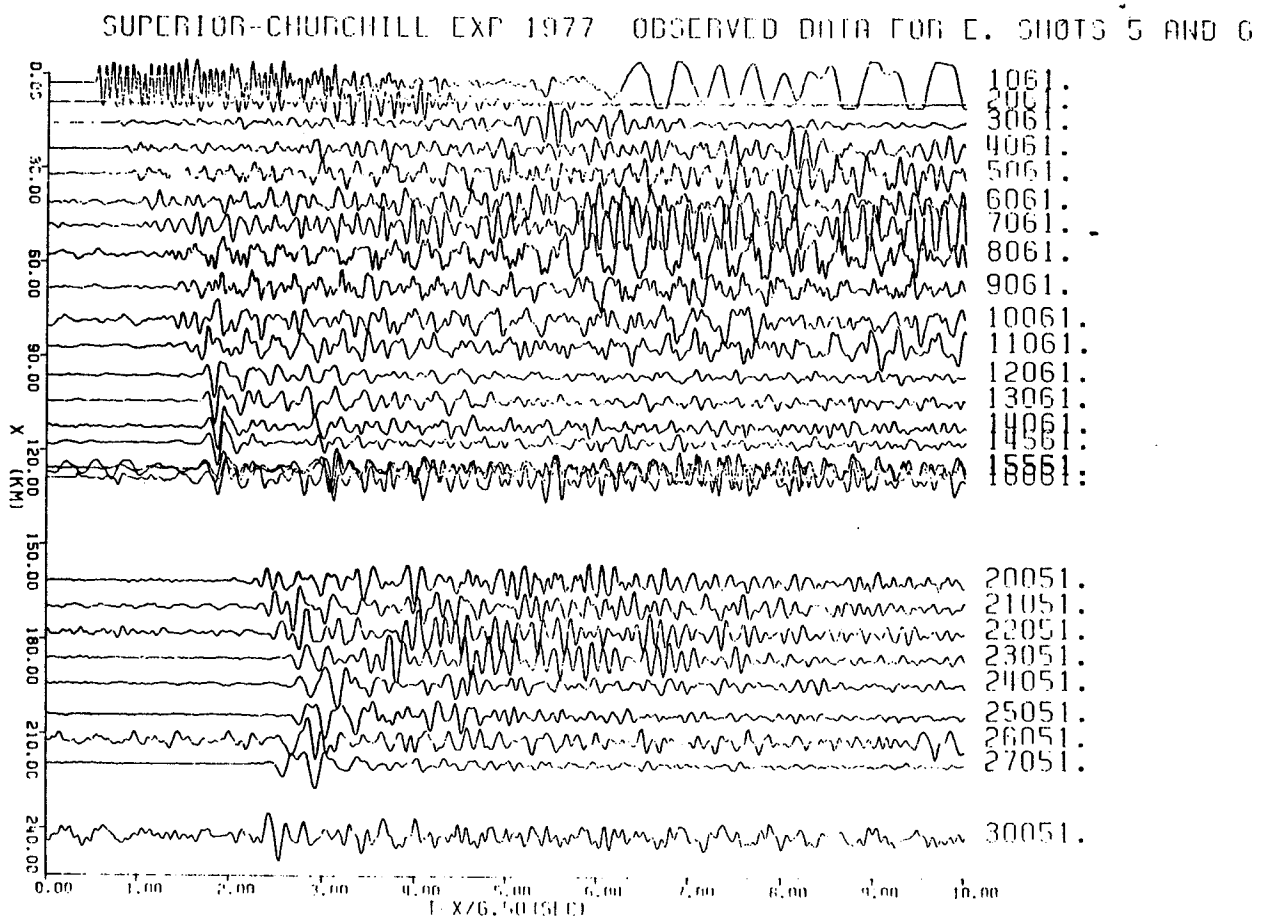

Figure 3.1 (c) - Record section for the east shot (local vertical).

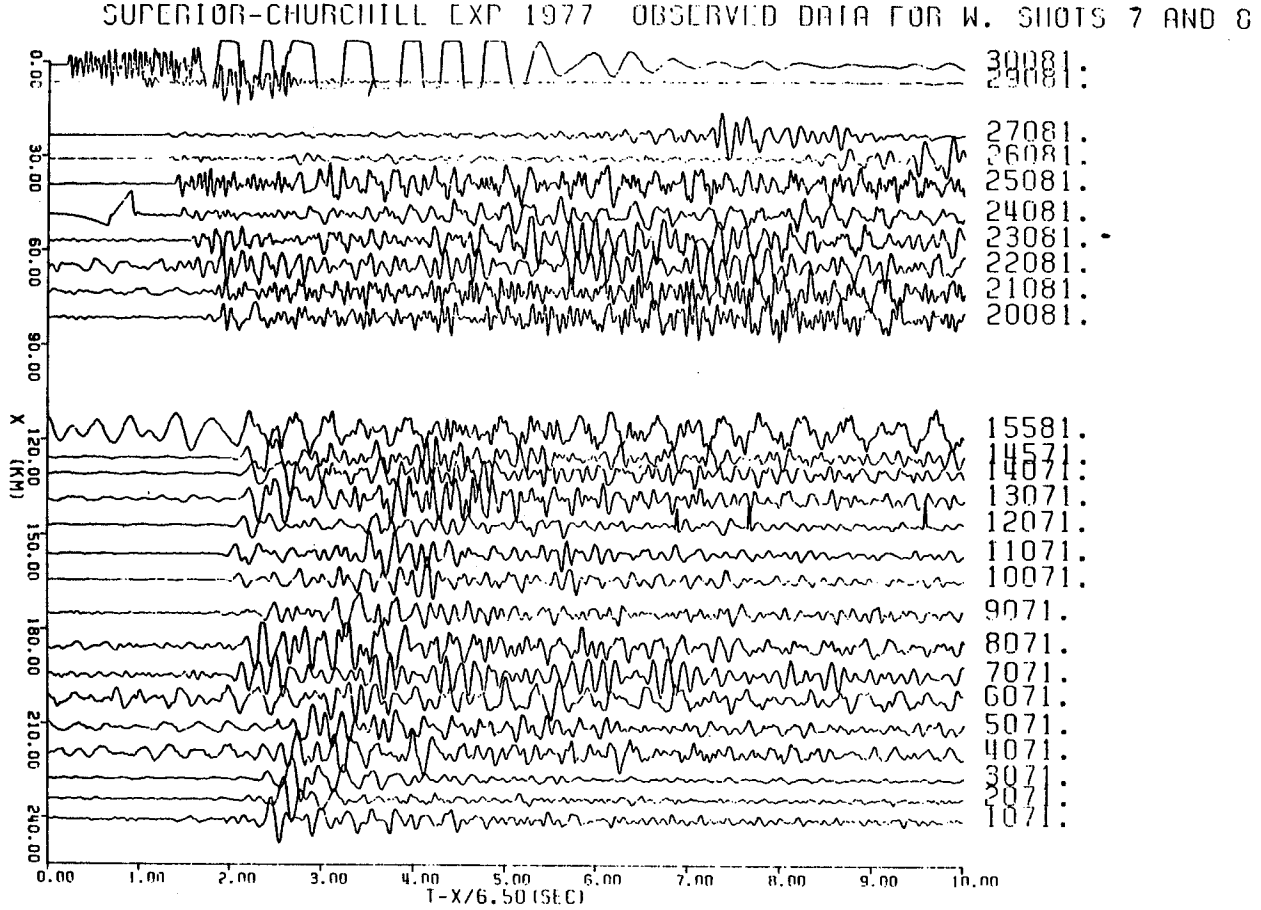

Figure 3.1 (d) - Record section for the west shot (local vertical).

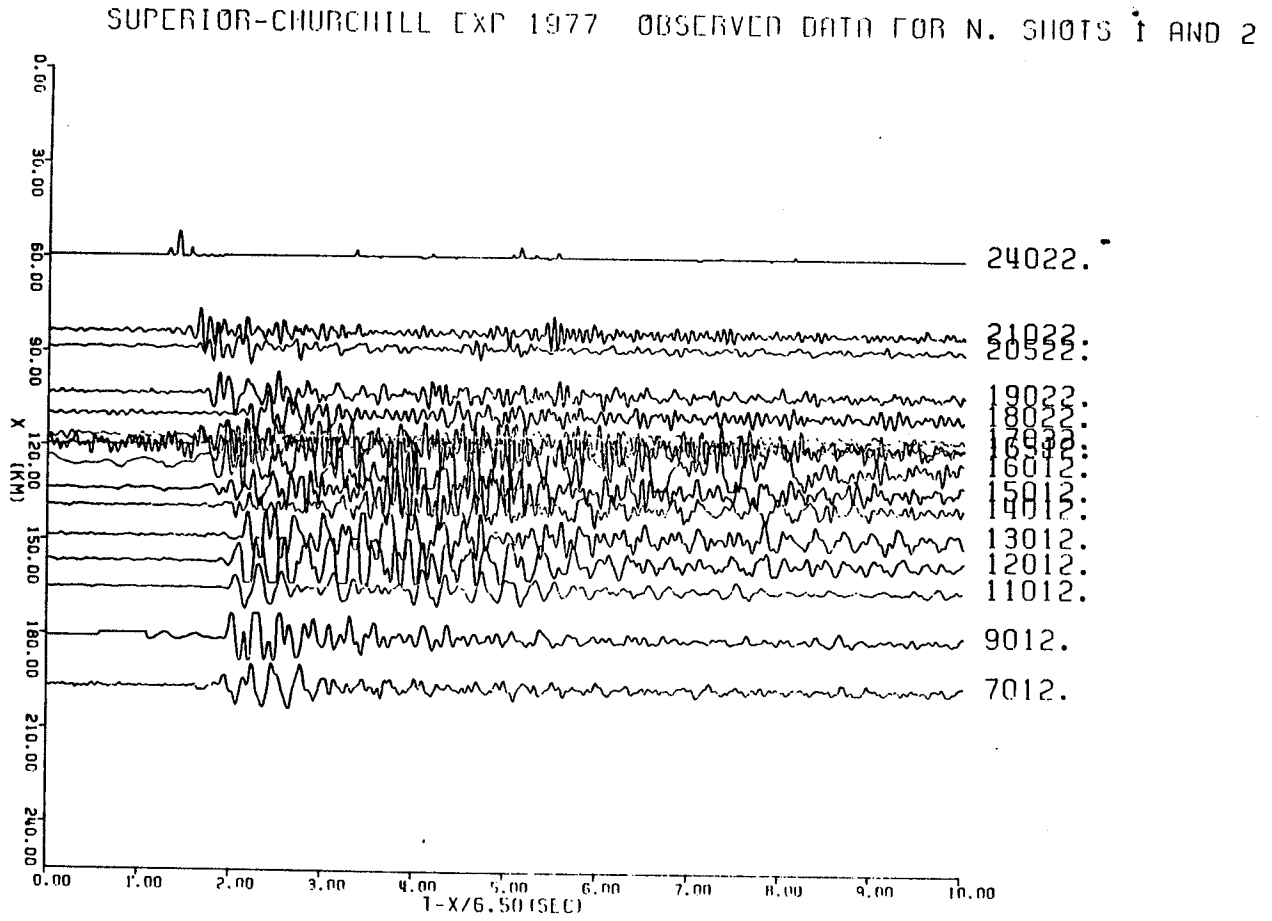

Figure 3.2 (a) - Record section for the north shot (remote vertical).

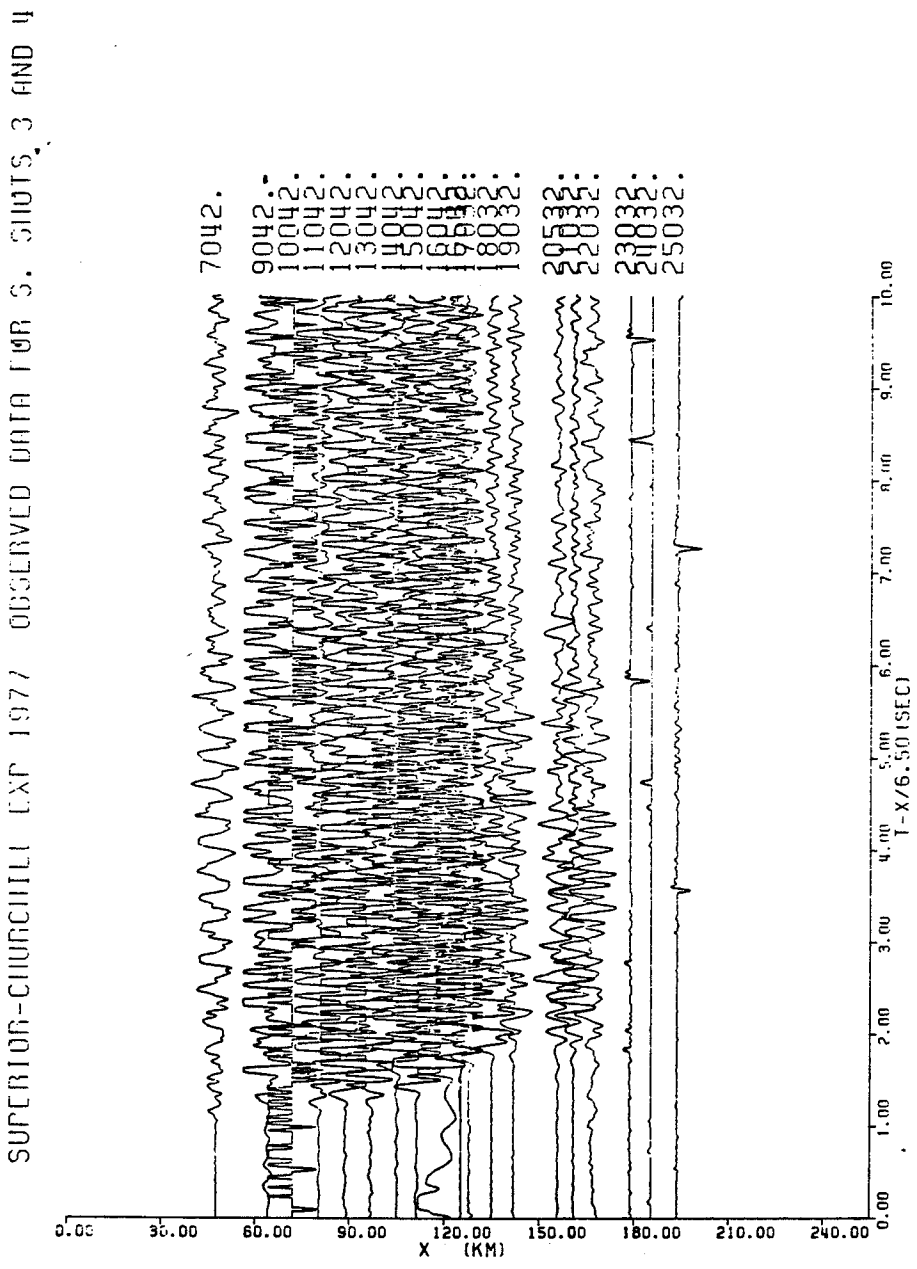

Figure 3.2 (b) - Record section for the south shot (remote vertical).

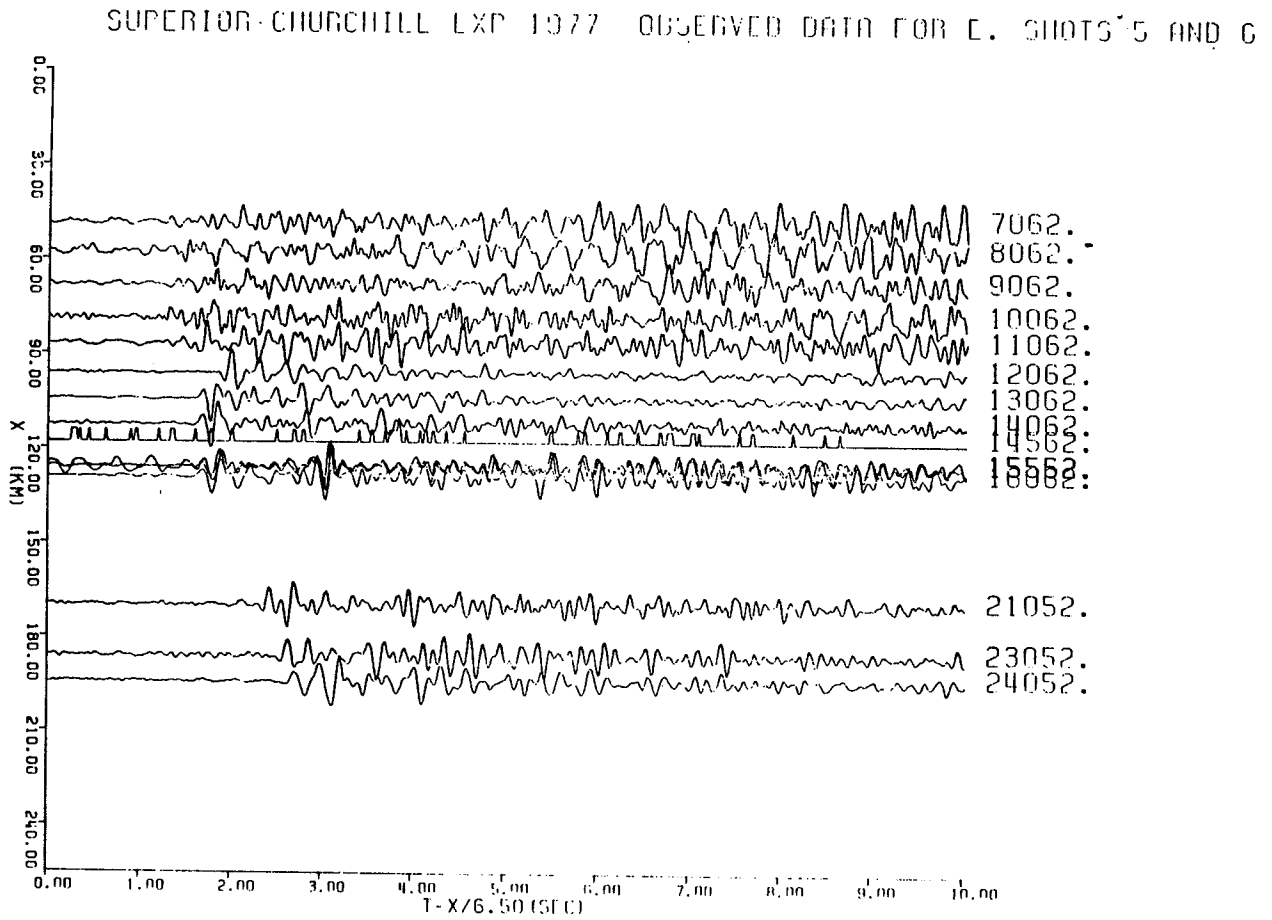

Figure 3.2 (c) - Record section for the east shot (remote vertical).

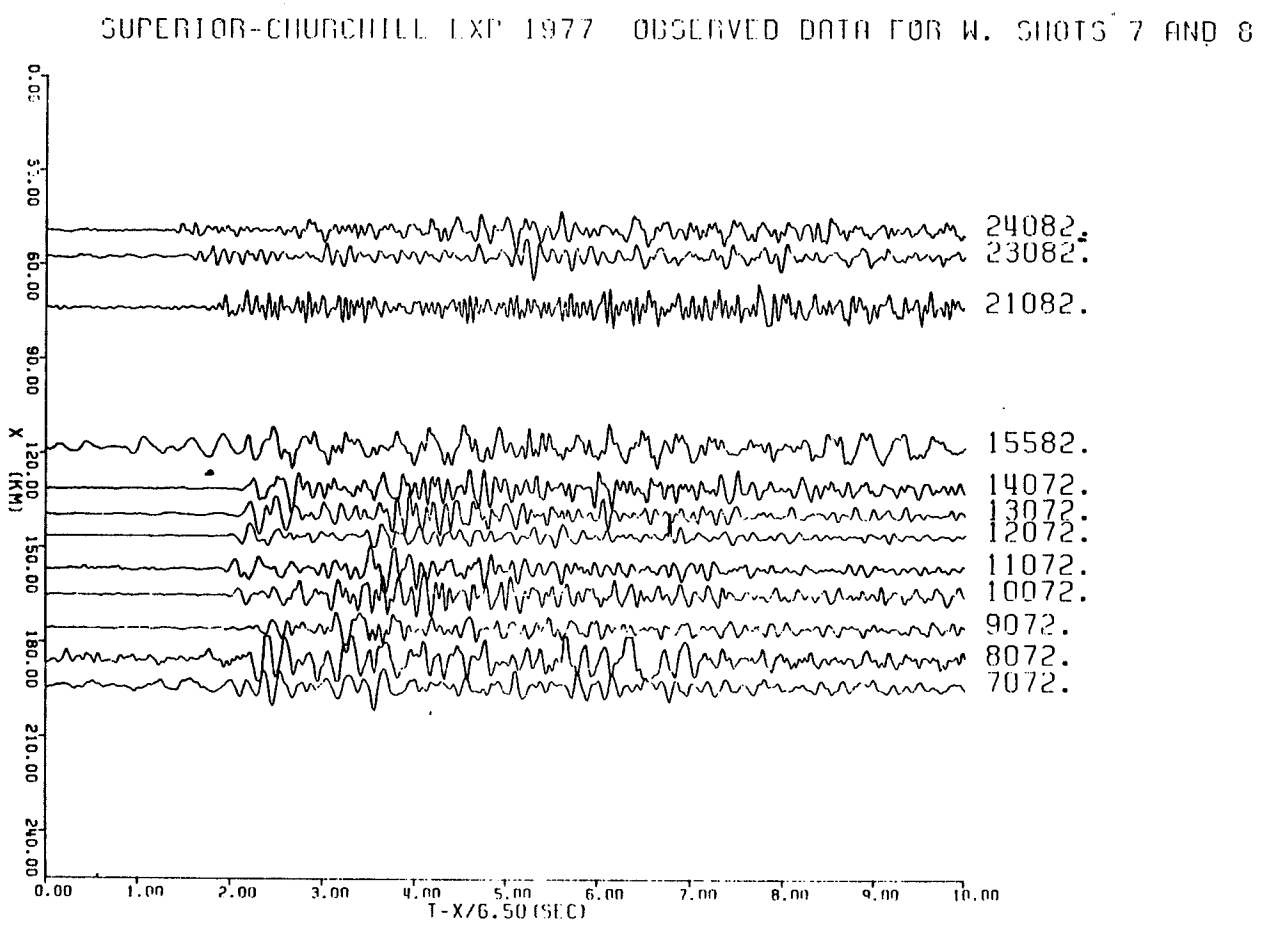

Figure 3.2 (d) - Record section for the west shot (remote vertical).

The data from the east/west and north/south horizontal and remote vertical receivers are of similar quality as the local vertical data, but because of the scarcity of receivers for each type signal detection there are many more gaps in the data recorded along each profile. For much of the subsequent processing it is the local vertical data that will be used. Use will be made of the horizontal data in one of the filtering methods to be discussed later in this chapter. Figures 3.2 to 3.4 show the raw data for each of the receiver types.

Source deconvolution is a very useful tool in seismic interpretation as it simplifies seismic sections and so allows for better recognition of first arrivals and secondary events. Past Attempts to deconvolve seismic data from the Superior Province have yeilded unsatisfactory and discouraging results. The complexity of the seismograms obtained in this project and the expected complexity of the subsurface in this region did not lead the author to expect any fruitful results from source deconvolution. So no attempt at deconvolution was made. For the purpose of synthetic seismogram modelling an approximate source function was convolved with the impulse response to give a more realistic seismogram.

The datasets were filtered using Butterworth bandpass and polarisation filters in order to increase the signal to

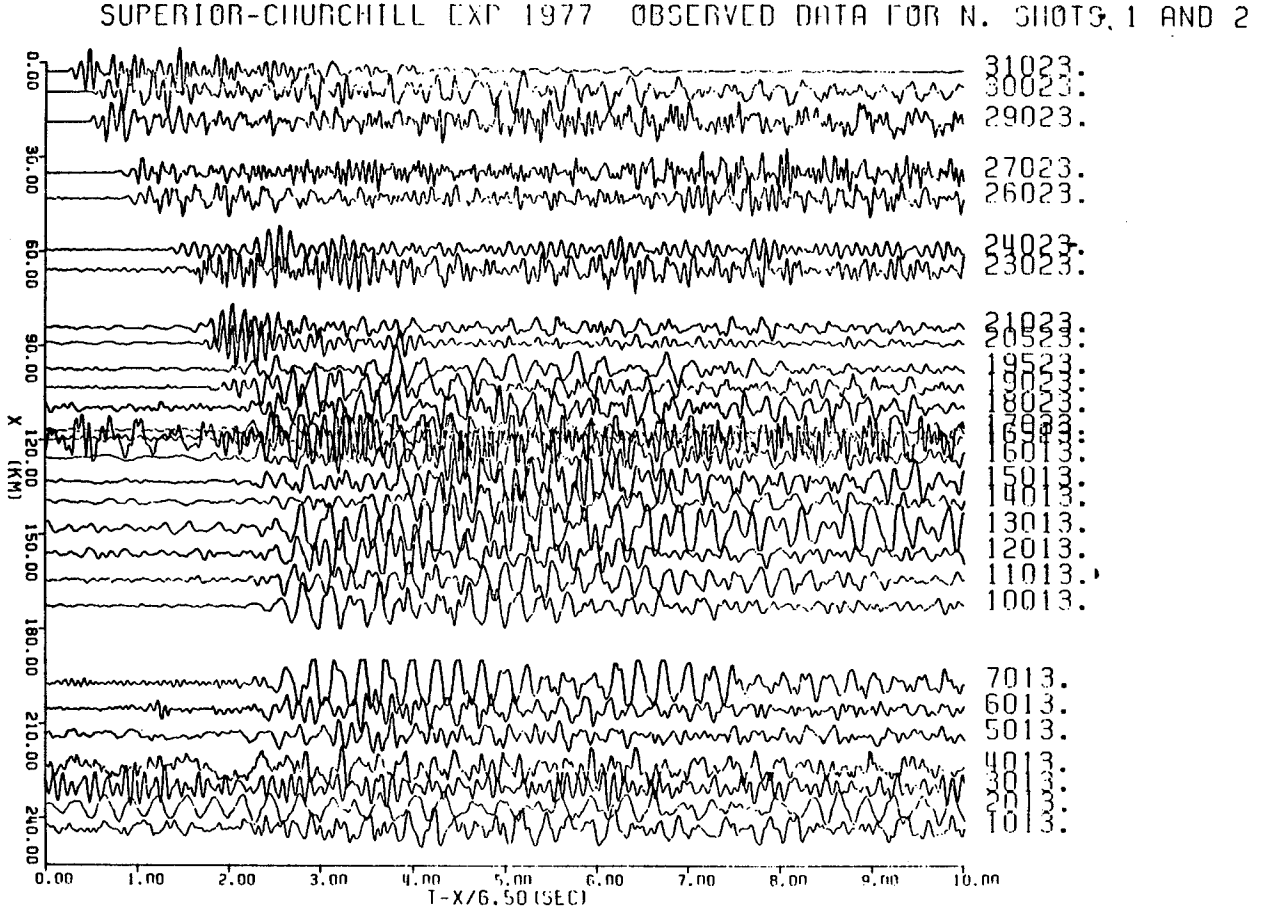

Figure 3.3 (a) - Record section for the north shot (E/W horizontal).

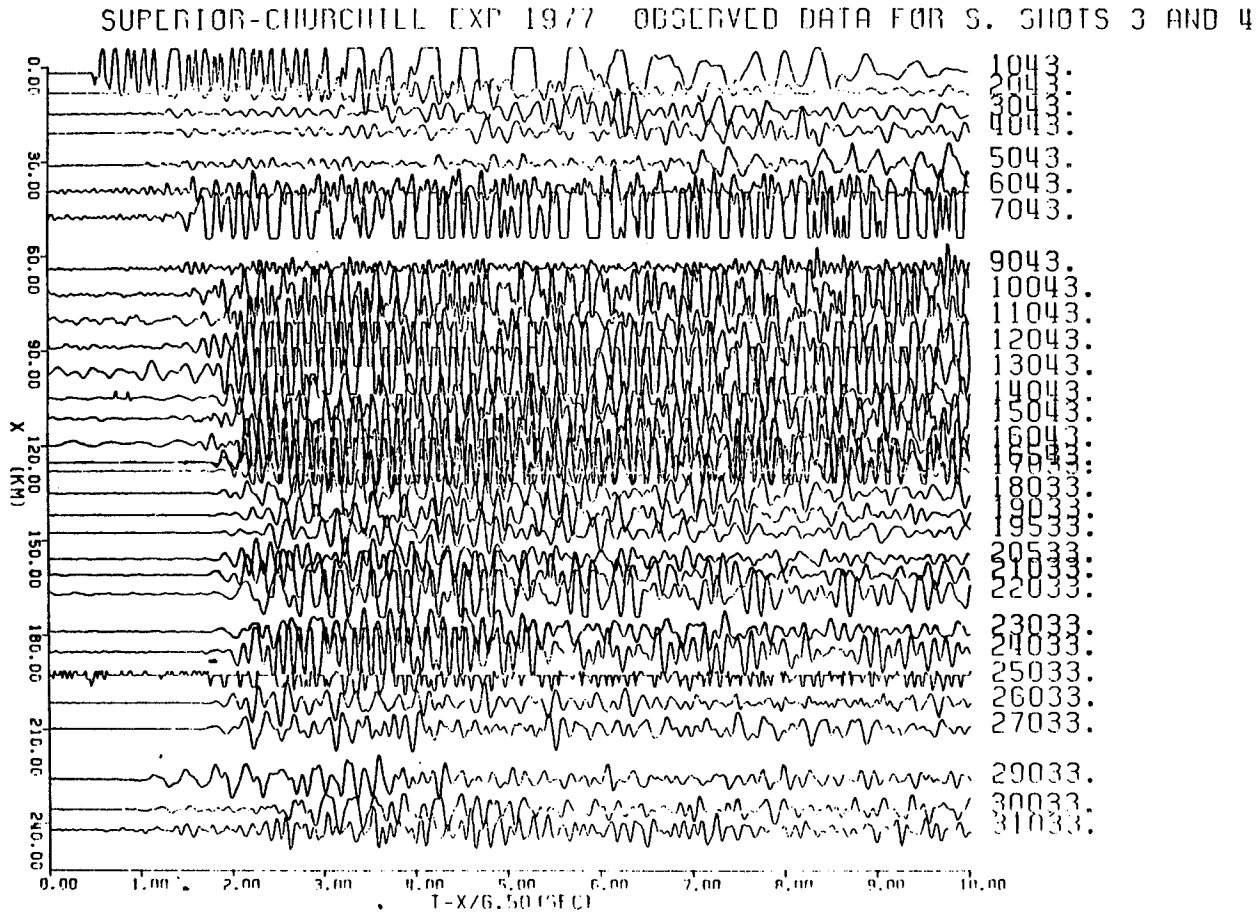

Figure 3.3 (b) - Record section for the south shot (E/W horizontal).

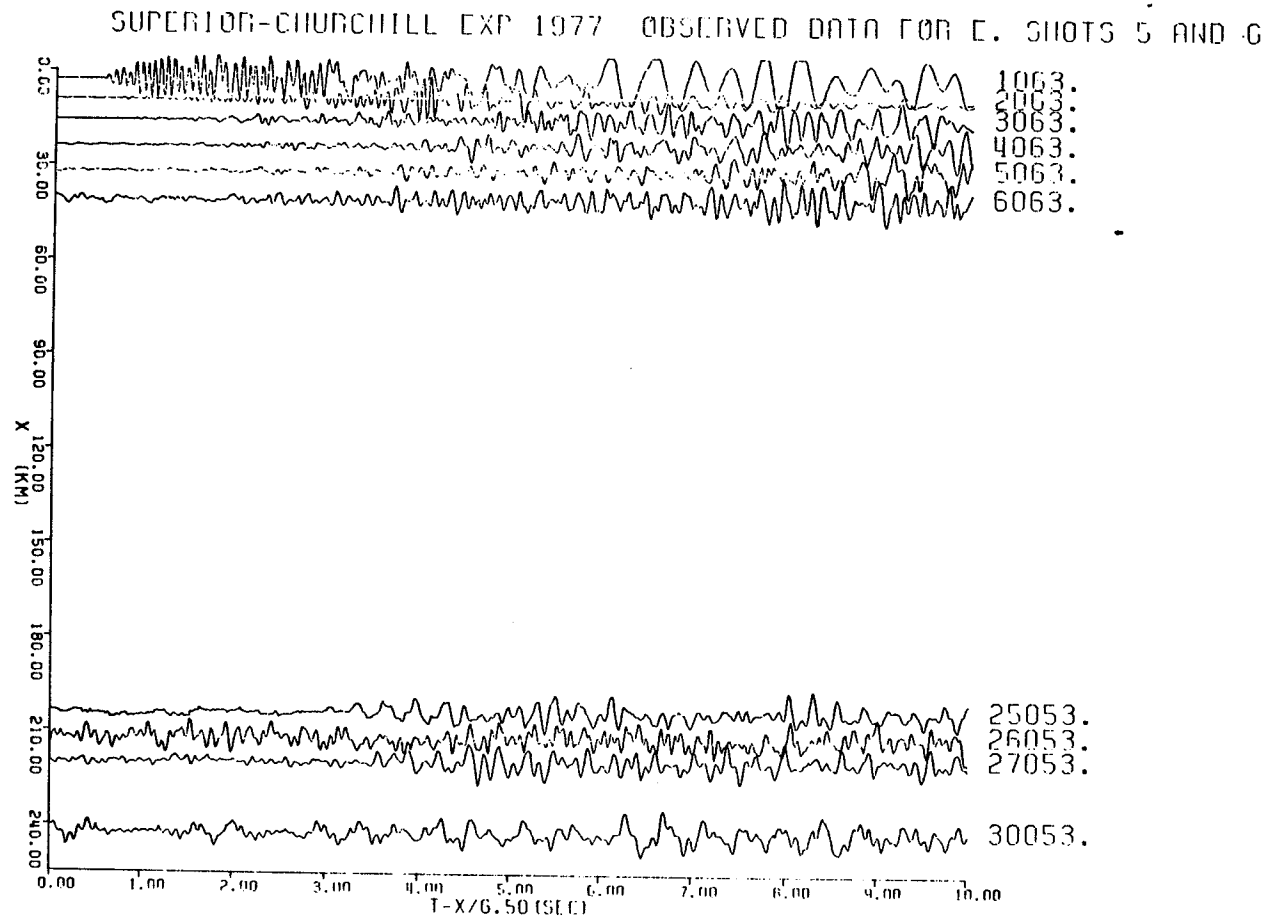

Figure 3.3 (c) - Record section for the east shot (E/W horizontal).

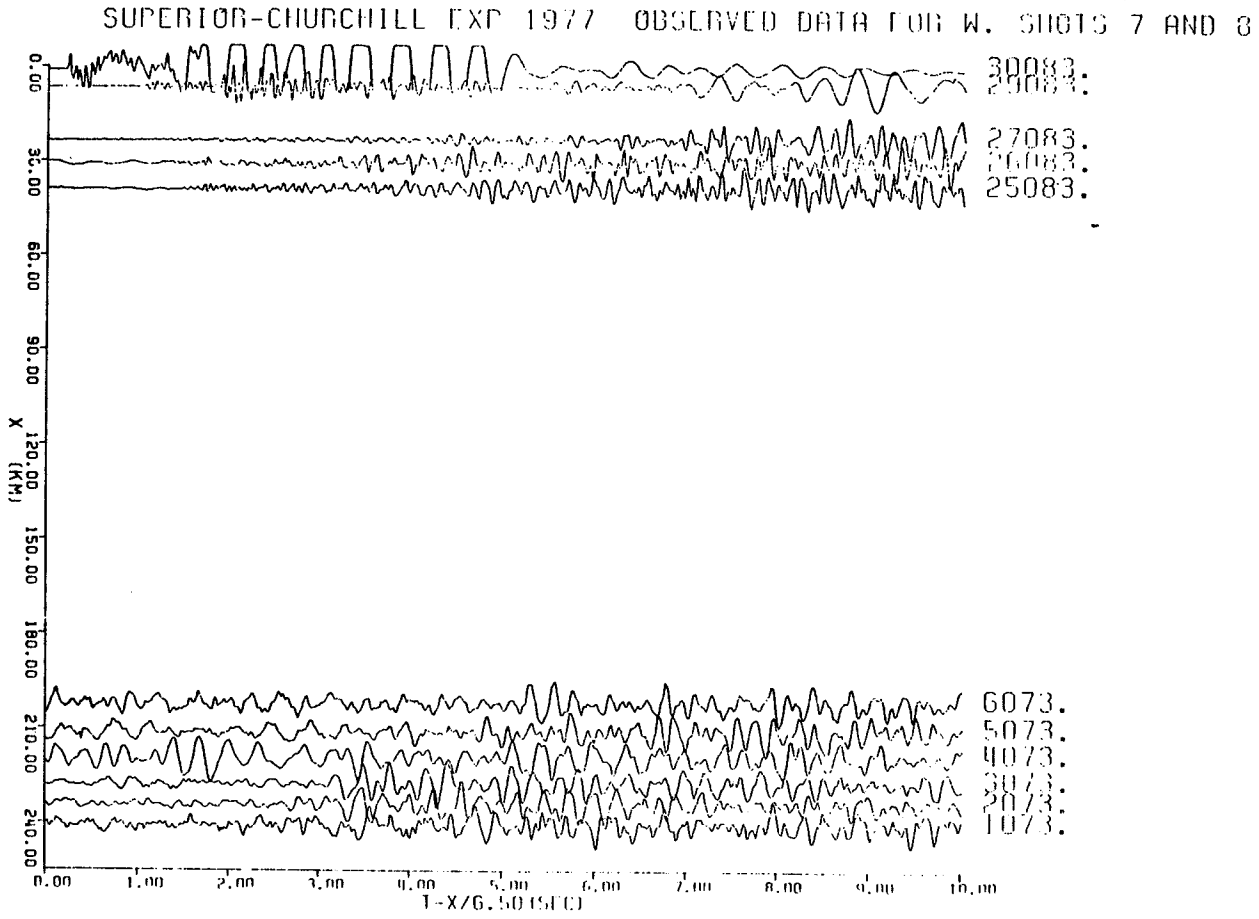

Figure 3.3 (d) - Record section for the west shot (E/W horizontal).

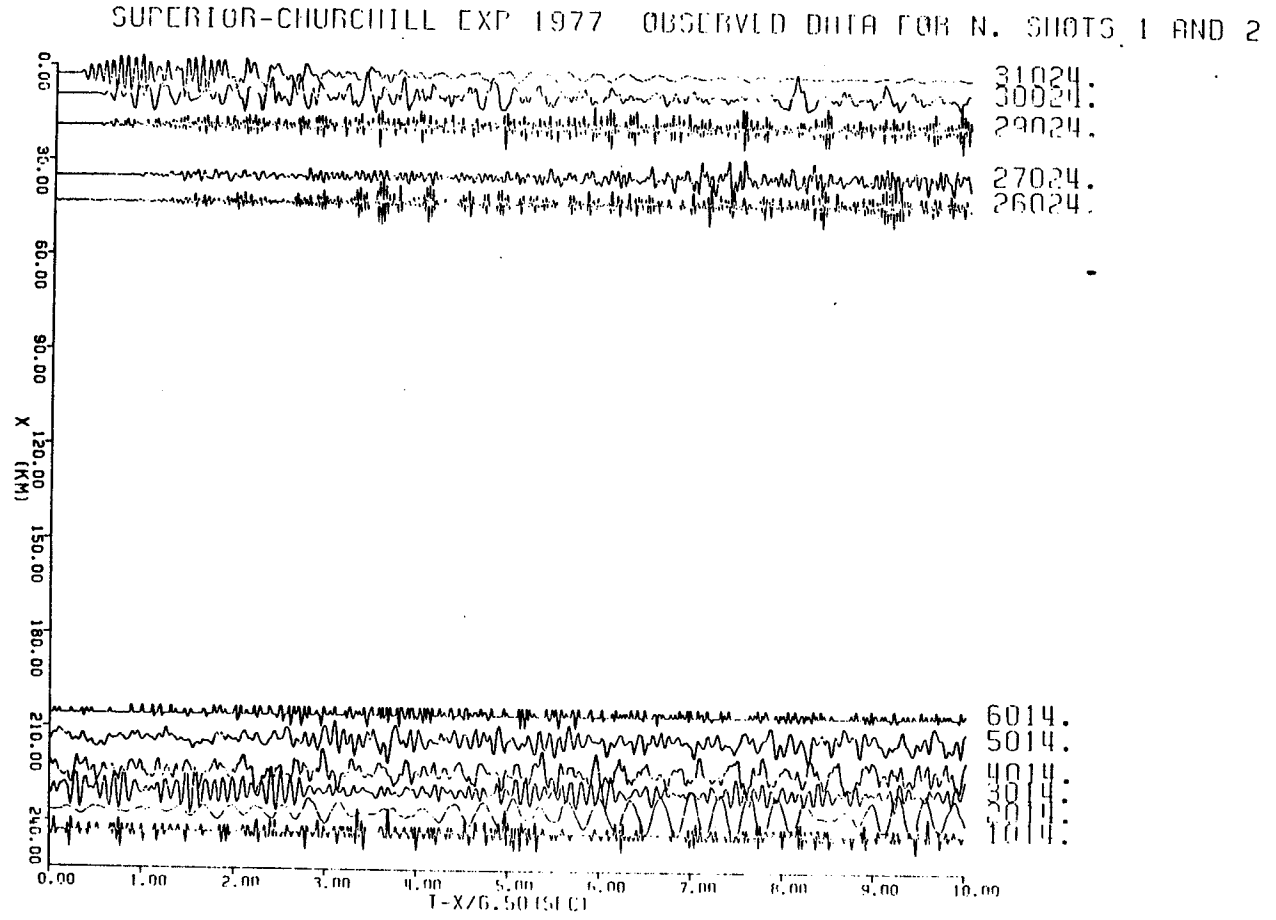

Figure 3.4 (a) - Record section for the north shot (N/S horizontal) .

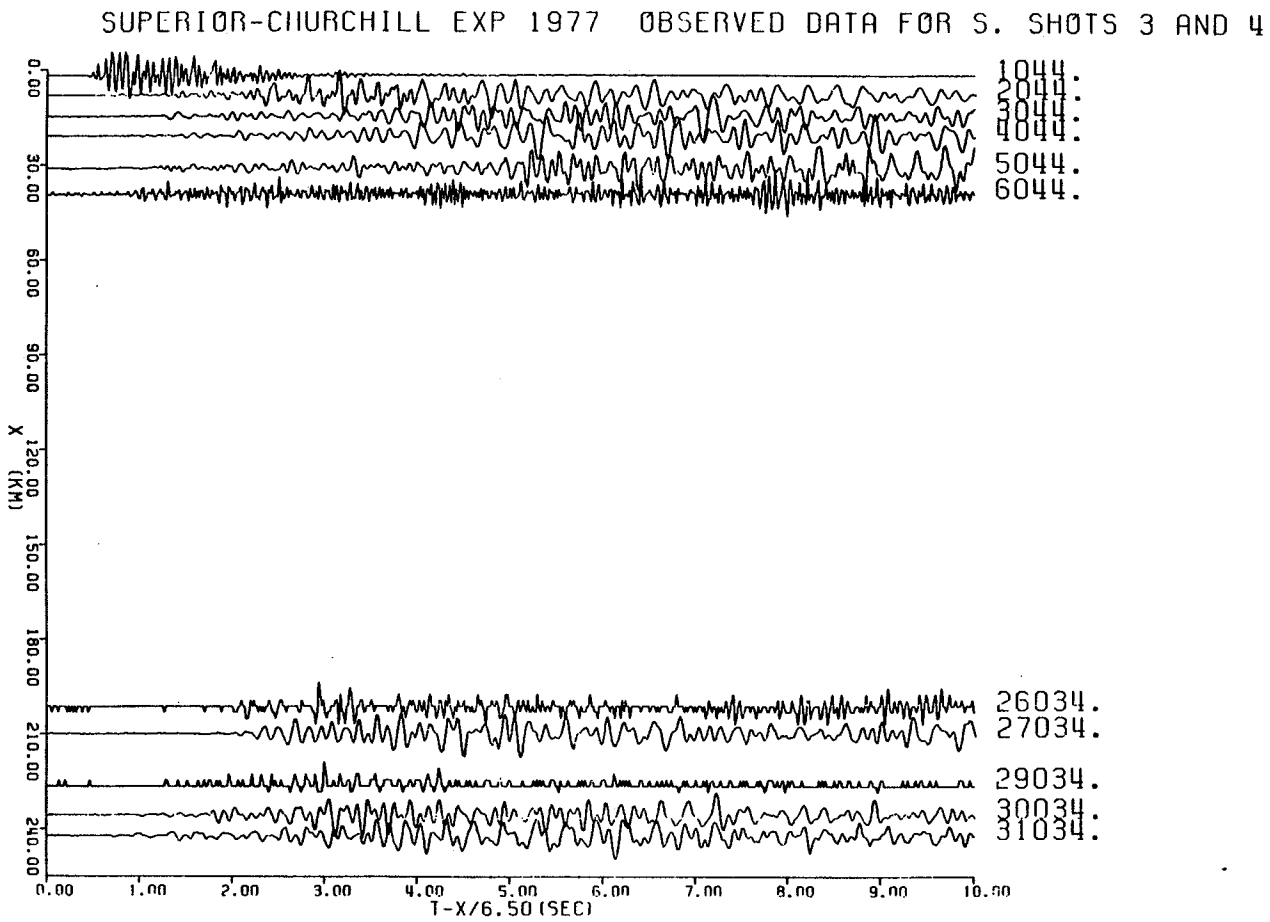

Figure 3.4 (b) - Record section for the south shot (N/S horizontal).

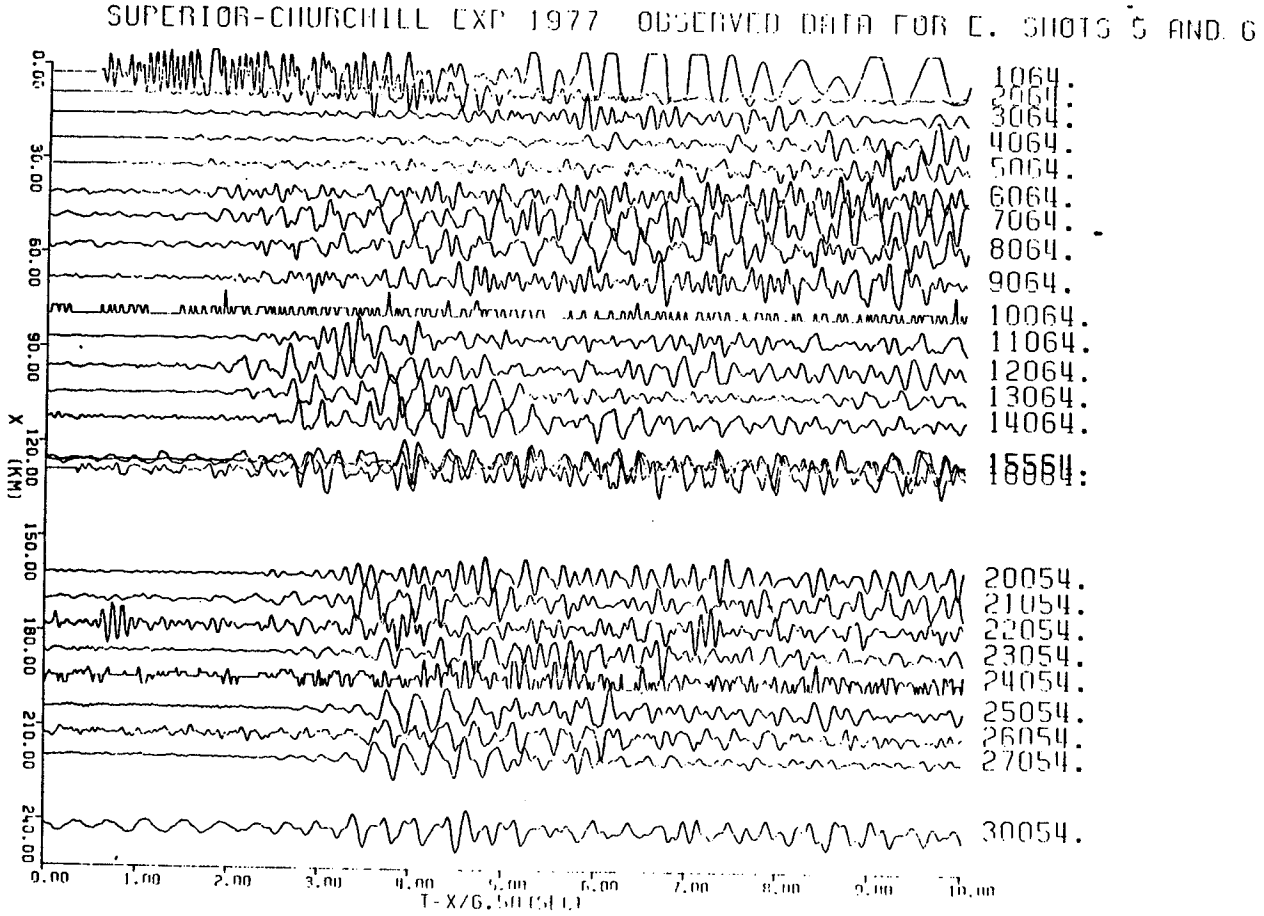

Figure 3.4 (c) - Record section for the east shot (N/S horizontal).

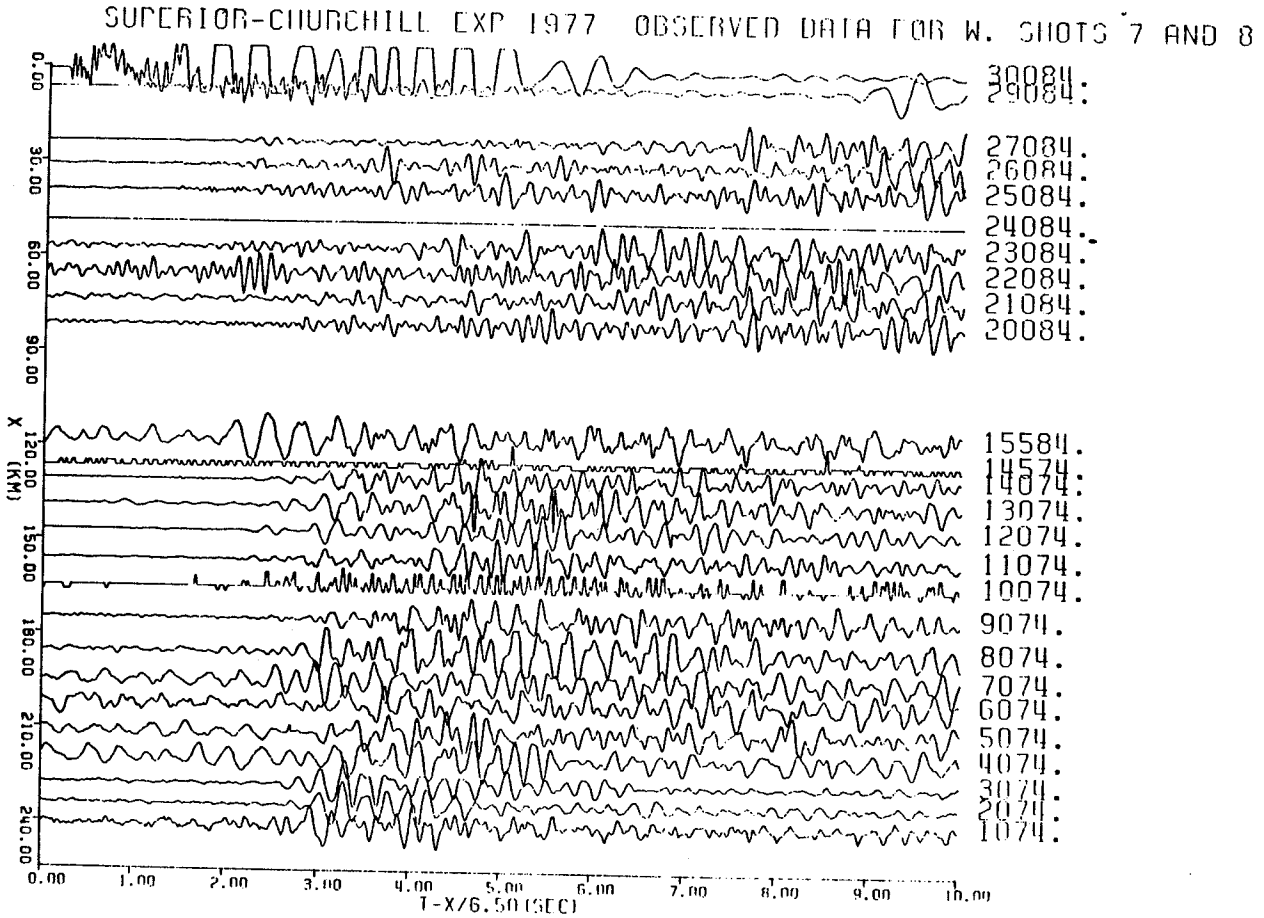

Figure 3.4 (d) - Record section for the west shot (N/S horizontal).

noise ratio. In addition particle motion displays are also obtained to aid in identification of late arrivals. The following sections provide a discussion of the theory of these filtering methods and the results of obtained from their use.

3.1 THE BUTTERWORTH BANDPASS FILTER

The ideal bandpass filter is one with a response of unity in the desired bandpass region and zero everywhere else. The impulse response of such a filter contains an infinite number of coefficients and in practice it is necessary to truncate it to a certain number of terms. This truncation produces oscillation and overshooting known as the Gibbs effect and leads to serious defects and errors when filtering. Several methods have been devised to eliminate this unwanted effect. The method proposed by Butterworth (1930) has achieved great popularity because of the closeness of the filter to the ideal case.

The ideal square response of a lowpass filter was approximated by Butterworth to be of the form:

$$|Y_L(\bar{\Omega})|^2 = \frac{1}{1+\bar{\Omega}^{2n}}$$

where $\bar{\Omega}$ = normalised frequency

By using the appropriate frequency transformations the bandpass filter response can be derived from the lowpass response.

The Laplace transform of the transfer function for an unnormalised Butterworth filter of degree 4 is given by

$$Y_{BP}(S) = \left(\frac{S}{S^2+b_1S+c_1}\right)\left(\frac{S}{S^2+b_2S+c_2}\right)\left(\frac{S}{S^2+b_3S+c_3}\right)\left(\frac{S}{S^2+b_4S+c_4}\right)$$

where s = the Laplace transform variable for normalised frequency

b_i, c_i = coefficients obtained from the pole position of the corresponding lowpass Butterworth filter of degree 4

Using a bilinear z transform developed by Golden and Kaiser (1964) for converting the continuous transfer function to one to be used for sampled data, the expression for the z transform of the Butterworth bandpass filter is

$$W(z) = \frac{(1-z^2)}{B_1(z)\,B_2(z)\,B_3(z)\,B_4(z)}$$

where B_i is a function of b_i, c_i and the sampling interval.

From trying several different bandwidths on the data, it was seen that most of the energy is concentrated between 1 and 9 hertz. In order to obtain as little distortion of the signal as possible a 1 to 9 hertz bandpass filter was used wherever it was feasable.

The data from the north shots 1 and 2 together with that from shots 7 and 8 were filtered using a 1 to 9 hertz bandpass filter. The recognition of firstbreaks was considerably improved in the case of traces from the northern shots. Even for the suite of seismograms for the western shot where the low signal to noise ratio made distinguishing firstbreaks off the raw data difficult, application of the filter was an improvement.

For south shots 3 and 4, a 4 to 10 hertz bandpass filter was used with only a marginal improvement in the records. Filtering of the seismograms from the east shots 5 and 6 with the same filter yielded similar results. The data obtained from both these pairs of shots were of generally poor quality and suggest some peculiarity in subsurface character in the region of the shot points. The filtered data for each of the shot pairs is given in Figures 3.5 (a) to (d).

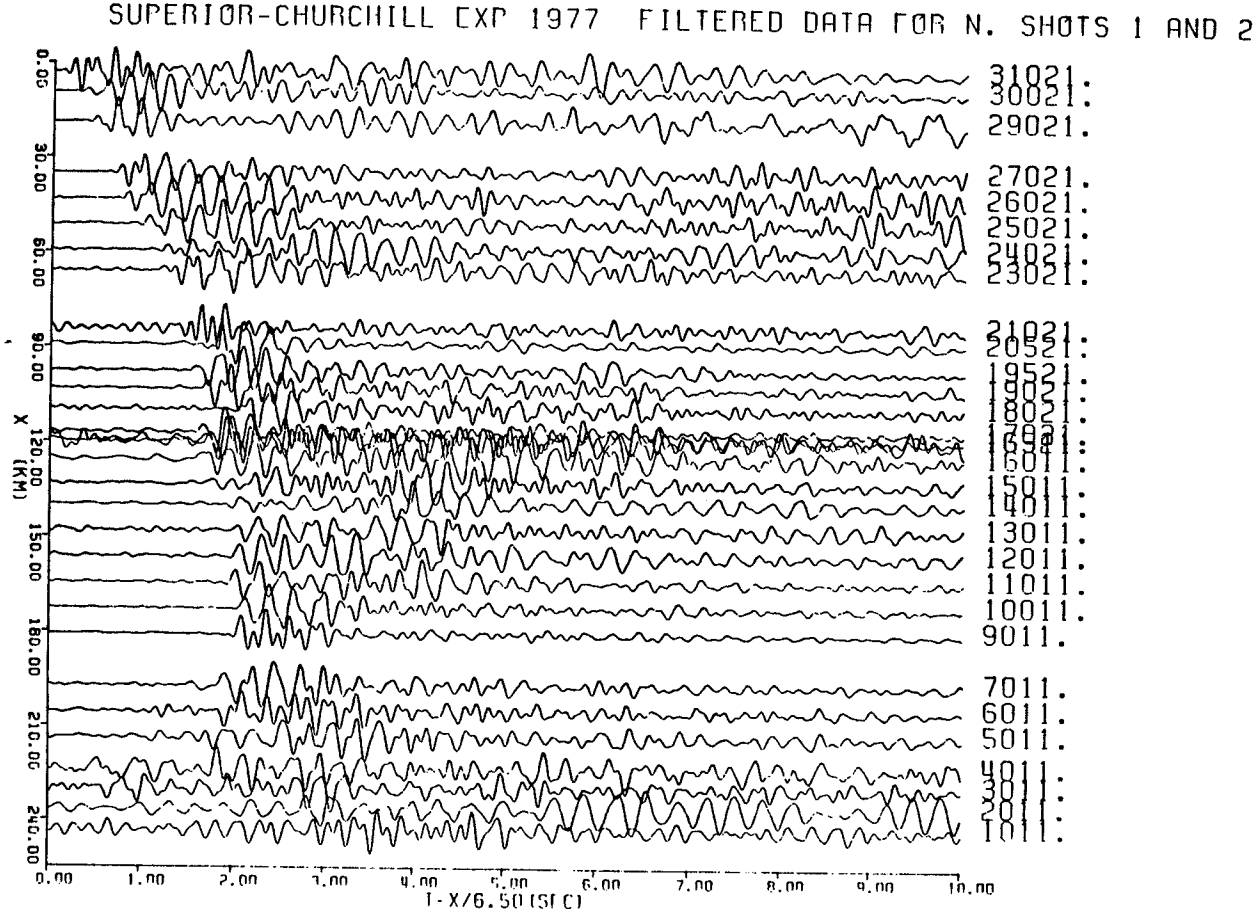

Figure 3.5 (a) - Bandpass filtered section for the north shot.

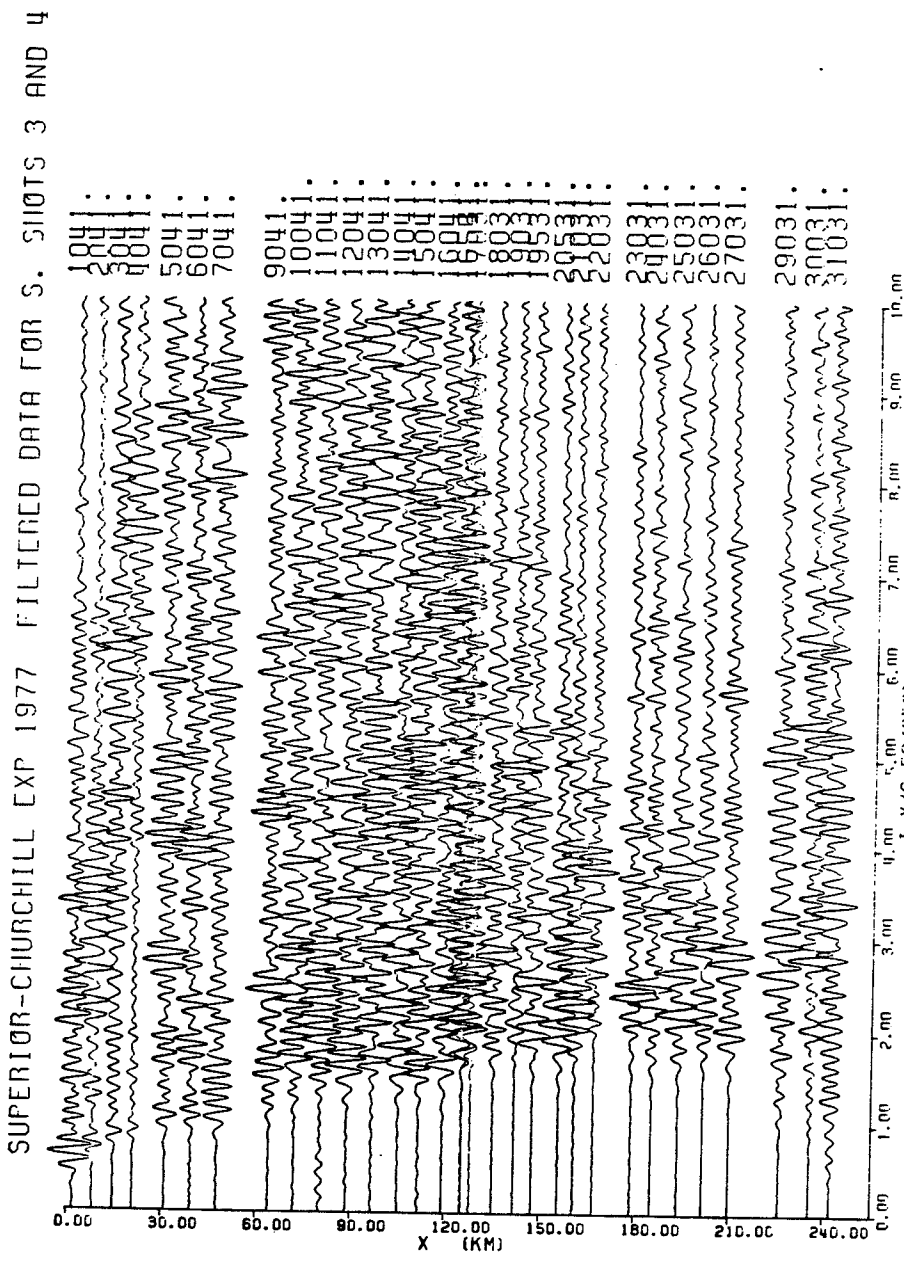

Figure 3.5 (b) - Bandpass filtered section for the south shot.

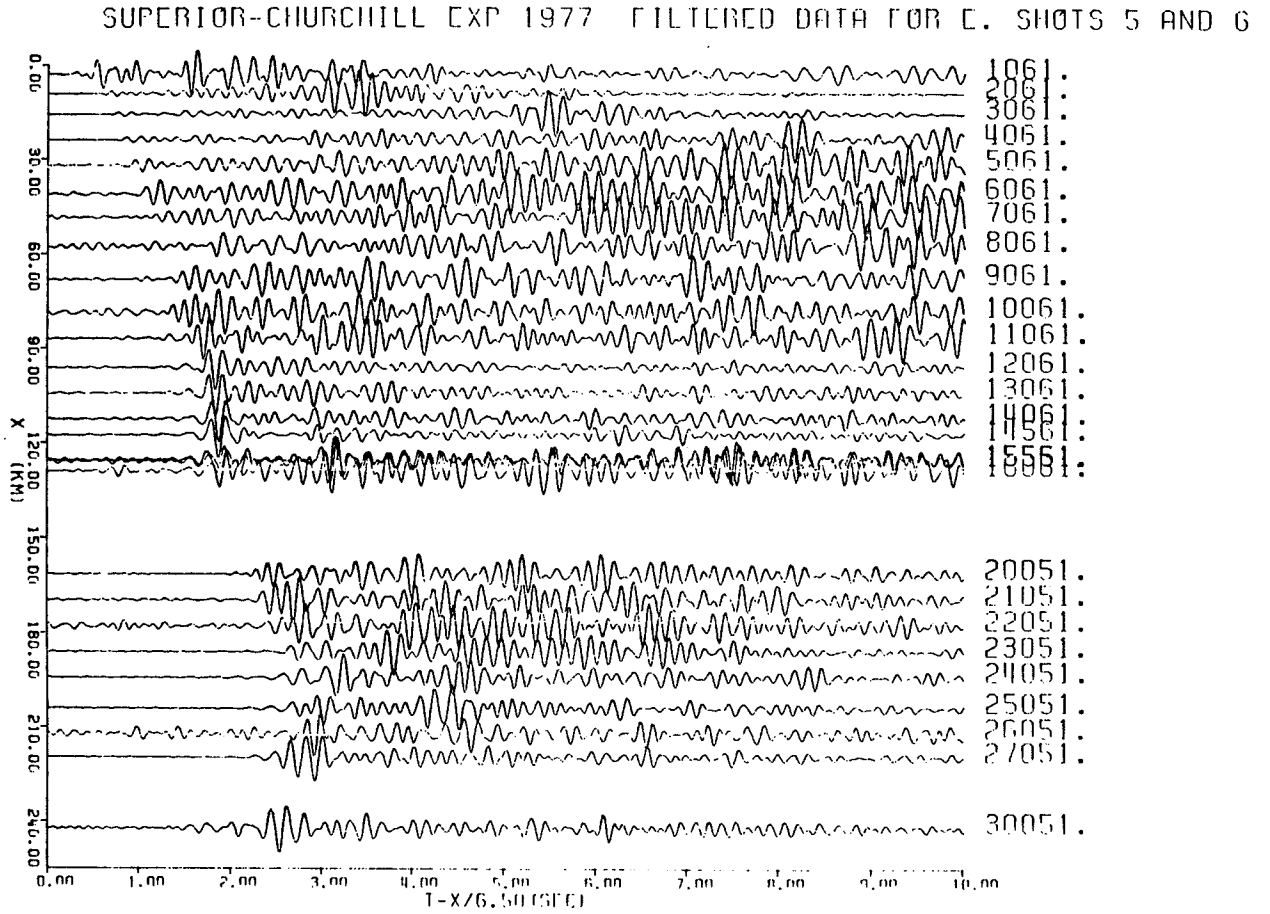

Figure 3.5 (c) - Bandpass filtered section for the east shot.

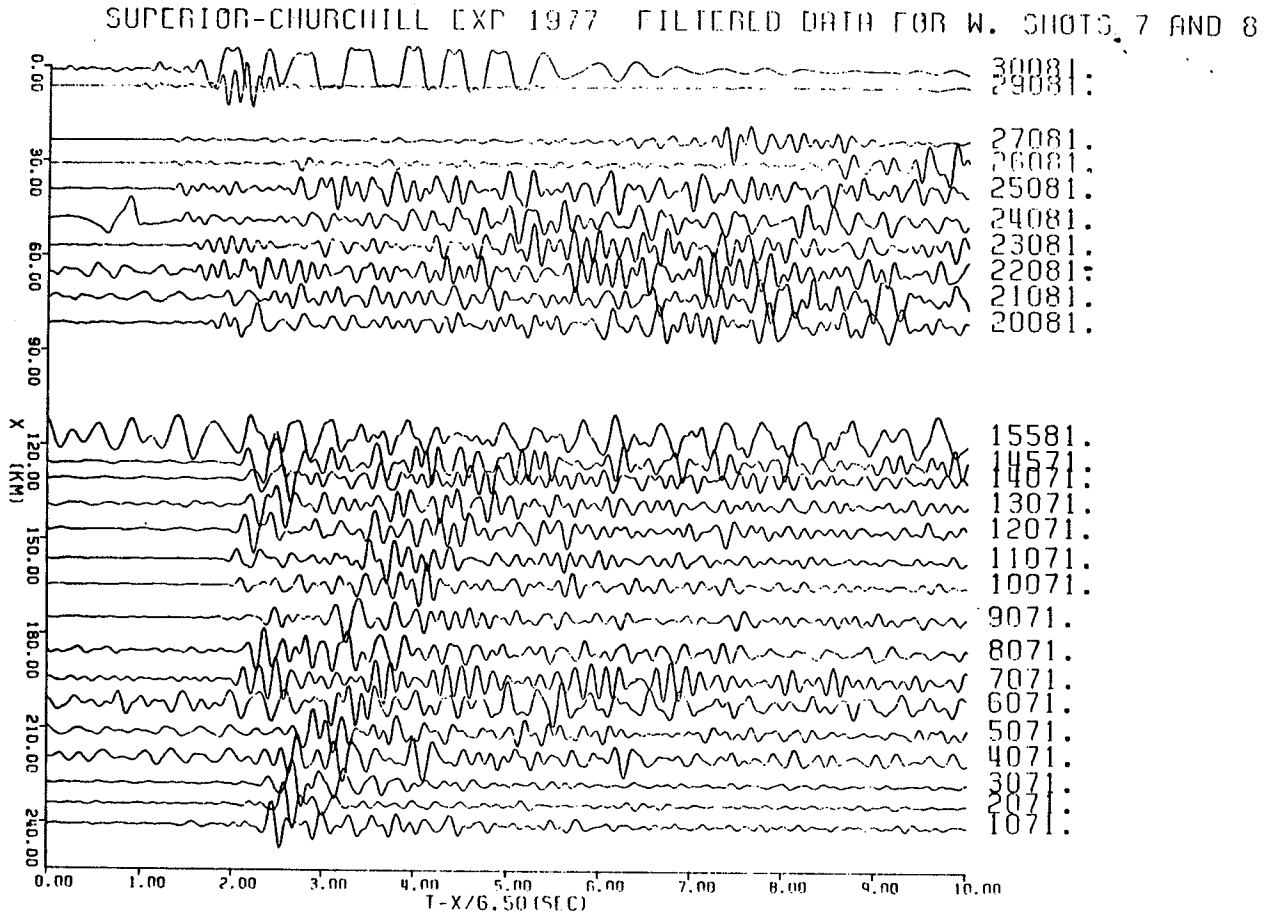

Figure 3.5 (d) - Bandpass filtered section for the west shot.

3.2 POLARISATION FILTERING

The non-linear polarisation filter is applied to data to isolate compressional phase pulses. To do this the vertical and horizontal components of the signal detected from the corresponding receiver types along the profile are cross-correlated. The cross-correlation coefficients being given by :

$$C_{t,w}(\tau) = \int_{t-w/2}^{t+w/2} Z(t)\, R(t+\tau)\, dt$$

where Z = vertical component of ground motion

R = horizontal component of ground motion

t = time at the centre of the record segment of length w

τ = lag

The SV motion is eliminated by ensuring that when Z.R is negative for $\tau = 0$, the cross-correlation $C_{t,w}(\tau)$ is zero. The cross-correlation coefficients are then convolved with Z and R, the output would then contain predominantly compressional motion.

Further enhancement of the largest of the compressional motions is done by convolving with the zero lag autocorrelation function.

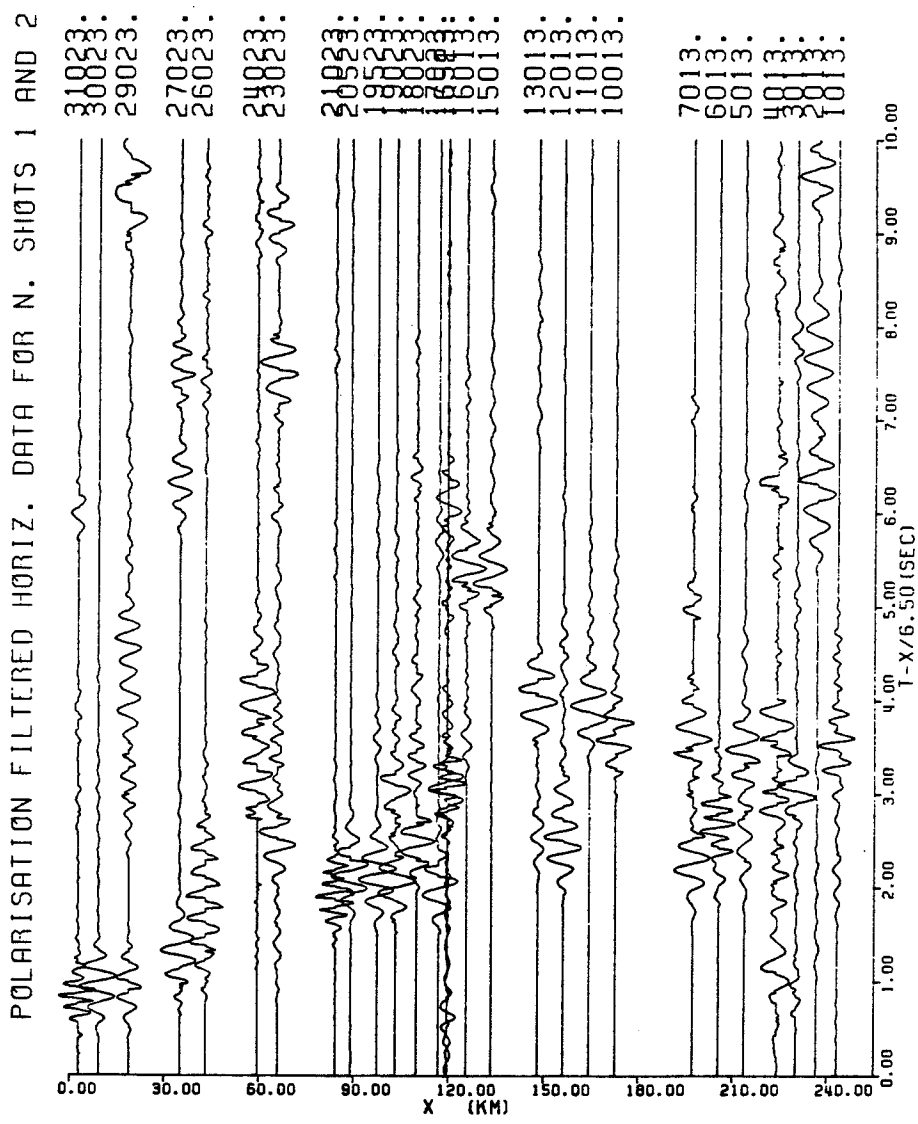

Figure 3.6 (a) - Polarisation filtering for the north shot (length = 41).

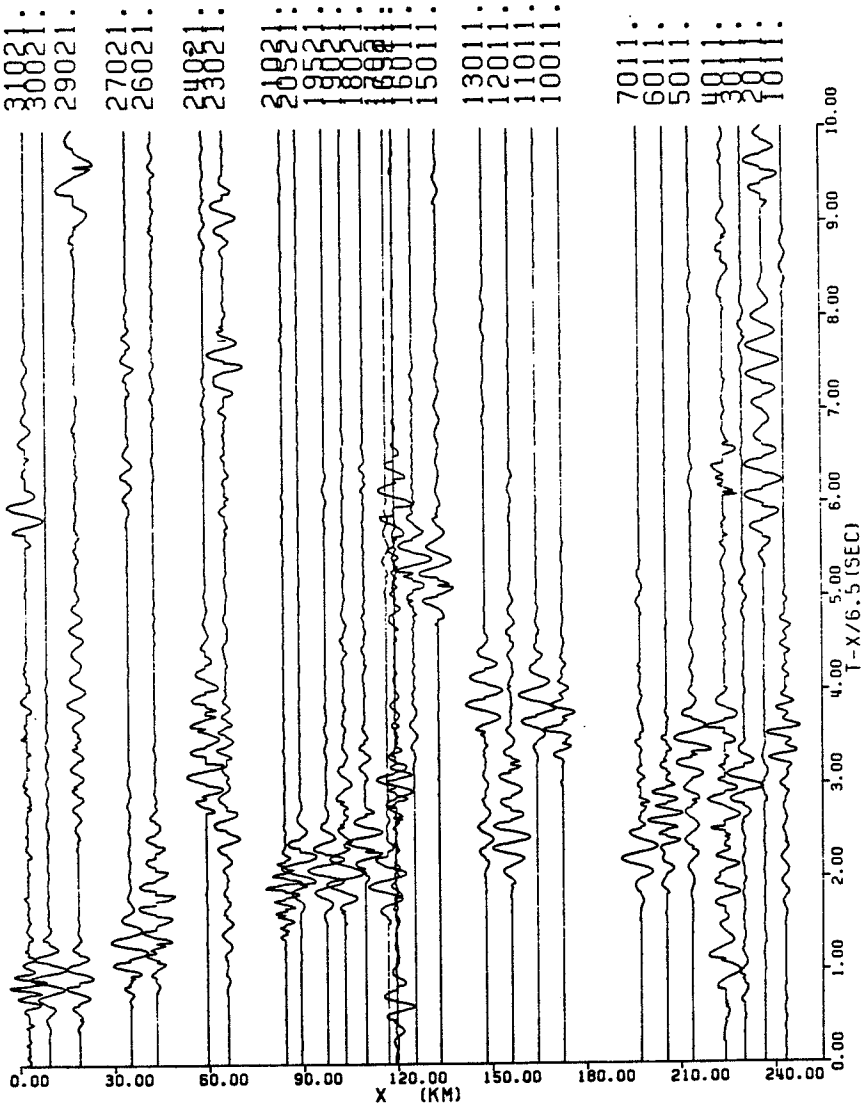

Figure 3.6 (b) - Polarisation filtering for the north shot (length = 41).

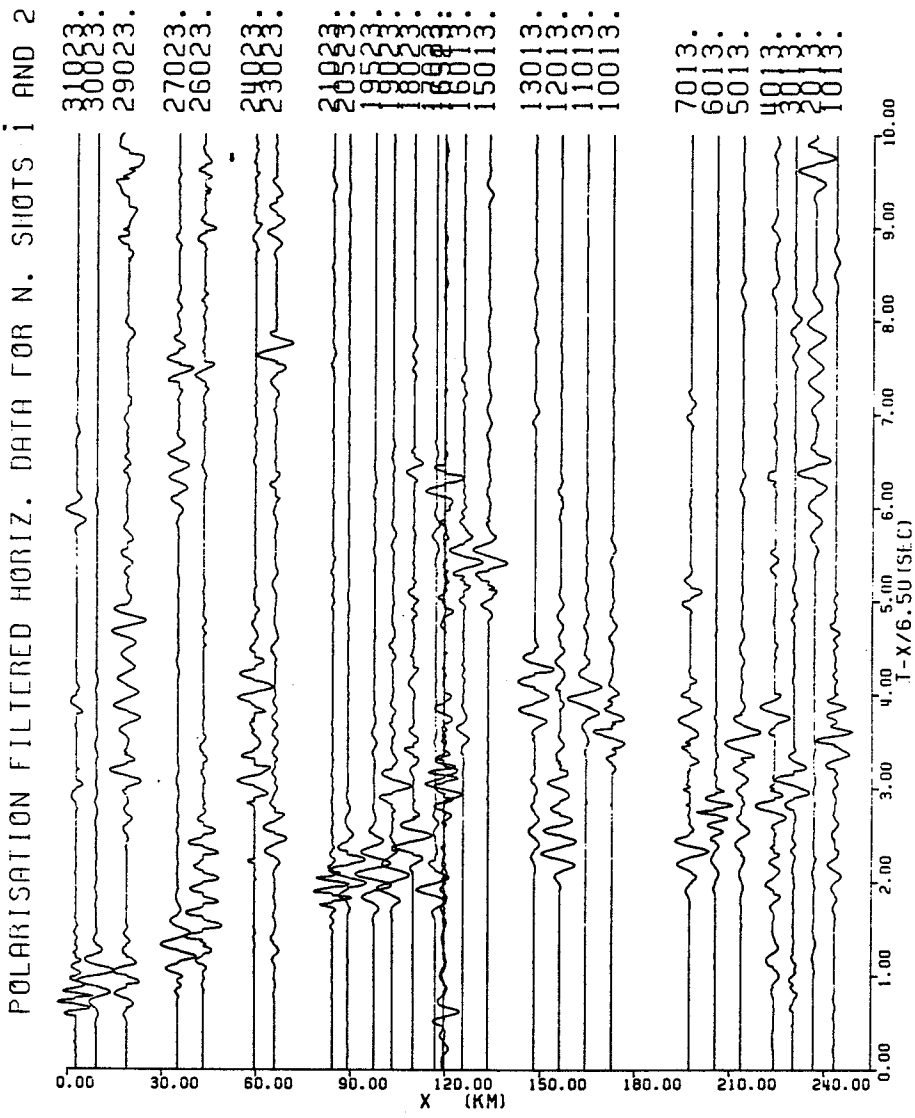

Figure 3.7(a) - Polarisation filtering for the north shot (length = 11).

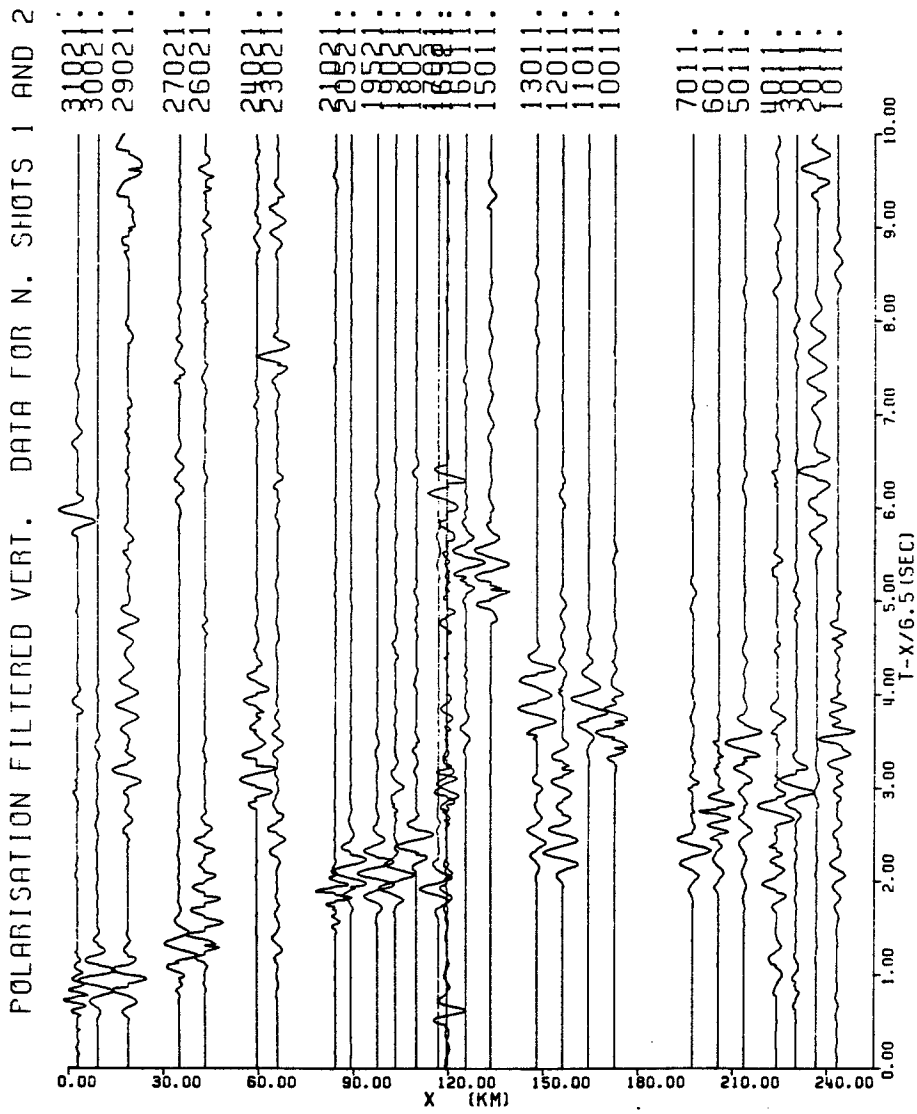

Figure 3.7(b) - Polarisation filtering for the north shot (length = 11).

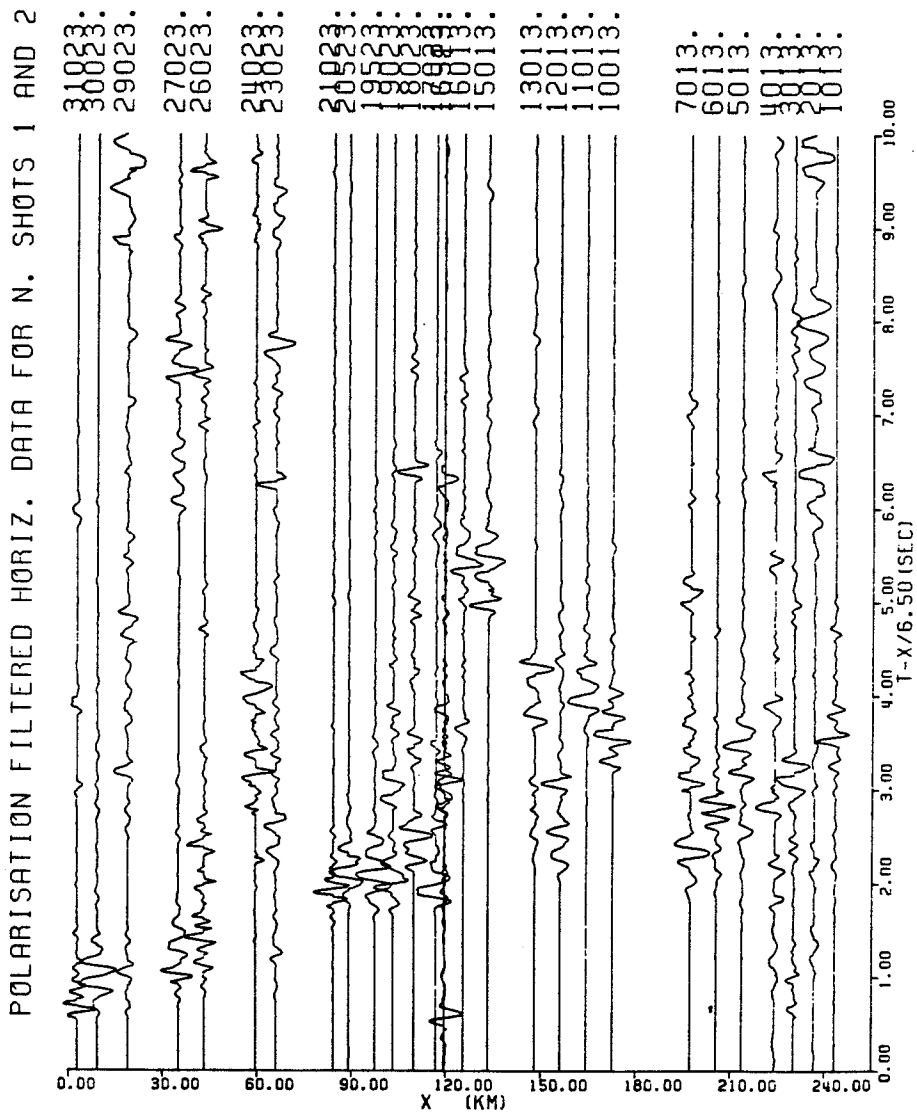

Figure 3.8(a) - Polarisation filtering for the north shot (length = 21).

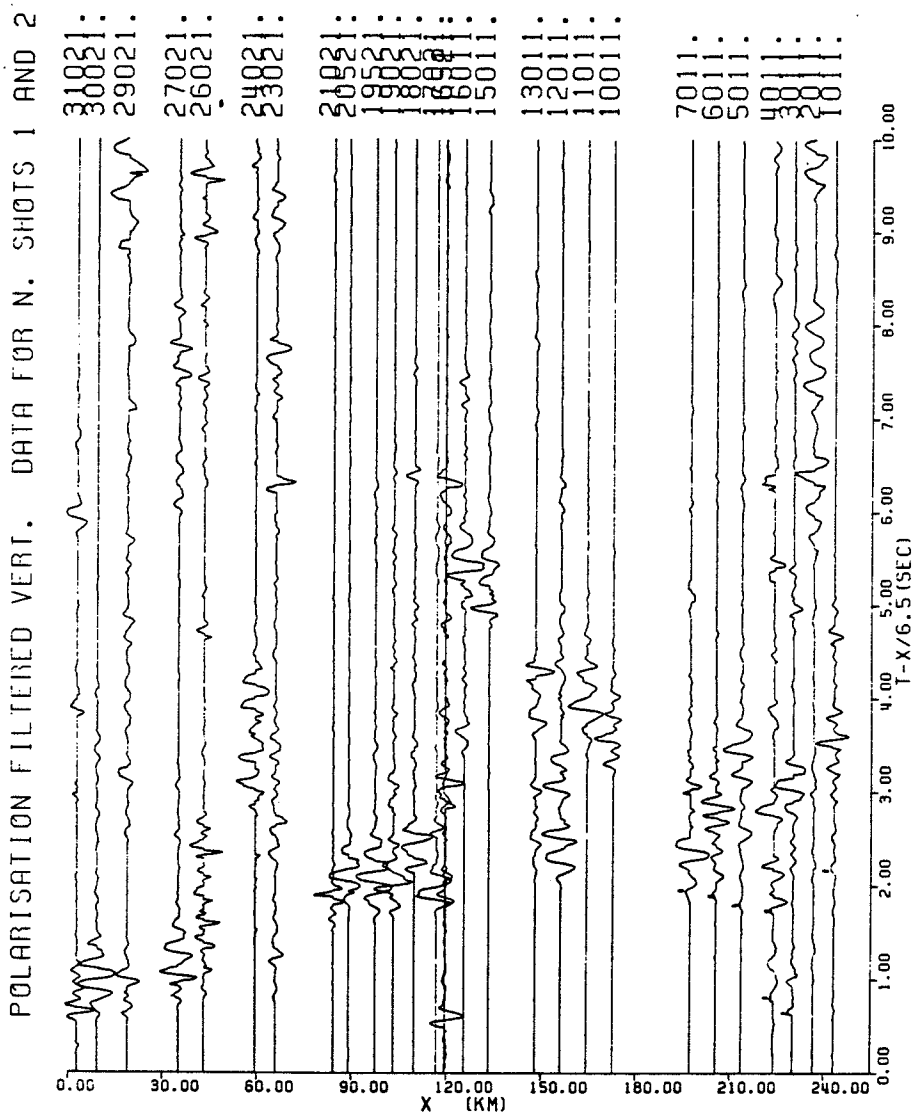

Figure 3.8(b) - Polarisation filtering for the north shot (length = 21).

The output is then normalised to maximum amplitude for plotting.

The polarisation filtered data for shots 1 and 2 using time windows of w = 41, 11 and 21, are shown in Figures 3.6 to 3.8. The use of a value w = 21 , gives much more clearly defined firstbreaks and it is this value that will be used throughout the the remainder of the analysis. Note that prior to polarisation filtering, the data was bandpass filtered with Butterworth filters of respective bandwidths to separate out the signal.

Figures 3.8 to 3.11 show the polarisation filtered data for each of the profile lines. On some of the traces the compressional phases are accompanied by small amplitude, short period noise. This is residual noise not removed by bandpass filtering. In general, the polarisation filtered data proved useful in delineating secondary arrivals, as these were far more visible here than for the bandpass filtered traces. In a few cases however the application of the polarisation filter cancelled out the signal. This is especially apparent in the case of traces 2061 to 5061 for the east shot and traces 27081 to 25081 for the west shot. This comes as no surprise for the signal to noise ratio for the east/west lines was low to begin with. For these traces the first arrivals and secondary events were chosen on the basis of the bandpass filtered data alone.

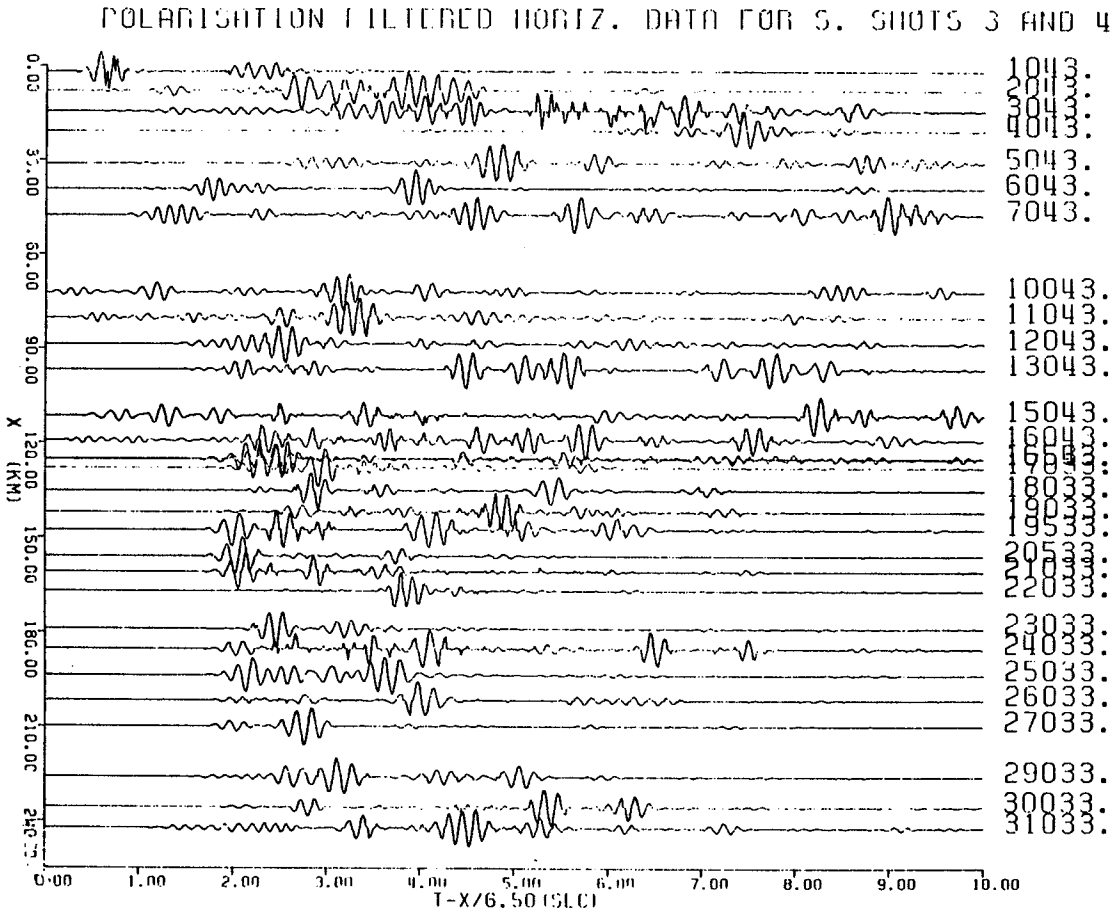

Figure 3.9(a) - Polarisation filtering for the south shot (length = 21).

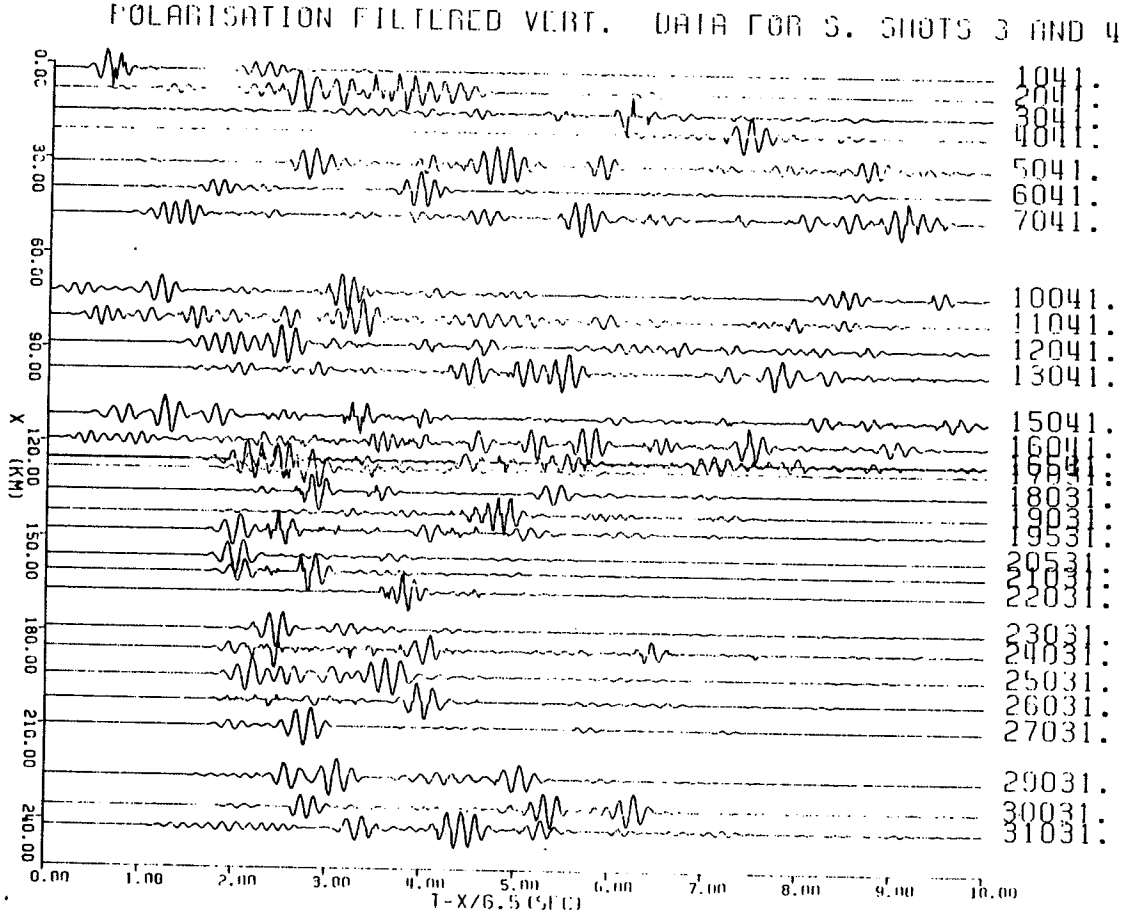

Figure 3.9(b) - Polarisation filtering for the south shot (length =21).

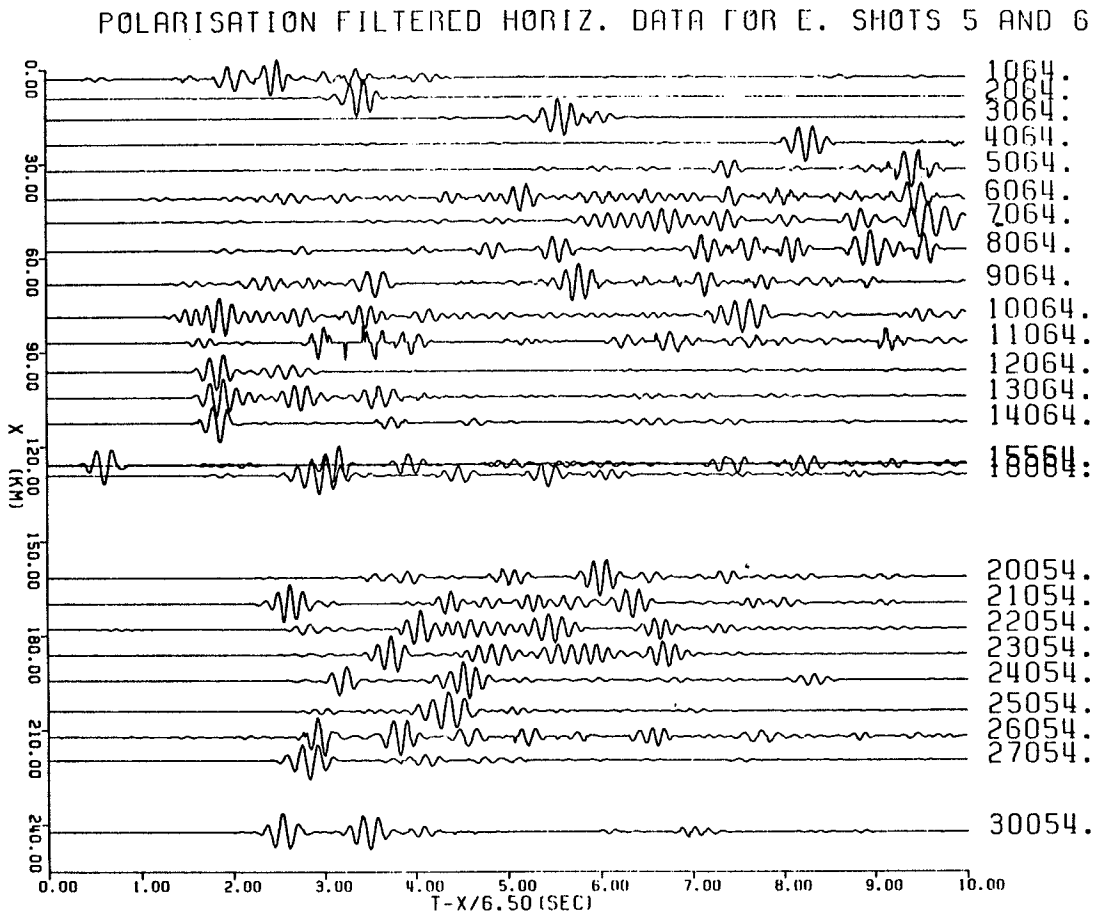

Figure 3.10(a) - Polarisation filtering for the east shot (length = 21).

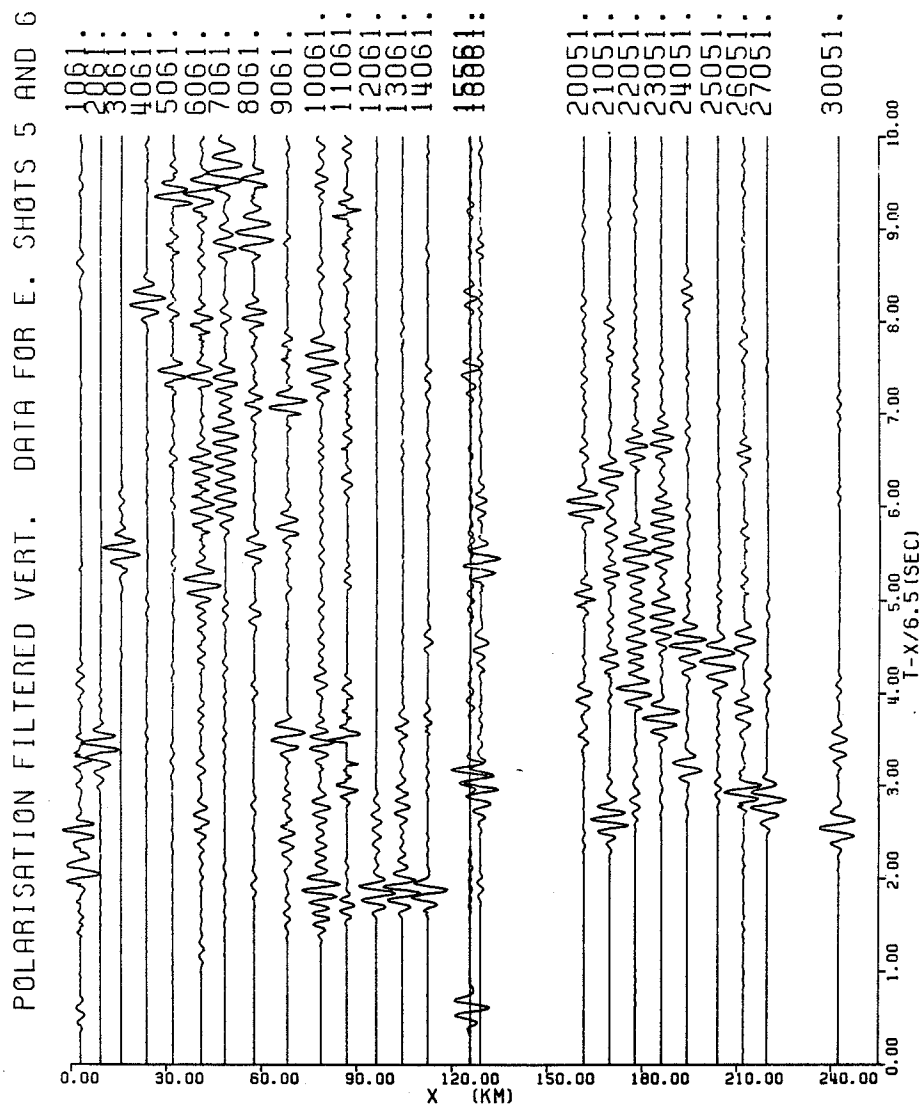

Figure 3.10(b) - Polarisation filtering for the east shot (length = 21).

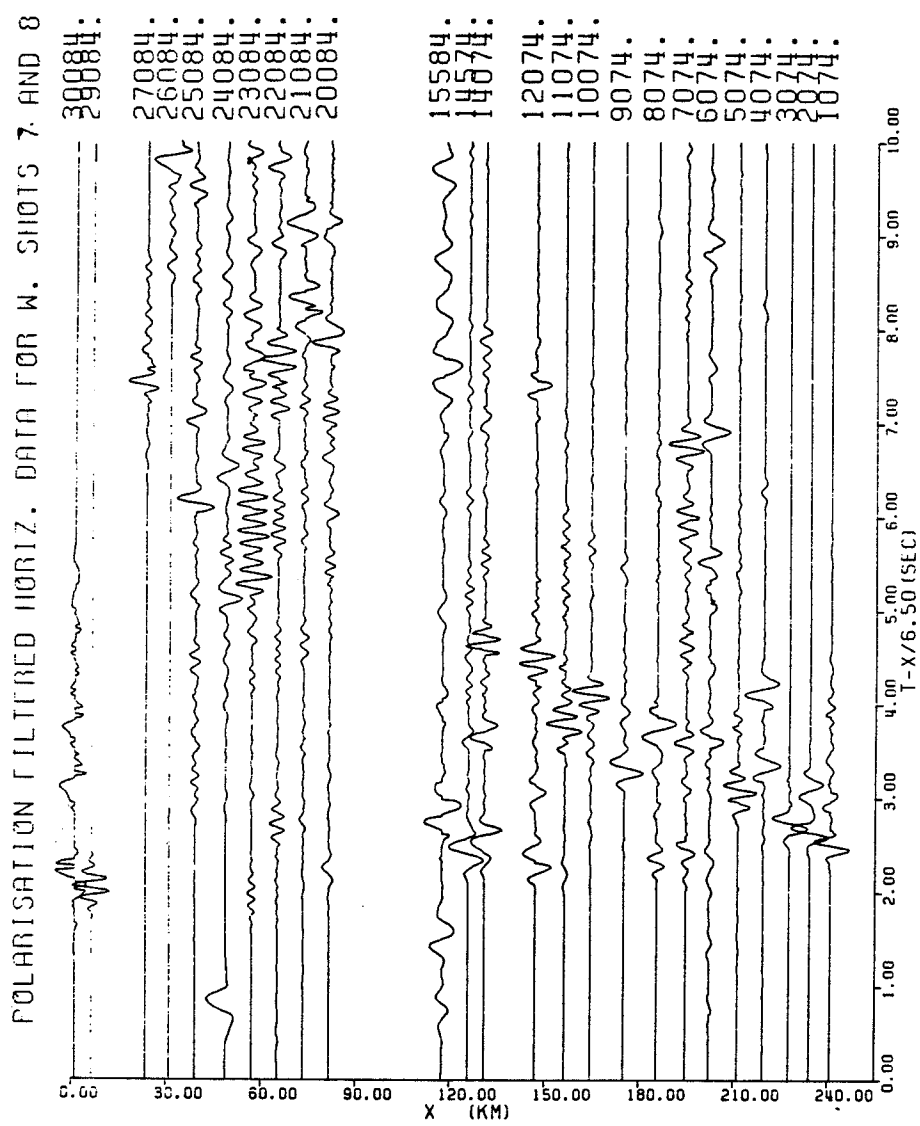

Figure 3.11(a) - Polarisation filtering for the west shot (length = 21).

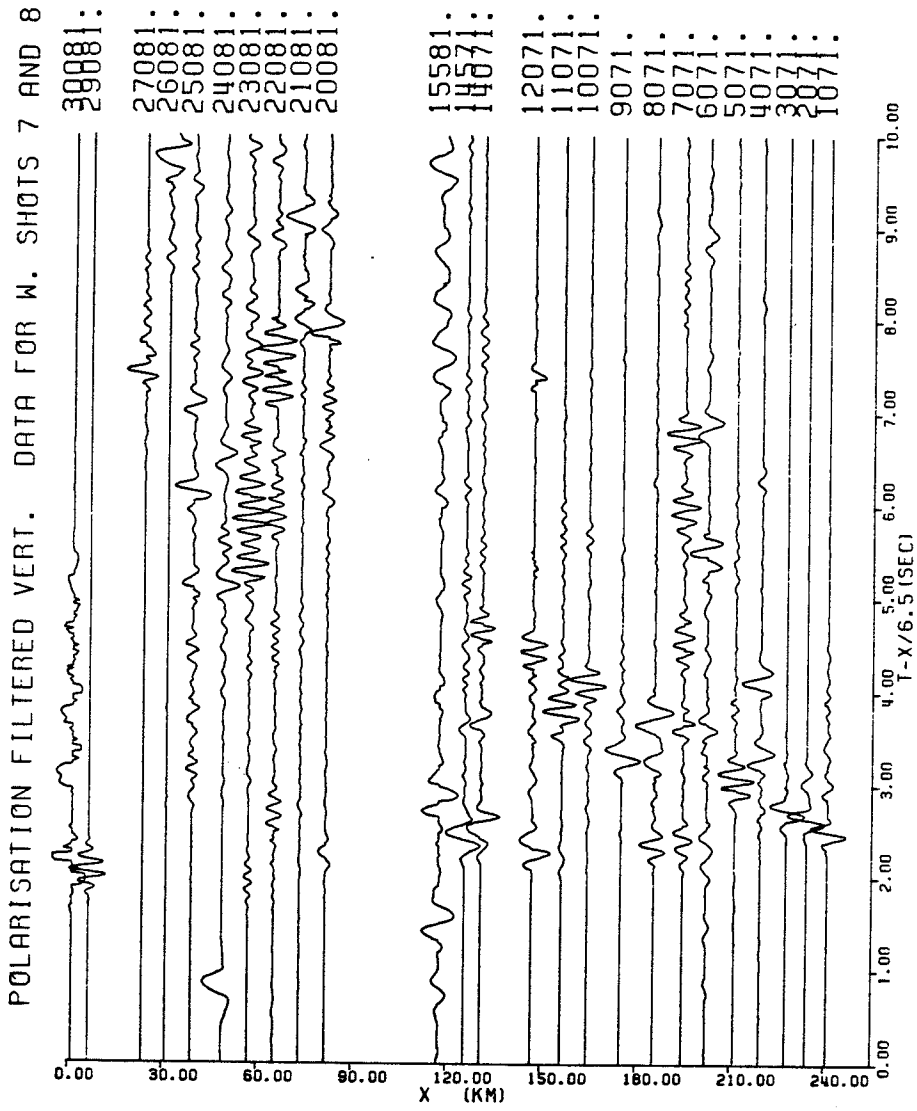

Figure 3.11(b) - Polarisation filtering for the west shot (length = 21).

3.3 PARTICLE MOTION DISPLAYS

Particle motion displays are plots of horizontal versus vertical ground motion as a function of time. The sections are divided into 0.5 second intervals for ten seconds of data. The beginning of each plot, where discernable, is signified by a number 1 and the end by the number 2. If there is only slight ground motion then the beginning of the plot and the end are almost coincedent. A large amount of vertical ground motion shows up on the plots as large amplitude rectilinear wanderings; with large amounts of horizontal motion the plots take on a more elliptical shape.

The particle motion displays for each of the profiles is given in Figures 3.12 (a) to (d). The presence of large amplitude signal at the tail end of the traces and the fact the the amplitudes were all normalised before plotting in some instances causes the first arrival to appear insignificant as compared to the rest of the section. The complexity of the signal and the variable nature of the subsurface through which it propogates makes correlation of particle motion plots from trace to trace unlikely. So in general the particle motion traces provided no additional help in the determination of first arrivals and secondary events.

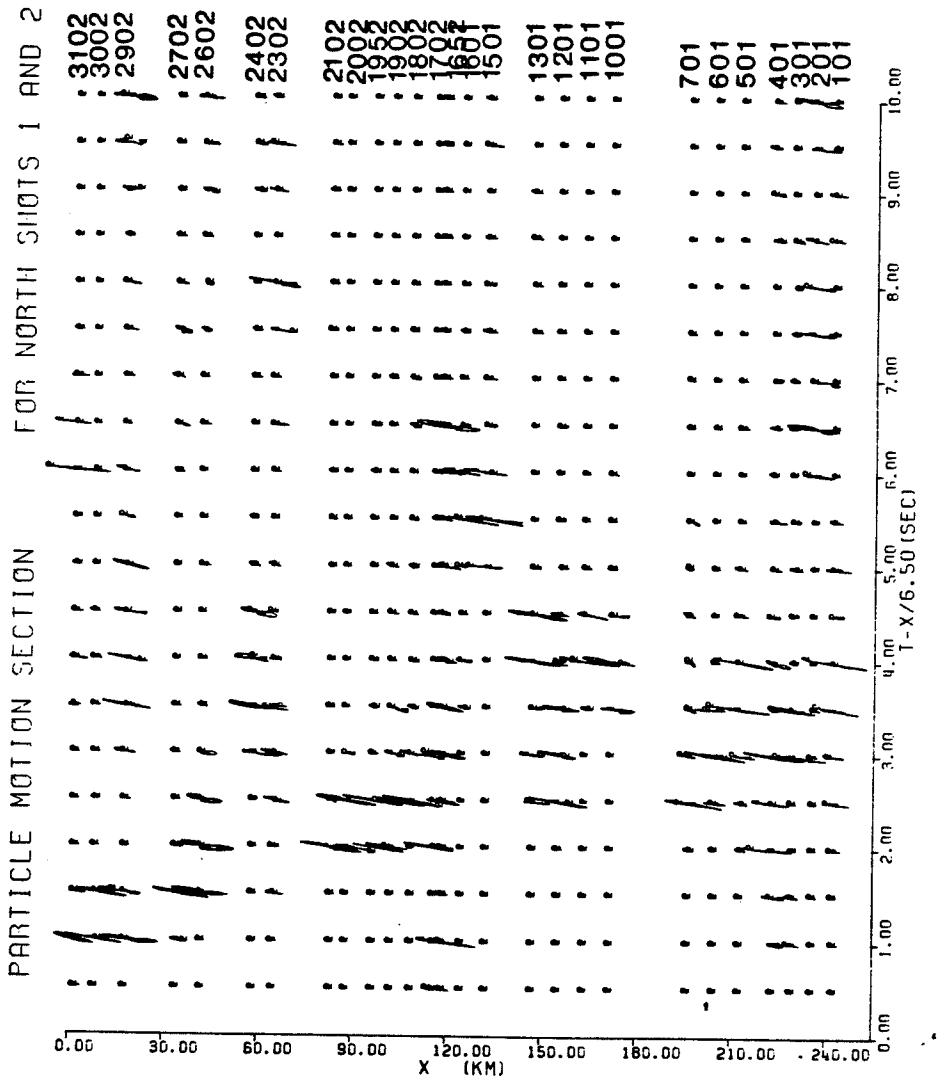

Figure 3.12(a) - Particle motion displays for the north shot.

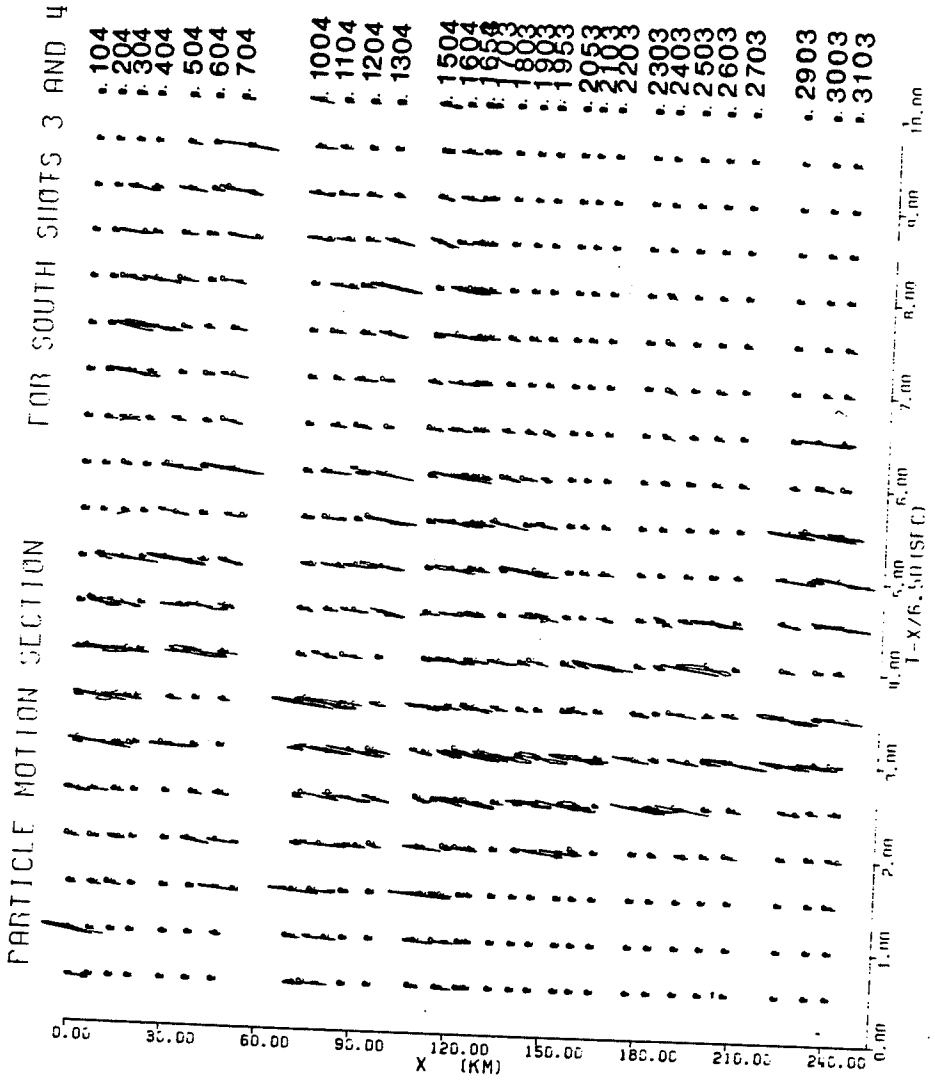

Figure 3.12(b) Particle motion displays for the south shot.

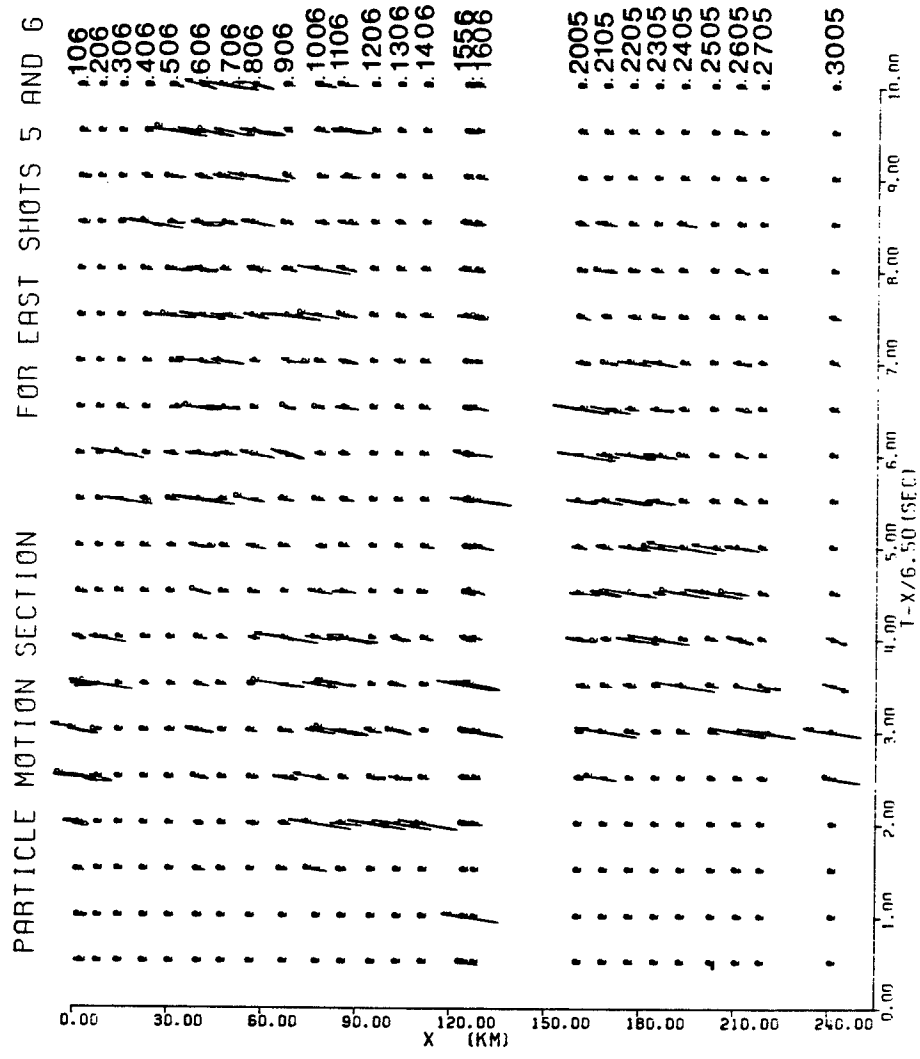

Figure 3.12(c) - Particle motion displays for the east shot.

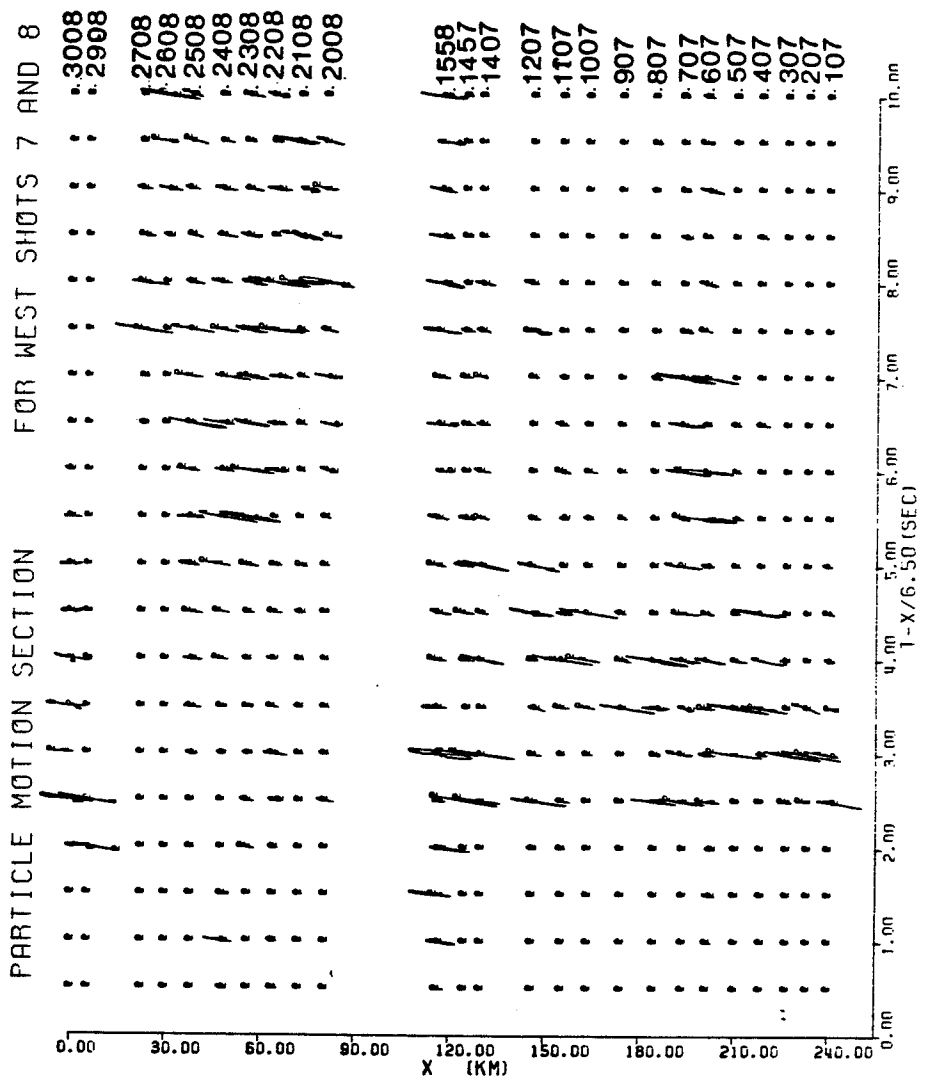

Figure 3.12(d) - Particle motion displays for the west shot.

In summary, application of bandpass filters on the data greatly improved the general appearance of seismograms and made for easy recognition of firstbreaks. Polarisation filtering simplified the complex P - wave signal and so allowed secondary arrivals which were not as easily recognised on the raw or bandpass filtered traces, to be distinguished. No new information could be gained from the particle motion displays, they did however serve to reinforce the findings of the previous filtering methods.

Chapter IV

PRELIMINARY INTERPRETATION

Prior to this study a preliminary interpretation and analysis of the data was done by Green et al. (1980). This analysis was based on first arrival picks from raw and 4 - 10 hertz filtered data using uniform velocity layers. The results of this preliminary velocity - depth determination will be dealt with in this chapter.

The travel time curves however, are of fundamental importance since all subsequent analysis is based on information obtained from them. With this in mind, and the fact that processing of the data has allowed for better recognition of events, a second interpretation making use of the same n - layer classical method from further processed data will be given. The similarities and differences between the models derived from this and the previous study will be discussed.

4.1 PRELIMINARY VELOCITY - DEPTH MODELS

Figures 4.1, 4.2 show picks of first arrival times for each of the shot pairs as done by Green et al. (1980). Least squares fitting of the travel times and distances was used to obtain apparent velocities and intercept times.

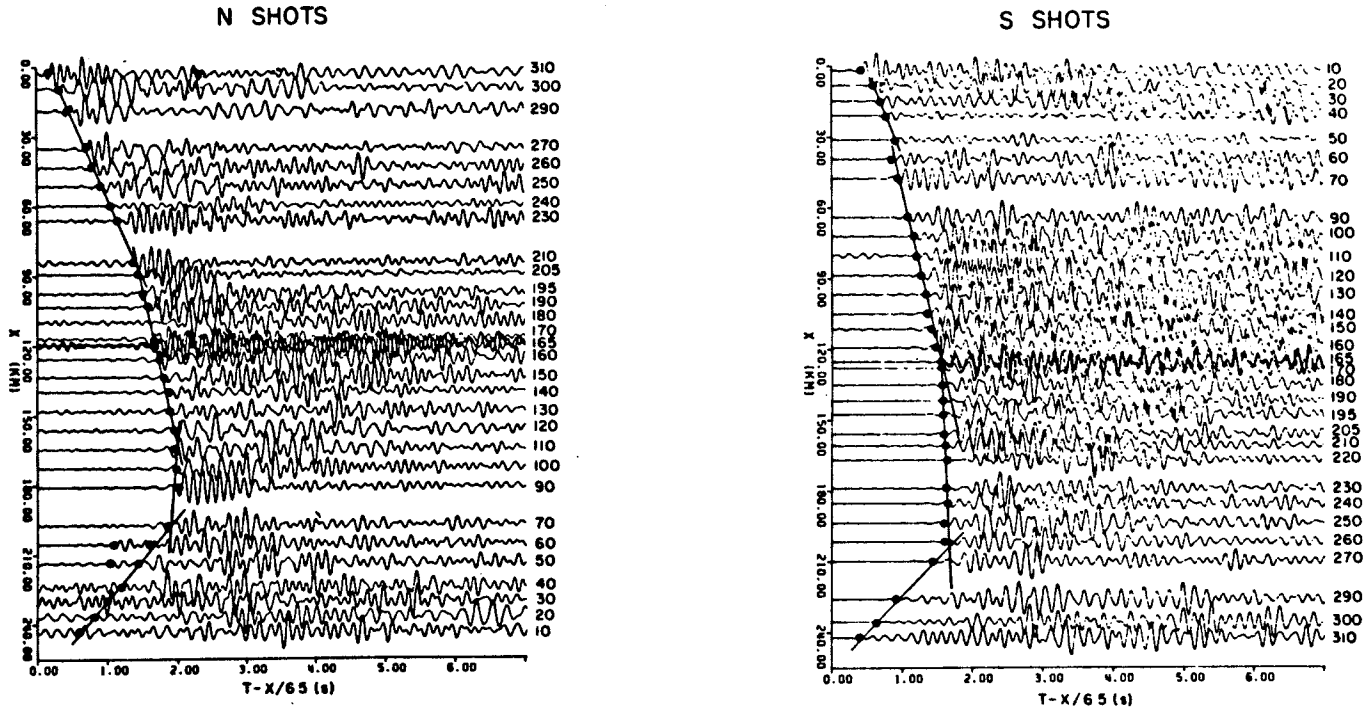

Figure 4.1 - First arrival picks for seismograms from the north/south line (Green et al., (1980))

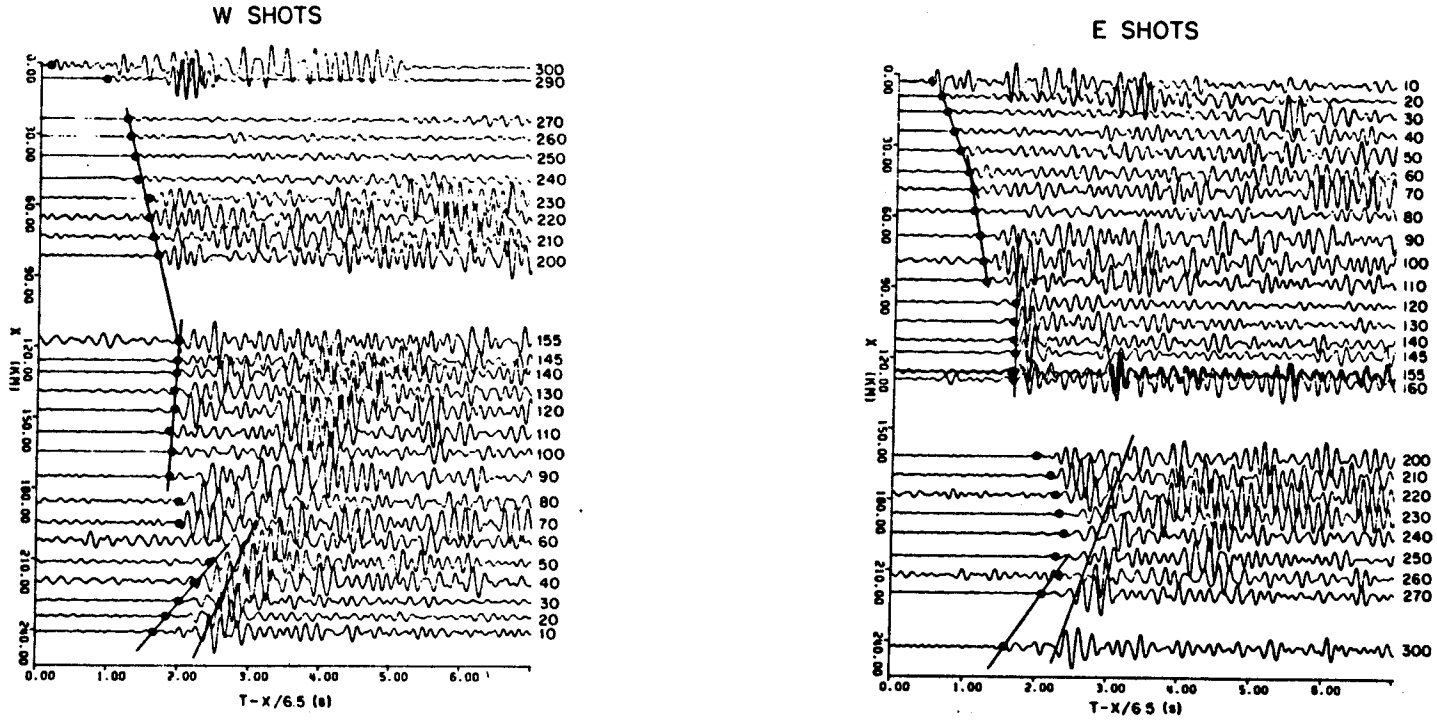

Figure 4.2 - First arrival picks for seismograms from the east/west line (Green et al., (1980)).

The first arrival data for the north - south profiles indicate a four layer crust. The first travel time branch yields an apparent velocity of 5.93 km/sec for the north and 5.98 km/sec for the south profile. The second and third branches of the profiles have velocities 6.20 and 6.65 km/sec and 6.21 - 6.45 km/sec for north and south respectively. The fourth travel time branch is less well developed and several first arrival picks are possible. An apparent velocity of 7.96 km/sec was determined by Green et al. (1980) for this event. Horizontal plane layered calculations based on these apparent velocities and least squares intercept times were carried out. Tables 4.1 (a) and (b) give the results of this calculation for north and south lines.

Reverse profile analysis on the north - south data was done after slight adjustment to the travel times. These alterations were required in order to satisfy the conditions for reverse profile analysis. Dipping layer analysis of the north-south line gave a five layered crustal section with two of the four interfaces dipping to the south. Figure 4.3 gives a diagramatic representation of the model.

The east - west profile lies directly across the Superior Province and boundary zone. Evidence from the magnetic and gravity studies on the boundary, indicate that a complex subsurface structure is to be expected in this region. The first arrival picks support these expectations.

Layer Number	Apparent Velocity (km/sec)	Depth to Interface (km)
1	3.55	0.41
2	5.93	6.95
3	6.20	19.22
4	6.65	39.14
5	7.96	

Table 4.1(a). Least squares apparent velocities and calculated depths to interfaces for model from north shot.

Layer Number	Apparent velocity (km/sec)	Depth to Interfaces (km)
1	3.55	1.13
2	5.98	2.12
3	6.21	10.68
4	6.45	38.45
5	8.11	

Table 4.1(b). Least squares apparent velocities and calculated depths to interfaces for model from south shot.

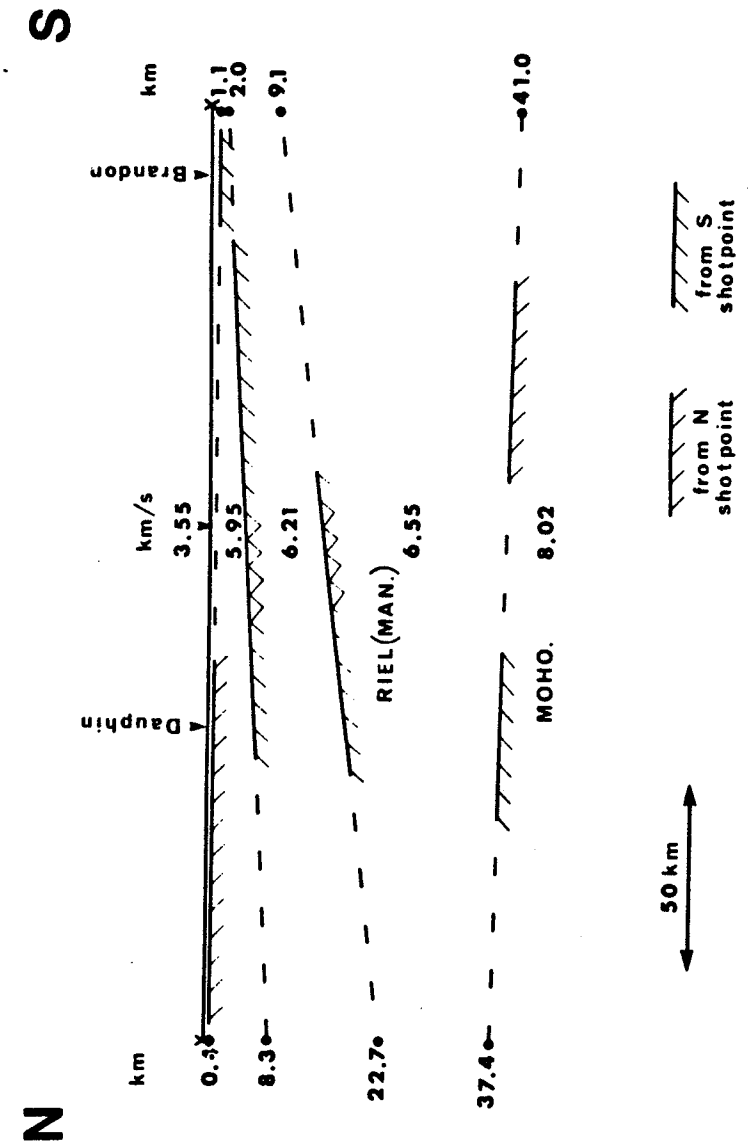

Figure 4.3 - Preliminary four layer model for the north/south line (Green et al., (1980)).

Layer Number	Apparent Velocity (km/sec)	Depth to Interfaces (km)
1	3.43	1.1
2A	6.04	2.9
2B	6.22	12.94
3	6.55	37.56
4	7.00	46.67
5	7.92	

Table 4.1(c). Least squares apparent velocities and calculated depths to interfaces for the east-shot model.

Layer Number	Apparent Velocity (km/sec)	Depth to Interfaces (km)
1	3.64	2.39
2	6.18	12.89
3	6.59	39.00
4	7.24	47.00
5	8.21	

Table 4.1(d). Least squares apparent velocities and calculated depths to interfaces for the west-shot model.

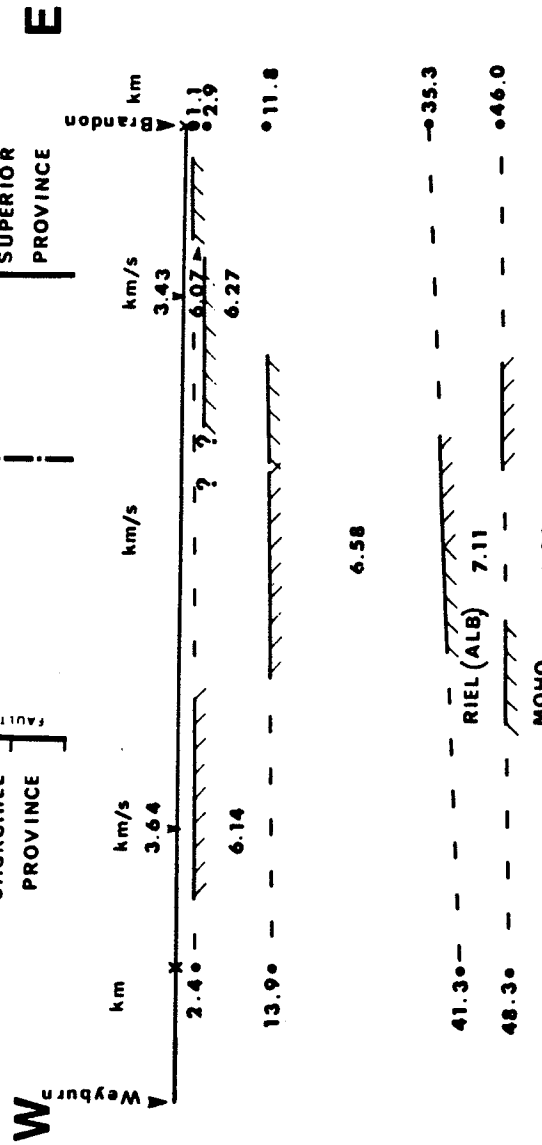

Figure 4.4 - Preliminary dipping layer model for the the east/west line (Green et al., (1980)).

In the analysis by Green et al. (1980), the crustal structure from the west- east profile showed a five layered crust where as for the east - west profile the travel time graph indicates a six layered crust. The extra travel time branch occurs between ~40 km to ~90 km. Further complexity is indicated in the seismograms at greater offset. The presence of a discontinuity in the seismic section between 161 km and 204 km is evidence for some low velocity zone and / or faulting in the subsurface in this area. The apparent velocities for the eastern and western profiles vary from 3.43 to 8.21 km/sec. Horizontal plane layer calculations revealed a depth to the Riel of approximately 37 km and Moho depth of approximately 47 km (see table 4.1 (c) and (d)).

Reverse profile calculations on this line could not be carried out for distances smaller than 90 km because of the discrepancy in the layers mentioned in the preceeding paragraphs. For distances greater than 100 km, reversed profile analysis was be done with slight adjustment to the travel times. The dipping layer model for the east - west profile is shown in Figure 4.4. It is a composite of velocity - depth information obtained from both the unreversed and reversed analyses.

The results for the the second analysis making use of the further processed records and those from the previous interpretation are broadly similar.

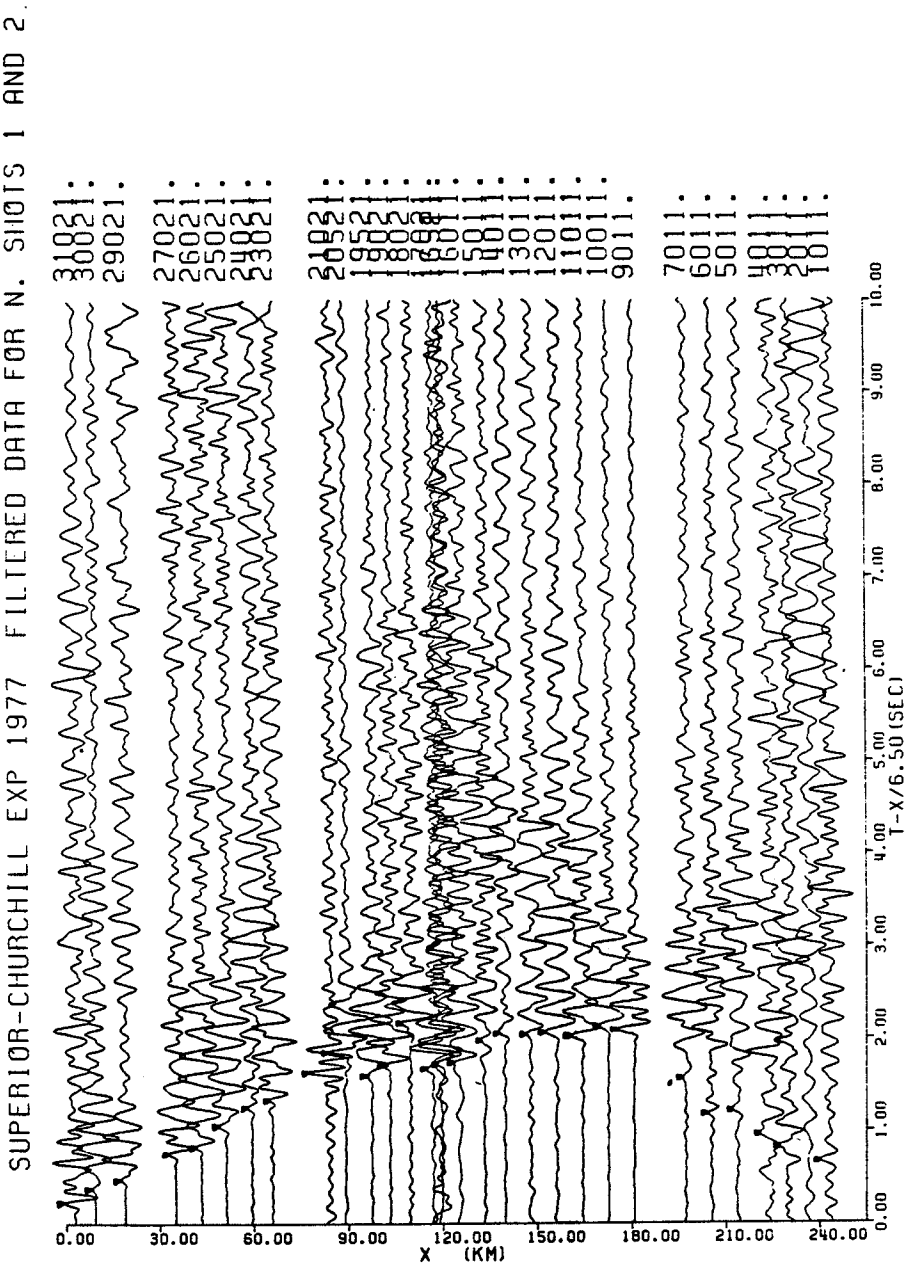

Figure 4.5 - First arrival picks for seismograms for the north shot.

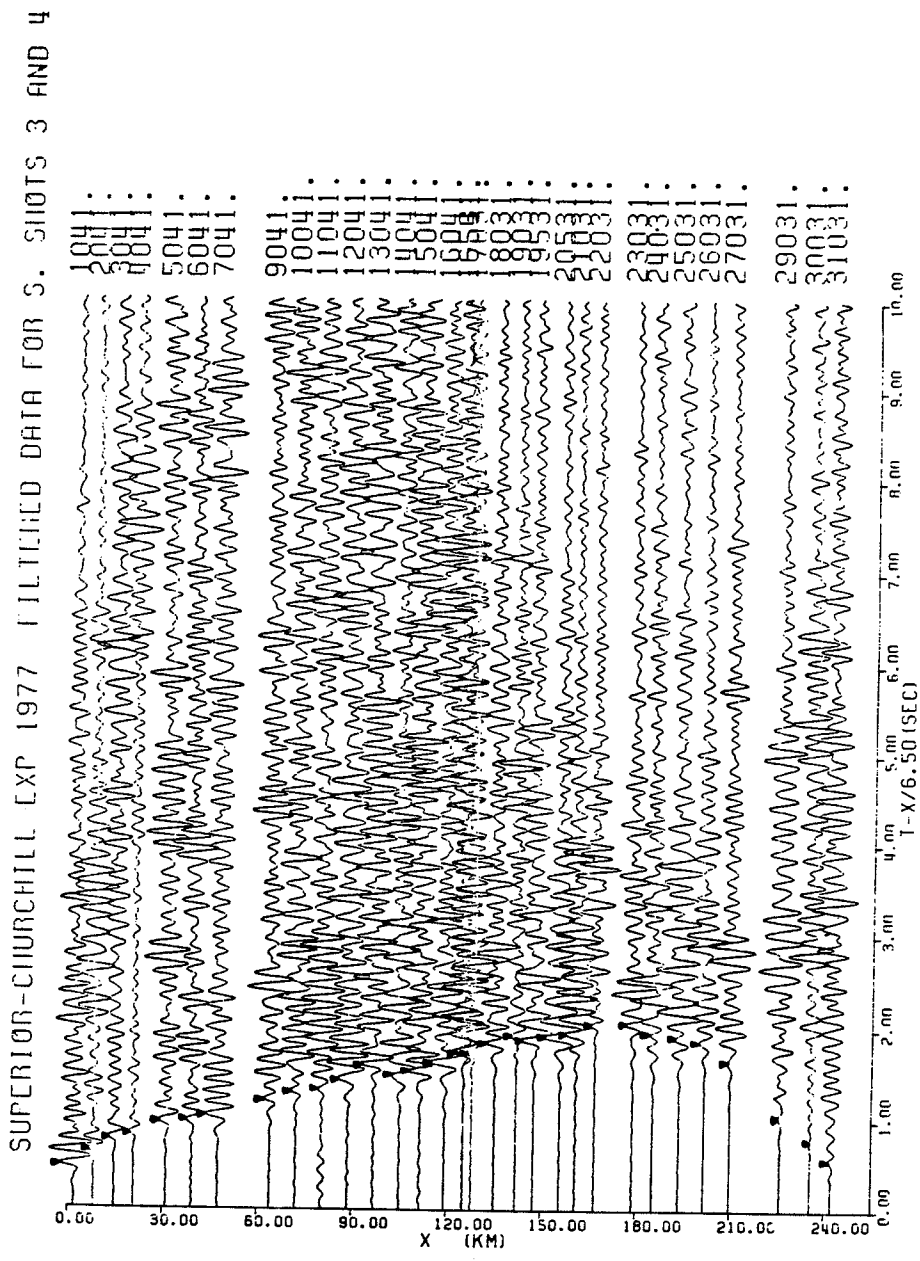

Figure 4.6 - First arrival picks for seismograms from the south shot.

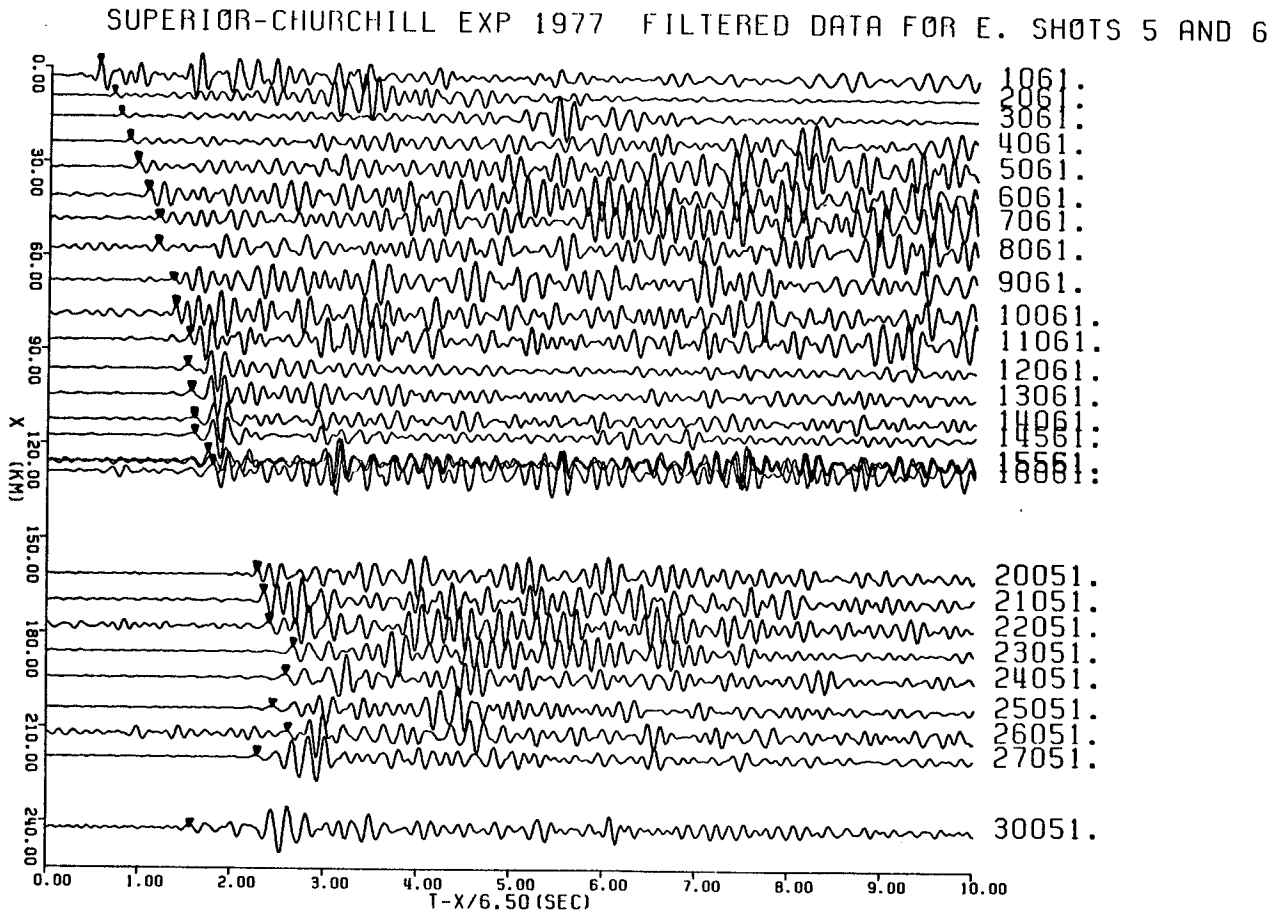

Figure 4.7 - First arrival picks for seismograms from the east shot.

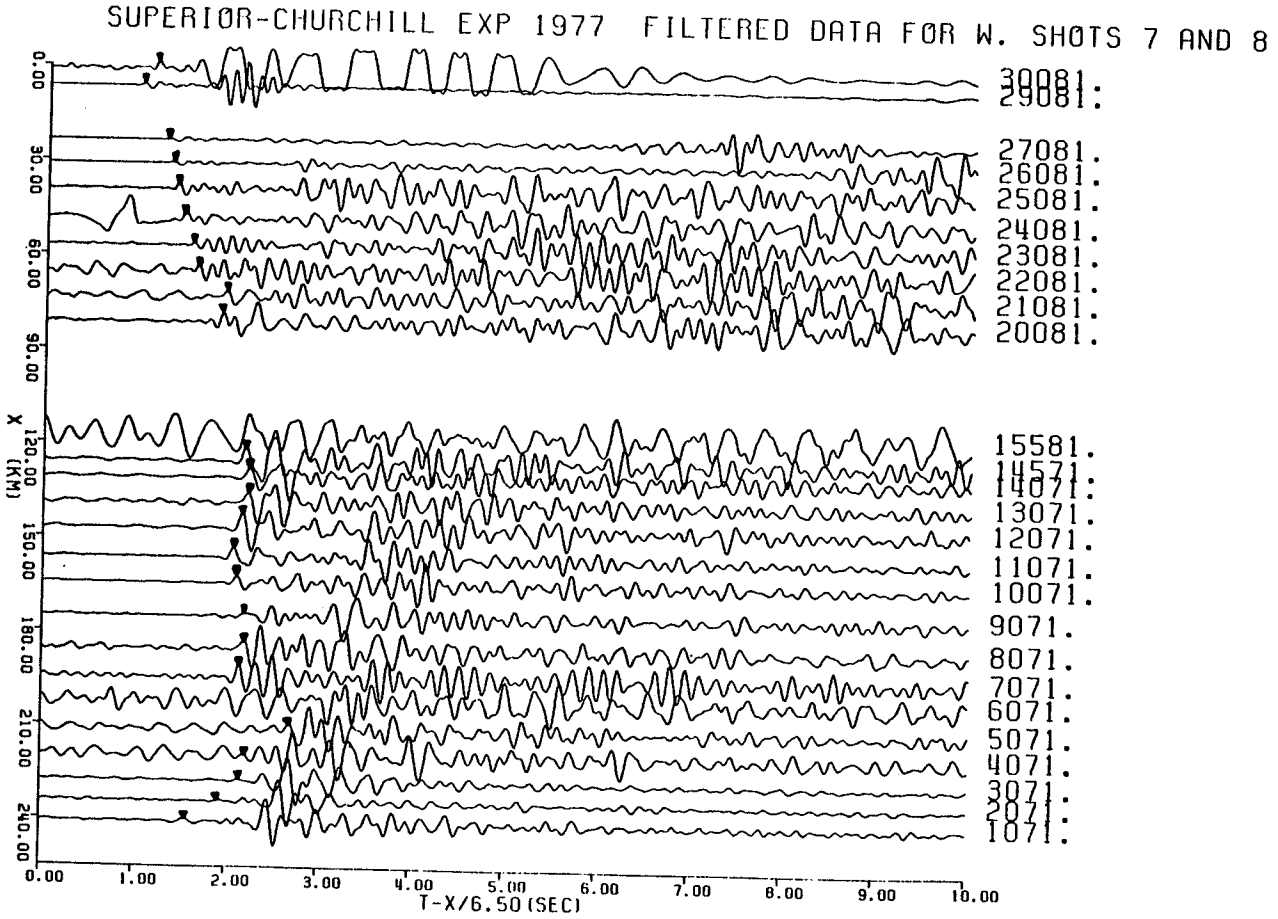

Figure 4.8 - First arrival picks for seismograms from the west shot.

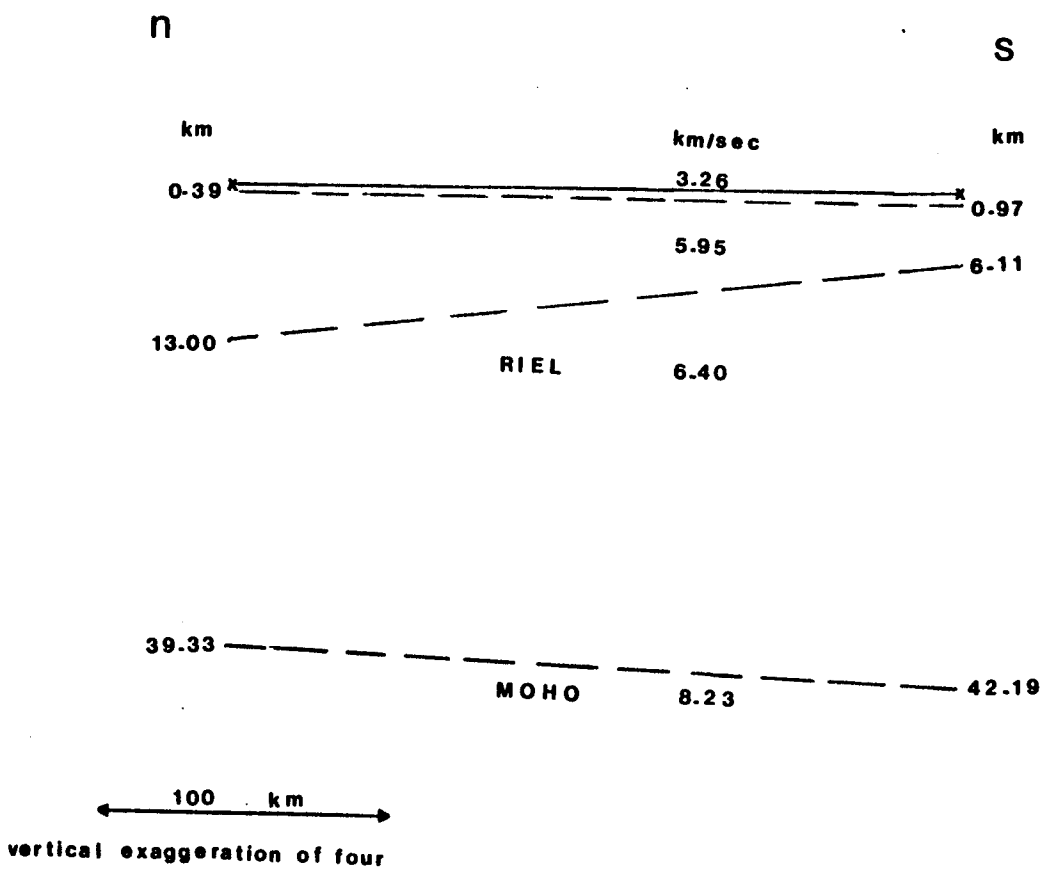

Figure 4.9 - Preliminary three layer model for the north/south line.

Velocity - depth distributions, based on the first arrival picks shown in Figure 4.5 to 4.8, are more or less the same, although there are some areas of discrepancy. The dips and depths of the major interfaces are very much similar.

The areas of discrepancy are :

(1) the presence of the 6.21 km/sec layer in the north - south profile. From the travel time picks in the second analysis there is little evidence for the presence of an extra layer. As a result of the exclusion of the 6.21 km/sec layer, the depths to the deeper interfaces for the north - south model differ from those of the previous interpretation. These differences are seen when the dipping layer models from the present interpretation (see Figure 4.9) are compared with the previous one,

(2) the inclusion of a 6.22 km/sec layer in Green's east to west model. This layer is not apparent from analysis of the processed data. The effect is again to vary the depth to the Riel and Moho discontinuities in the two models.

From the above, it can be seen that the data lends itself to a variety of interpretations. The true model may

be a modified version of one or both of these interpretations or some new velocity - depth structure. It now remains for ray tracing and theoretical modelling techniques to resolve these areas of discrepancy in the different models and provide a suitable solution of the structure of the subsurface in the Churchill - Superior boundary zone.

Chapter V

INTERPRETATION

This chapter is divided into two parts. In the first part, a brief discussion of the interpretation techniques used in obtaining the final best fit velocity - depth profile is given. These interpretation techniques include travel time inversion, synthetic seismogram analysis and travel time fitting using the WKBJ method and ray theory method respectively. The second part of this chapter provides a detailed commentary of the steps leading up to the final crustal models. It gives the velocity - depth models obtained from inversion of the observed travel times and the synthetic seismograms and computed travel time curves derived from these and various other models.

PART I

5.1 TRAVEL TIME INVERSION

The inversion problem involves the finding of a set of model cross- sections to fit all the given observations. There are two general methods of solving the problem, either by a trial and error method or through direct inversion.

The trial and error method finds cross-sections for which the theoretically calculated properties of waves are in agreement with the observations. Direct inversion provides a mathematical solution of some function that characterises the propogation of the waves. With the trial and error method it is possible to analyse not only seismic data but also other types of data for example potential field or heat flow data. The direct method is less versatile but saves on computation time.

The Weichert-Herglotz inversion method is one of the direct inversion methods. A brief account of the Wiechert-Herglotz-Bateman solution and the extension of this solution by Gerver and Markushevich (1966, 1967) to include inversion of a finite number of low velocity zones is given in the following paragraphs.

5.2 WEICHERT-HERGLOTZ-BATEMAN INTEGRAL

This derivation follows that given by Grant and West (1965). From Figure 5.1(b) the equation relating horizontal distance and depth increments is:

$$dx = \tan i_o \, dz \quad \ldots\ldots (1)$$

where i_o = angle which turning ray makes with the normal

Rewriting this equation in terms of ray parameter, p ,

$$dx = dz \quad (\sin i_o / \cos i_o)$$

(a)

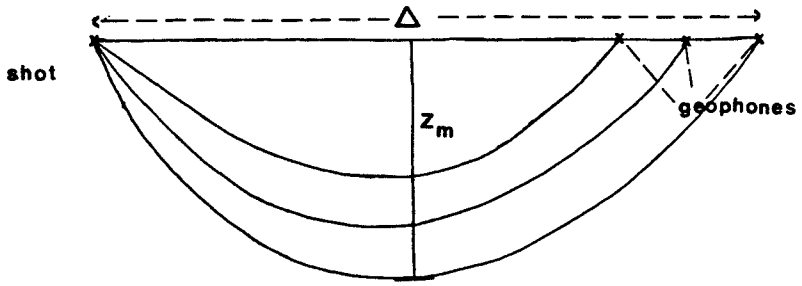

(b)

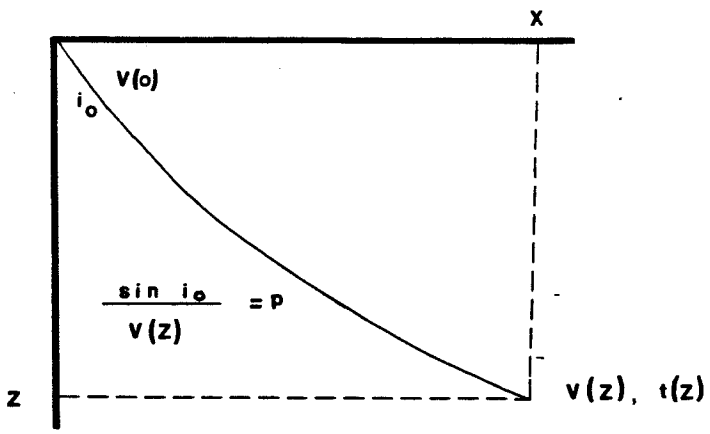

Figure 5.1 - Ray path in vertically inhomogenous medium.

$$= \frac{dz\ p\ v(z)}{1 - p\ v(z)}$$

$$x = p \int_{z_1}^{z_2} \frac{v(\xi)}{1 - p^2 v(\xi)}\, d\xi$$

from Figures 5.1(a) and (b),

$$\Delta = 2x$$

$$= 2p(z_m) \int_0^{z_m} \frac{v(\xi)}{1 - p^2(z_m)\, v^2(\xi)}\, d\xi \quad \ldots\ldots (2)$$

where z_m is the maximum depth of penetration of the ray.

By changing variables

$$y(z_m) = p^2(z_m),\quad \eta(\xi) = \frac{1}{v^2(\xi)},\quad f(y) = \frac{\Delta}{2p}$$

rewriting equation (2)

$$f(y) = \int_{\eta_0}^{y} \frac{\xi' \eta}{\sqrt{\eta - y}}\, d\eta \quad \ldots\ldots (3)$$

where $\xi' = \frac{d\xi}{d\eta}$ and $\eta_0 = 1/v(0)$

From Abel's integral equation

$$f(\eta) = \int_a^{\eta} \frac{u(x)}{(\eta - x)^n}\, dx \quad \text{for } 0 < n < 1$$

the solution of which is

$$u(x) = \frac{\sin n\pi}{\pi} \frac{d}{dx} \int_a^x \frac{f(\xi)}{(x-\xi)^n} \, d\xi$$

the solution of equation (3) is as follows:

$$\frac{1}{i} \frac{dz}{d\eta} = \frac{1}{\pi} \frac{d}{d\eta} \int_{\eta_0}^{\eta} \frac{f(y)}{\sqrt{(\eta - y)}} \, dy$$

which becomes

$$z(\eta) = -\frac{1}{\pi} \int_{\eta_0}^{\eta} \frac{f(y)}{\sqrt{y - \eta}} \, dy$$

This solution however assumes that velocity increases continuously with depth. Gerver and Markushevich (1966, 1967) extended this solution to take into account the presence of finite numbers of low velocity layers. This solution places bounds on the depth extent and velocity in the low velocity zone obtained.

The computer algorithm HRGLTZ which performs the inversion and is applied in this research, makes use of this modified solution and produces velocity-depth profiles from

values of ray parameter, dT/dX vs distance. Because of the widely spaced receiver distances for the observed data, smoothening of travel time graphs had to be done in order to obtain monotonically decreasing ray parameter values (Mc Mechan, 1972,1979a, 1979b).

5.3 THE WKBJ METHOD

Improvements in instrumentation within the last ten years have facilitated the use of synthetic seismograms as an aid in seismic data interpretation. Various techniques have been developed to compute theoretical seismograms, one of the more recent of these being the WKBJ method. This method was devised by Prof. C. H. Chapman (1978) and owes its popularity to the fact that computation time is far less than that for other methods.

In the evaluation of synthetic seismograms by this method, the WKBJ approximate solution of the wave equation is assumed. This assumption is valid as long as the frequencies are sufficiently high compared to the velocity gradients. The WKBJ approximation is

$$\hat{\tilde{v}}(\omega,\rho) = i\,\mathrm{sgn}(\omega)\,\exp[i\omega\tau(\rho)]\,R(\rho)$$

where

$$\tau(\rho) = 2\int_{z_a}^{z_b} q(\rho,\epsilon)\,d\epsilon$$

$\tau(p)$ = vertical slowness integral

$\hat{v}$ = the Fourier Transform of v with respect to frequency (w) and horizontal wave slowness (p)

R(p) = a function of the source and receiver directivity and transmission ceofficients.

This approximation is used in the inverse transform of the displacement field

$$u(t,x) = \frac{1}{4\pi^2}\int_{-\infty}^{\infty}\int_{B} \hat{u}(\omega,p)(i\omega)[i\,\mathrm{sgn}(\omega)] \{\exp[i\omega(t-px)]\}\,d\omega\,dp$$

which reduces to

$$u(t,x) = \frac{1}{2\pi}\,\dot{s}(t) \sum_{t=\theta(p,x)} \frac{R(p)}{|\theta'(p,x)|}$$

$\dot{s}(t)$ = source function including the transform function of the geophones

$$\theta = px + \tau(p)$$

This solution is valid for reflected, direct and turning and head waves.

5.4 THE RAY TRACING METHOD

The interpretation of the previous chapter indicated a dipping subsurface strata for both east/west and north/south lines, in addition there is evidence of lateral inhomogeneity in the boundary zone. The WKBJ method assumes horizontal layering and lateral homogeneity and cannot adequately model these details of the subsurface. The ray tracing method is one method capable of doing this.

There are several approaches to calculate the travel times of rays through laterally and vertically inhomogeneous media. Many of these techniques however, are complex and have the disadvantage of taking up excessive amounts of computer time. For the purposes of this thesis, because of the number of models which were going to be tried, a simpler, more efficient means of computing ray paths and travel times was sought. The method developed by Whittall and Clowes (1980) was chosen.

The Whittall-Clowes method uses plane interfaces with any specified amount of dip. Velocities at boundaries between layers are constant and non-zero with linear gradient perpendicular to the dip direction. As a result of this, the ray paths are circular arcs, the equation of which is given by:

$$RHO = VOUT \; (\; GRAD * \sin (IOUT) \;)$$

where 'RHO' is the radius of the circle

'VOUT' is the velocity at the boundary from which the ray departs.

'GRAD' is the gradient in the layer

'IOUT' is the angle of departure of the ray

measured with respect to the gradient.

Once the ray path is found the intersection of the ray with the nearest boundary is obtained. The velocity of the ray at the point of intersection is determined by the following relation:

$$V = V(0) + GRAD * \cos (I) * Z$$

where V (0) is the velocity along the nearest overlying boundary I is the dip

Z is the vertical distance to the boundary from the point in question.

Snell's law is then used to compute the angle of intersection of the ray on the next boundary.

The travel time is calculated from the equation:

$$dt = 1/GRAD * (\text{arctanh} (\cos (IOUT)) - \text{arctanh} (\cos (IIN)))$$

where dt is the travel time between the two boundaries and IIN the ray-intersection angle with the next boundary

By the above method travel times and distances for all surface arrivals are calculated. Because of the low probability of critically refracted waves impinging on a boundary at the precise critical angle, in most cases true critically refracted wave travel times are not calculated. Instead the travel times for pseudo-headwaves are calculated, these pseudo-headwaves are waves which are incident on the boundary at an angle which is within a small range of the critical angle. Converted phases, multiply reflected ray paths and subcritical reflected events are not considered.

PART II

5.5 WEICHERT-HERGLOTZ INVERSION AND WKBJ MODELLING

Wiechert - Herglotz inversion of the north-south and east-west profile data produced the results shown in Figures 5.2 (a) to (d). Smoothly increasing velocity distributions characterise both profiles. Depths to the Moho of between 40.0 to 57.0 km and velocities of 6.9 and 8.4 km/sec are determined for the north-south line; while for the east-west line the calculated depth and velocities are 65.4 km, 8.06 km/sec and 55 km, 8.26 km/sec respectively. It should be noted that a similar type of smooth velocity variation was predicted by Lau (1979) from synthetic seismic modelling.

The large receiver spacing used in data collection meant that there were few data points with which to determine ray parameter, p. Therefore considerable smoothening of the ray parameter vs. distance curve had to be done, placing severe limitations on the inversion technique. The inverted models, therefore indicate only broad trends in the velocity distribution rather than the detailed velocity structure.

The WKBJ method at this stage of development, assumes horizontal layering. The large dips suggested by the preliminary reverse profile calculations eliminate the use of this method for obtaining accurate approximations of the

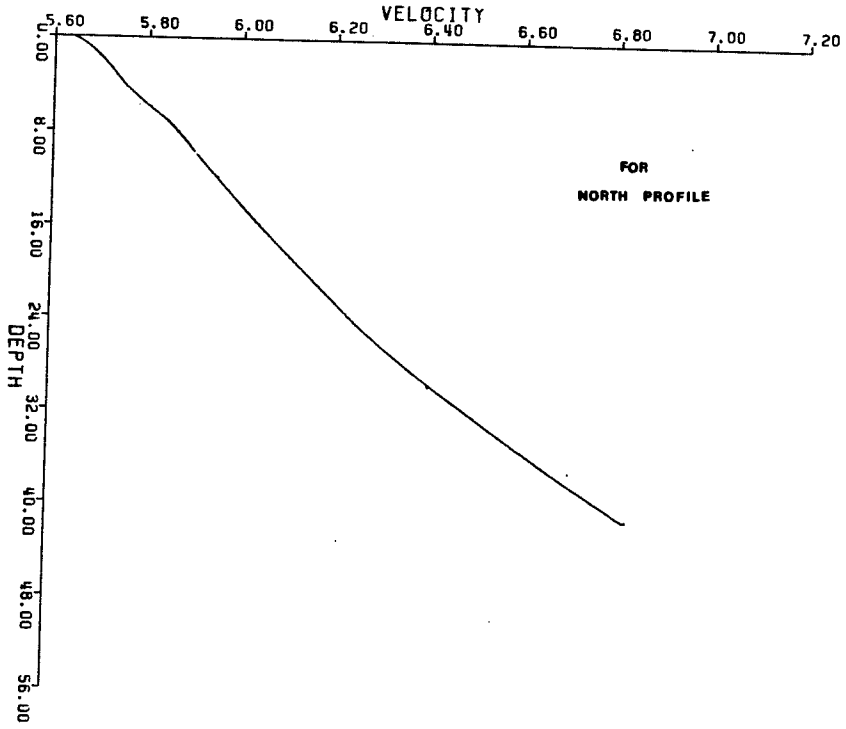

Figure 5.2 (a) - Weichert-Herglotz inversion for the north shot.

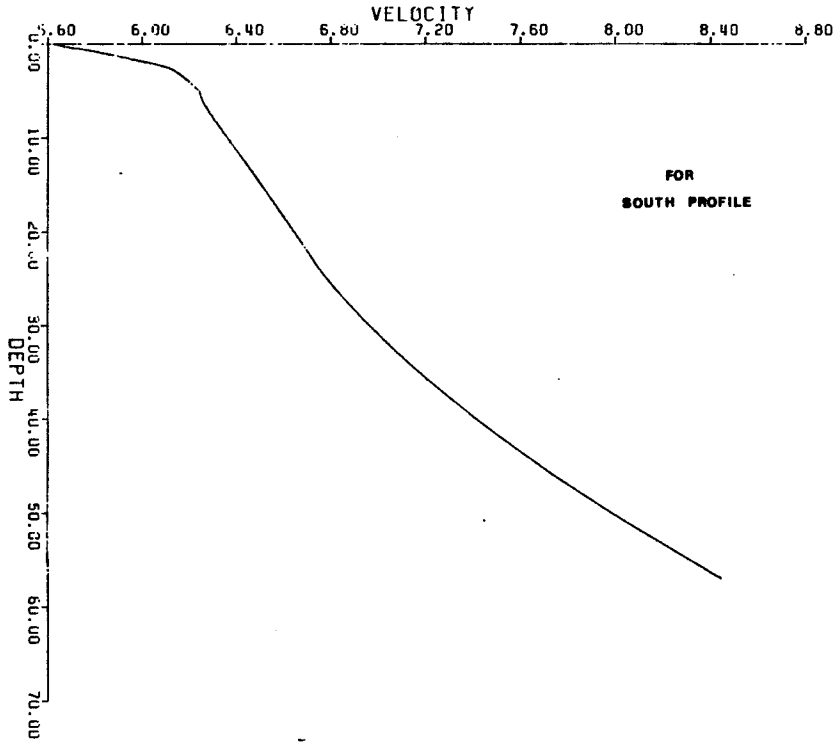

Figure 5.2 (b) - Weichert-Herglotz inversion for the south shot.

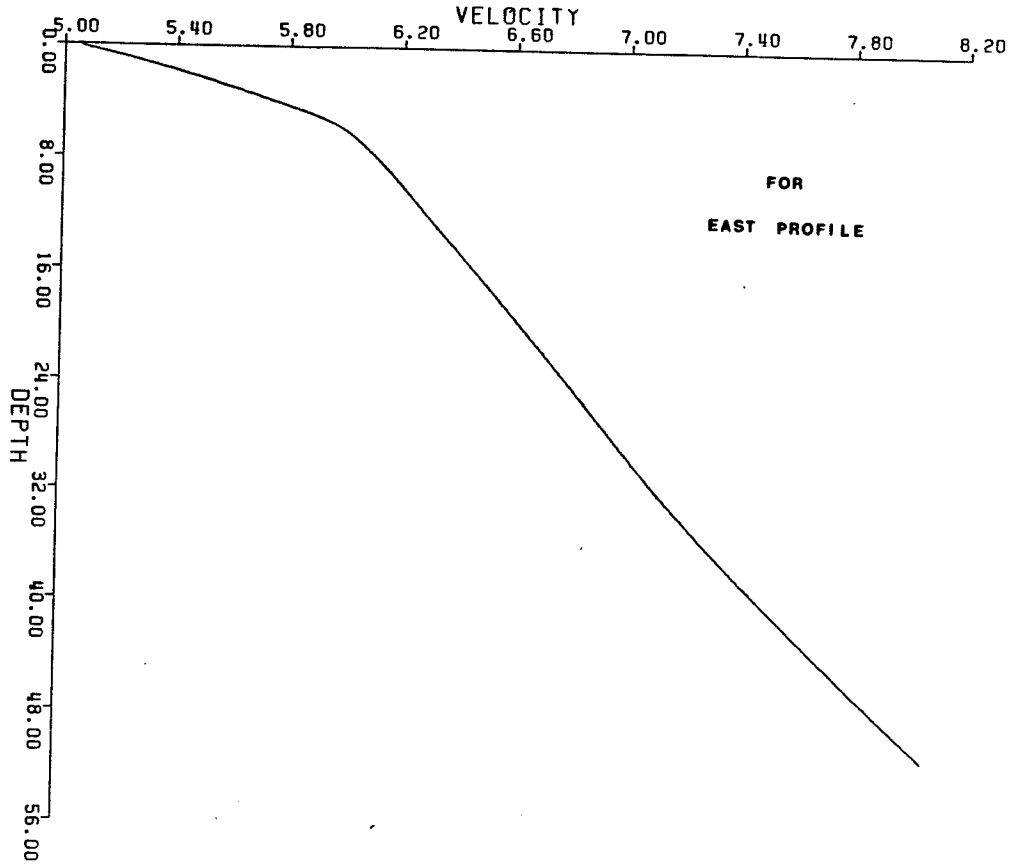

Figure 5.2 (c) - Weichert-Herglotz inversion for the east shot.

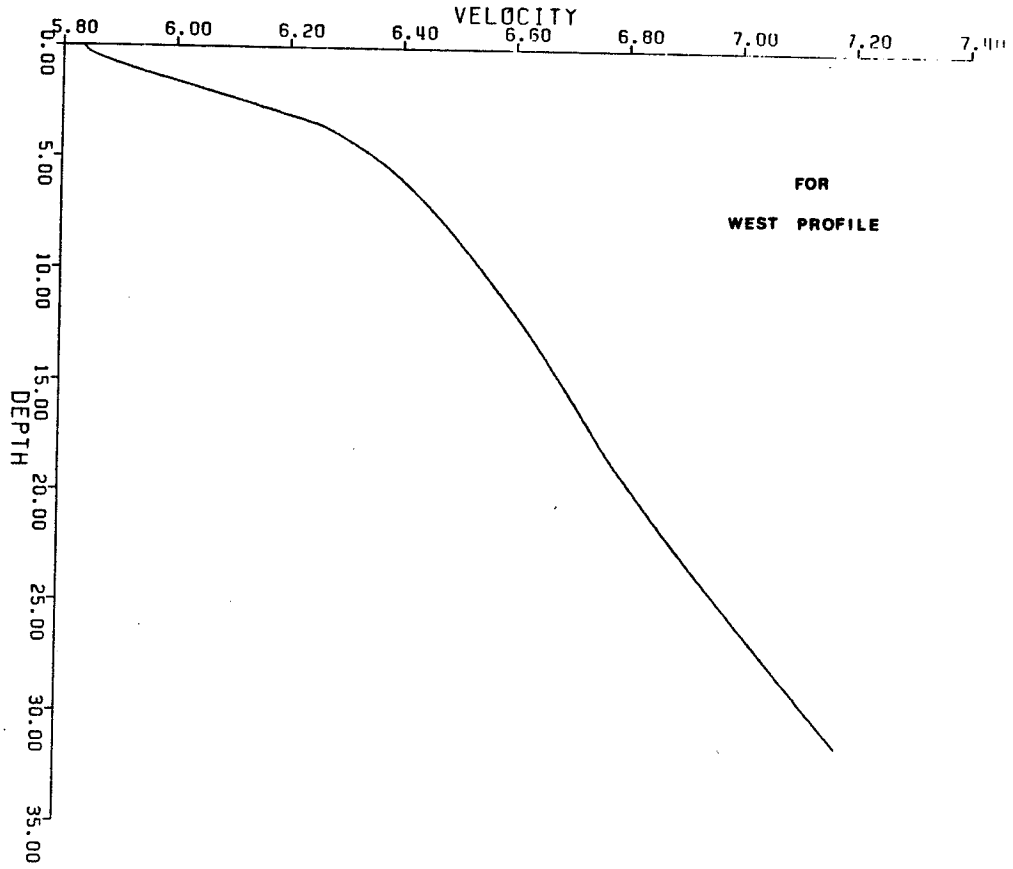

Figure 5.2 (d) - Weichert-Herglotz inversion for the west shot.

observed seismograms. However, after initial velocity-depth modelling was done using ray tracing, the WKBJ method was used to establish amplitude relations between refracted and reflected events for the final models.

5.6 INTERPRETATION OF THE NORTH-SOUTH LINE

Ray tracing results for the north/south profile using the author's three layered model are shown in Figures 5.2 (a) and (b). Figure 5.3 (a) shows the ray tracing results for the northern shot and Figure 5.3 (b) show the results for a shot at the southern end of the profile. In each of these figures and all other ray tracing diagrams to follow, the bottom diagram represents the velocity-depth model for which the calculated ray paths for near critically refracted and reflected events are shown. The velocities, non-zero velocity gradients and depths to interfaces are given for each layer. In the top diagram the calculated travel times for the reflected and refracted events are shown as x's and diamonds respectively. The observed first arrival times are plotted as circles joined together by lines.

From the lack of fit of the calculated and observed data for this original three layer model and modified versions of this model between 60 km to 120 km, it was concluded that a three layered crust was insufficient to model this dataset. A more complicated crustal model was needed. As a first approximation, the four layer model by

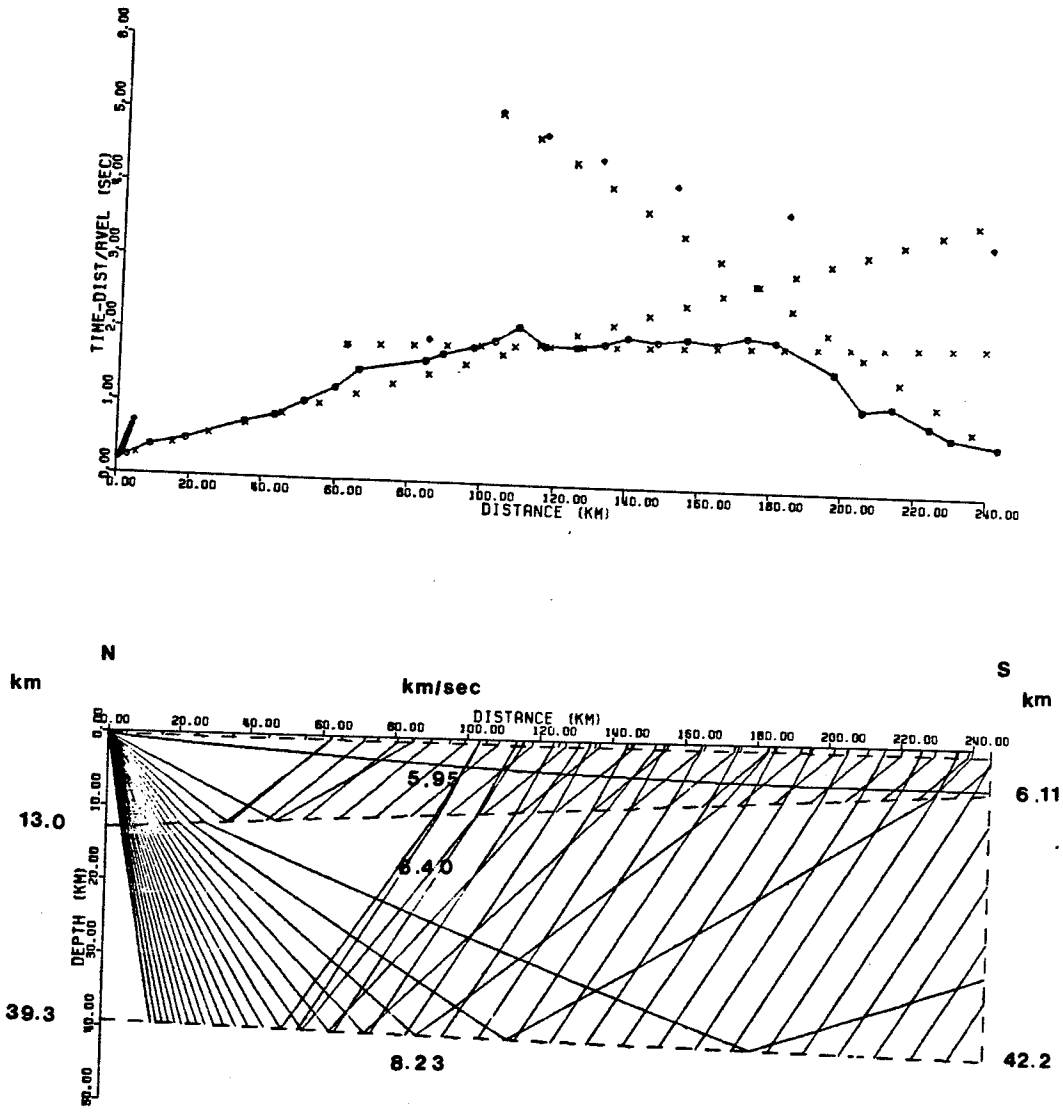

Figure 5.3 (a) - Ray tracing results for the preliminary three layer N/S model (north shot).

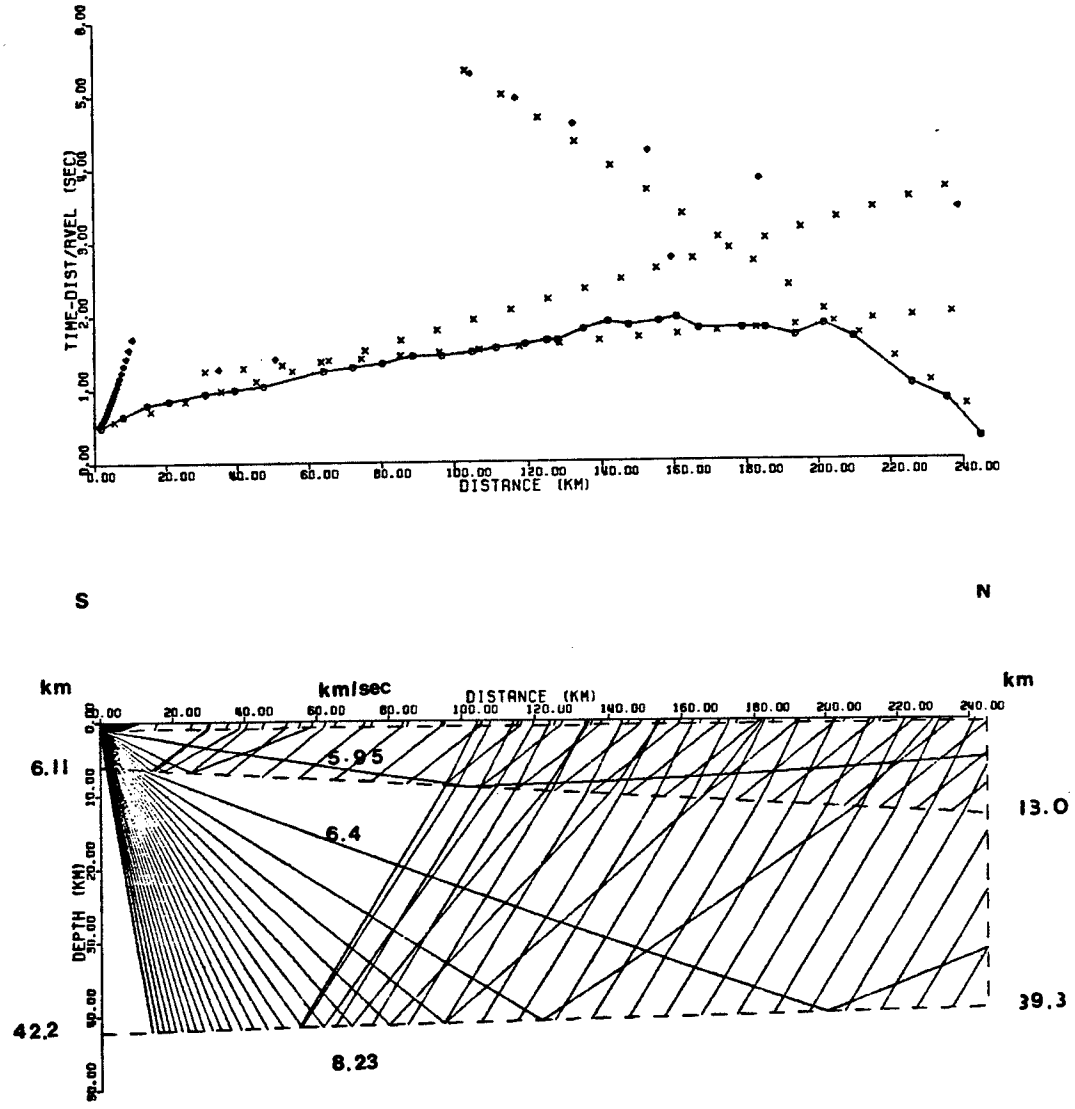

Figure 5.3 (b) - Ray tracing results for the preliminary three layer N/S model (south shot).

Green et al. (1980) was tried. The results of ray tracing using this model are shown in Figures 5.4 (a) and (b). Even though there was improved correspondence between the computed and observed travel times, there still existed some discrepancy in the fit at the 60 to 120 km distance and for the deeper arrivals. Other velocity-depth models were tried and by a process of trial and error a final best-fit model was attained.

The final best-fit model for the north/south profile is shown in Figures 5.5 (a) and (b). It is a four layered crustal model comprising of a thin (0.39 to .97 km) near surface layer of velocity 3.46 km/sec underlain by layers of heterogenous and homogenous material. Beneath the near surface layer is an intermediate upper crustal layer of velocity 5.80 km/sec extending down to a depth of 8.3 km in the north and 3.5 km in the south. A heterogenous layer of increasing velocity underlies this 5.80 km/sec layer. Velocities in this layer increase from a value of 6.22 km/sec at a rate of 0.005 km/sec/km down to the lower interface. The lower crust shows less differentiation although there is heterogeneity indicated by the high 0.015 km/sec/km velocity gradient. Velocity increases from a value of 6.45 km/sec at the uppermost interface to a value of 8.00km/sec at the Moho. Depths to the Moho discontinuity range from 37.0 km in the north to 43.0 km in the south.

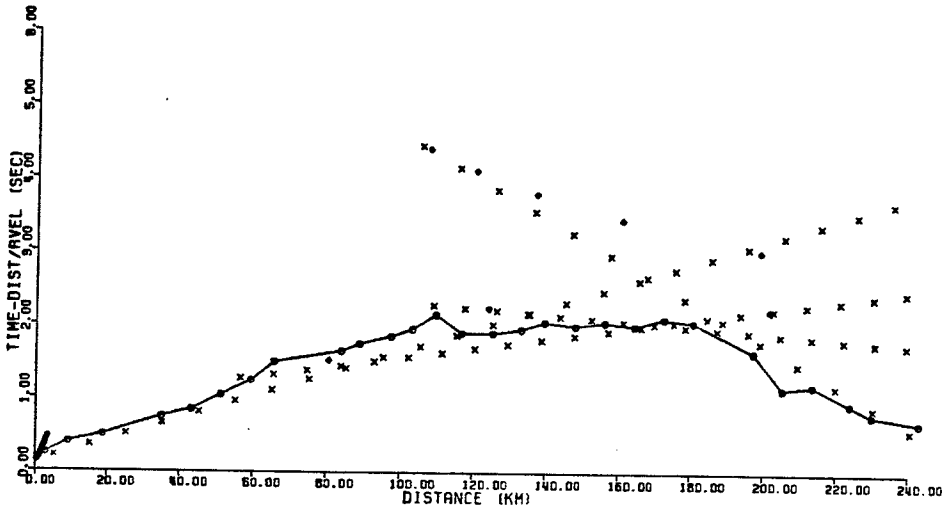

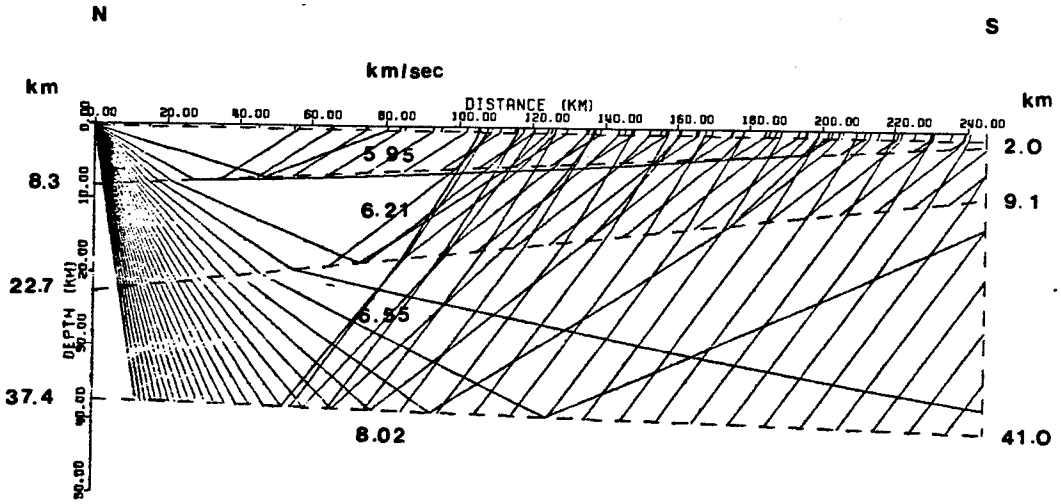

Figure 5.4 (a) - Ray tracing results for the preliminary four layer N/S model (north shot).

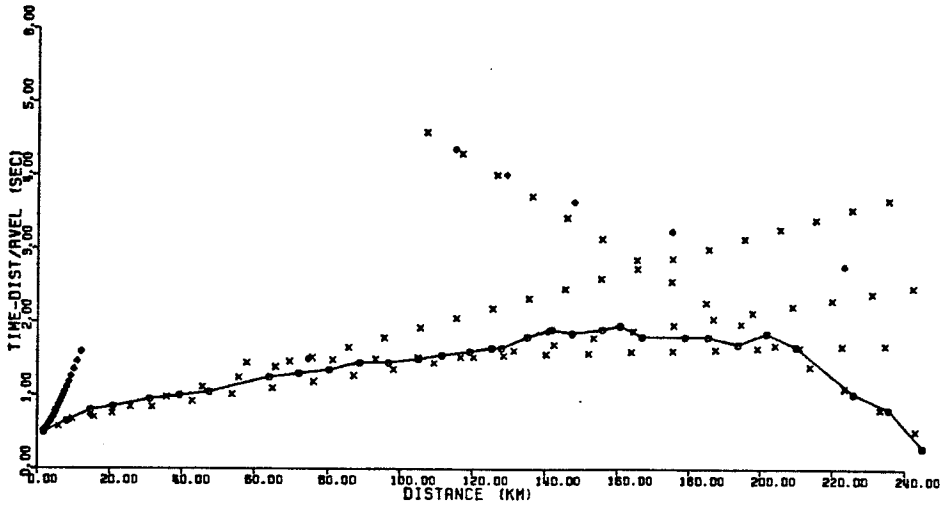

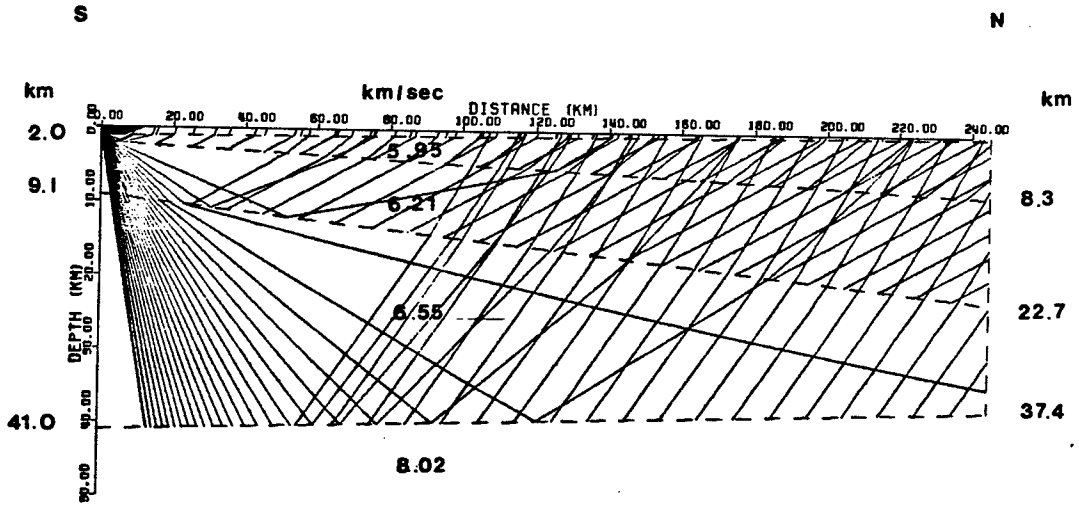

Figure 5.4 (b) - Ray tracing results for the preliminary four layer N/S model (south shot).

In general the fits of the calculated events with those picked from the observed data is good (see Figures 5.5 and 5.6). One exception is late arrival alluded to in the polarisation filtered traces for the north and south shots (see Figure 5.7). This event, beginning at a distance of 120 km and at approximately 6.0 seconds (reduced time), could not be predicted by the final model. Attempts at obtaining this late arrival led to the introduction of sub-Moho interfaces at depths of between 3.0 - 6.0 km beneath the Moho. The high degree of curvature of the reflection event could not however be approximated by the reflections off these interfaces. It should be noted here that even though the late reflection is seen on the polarisation traces for the north/south shots, it is not as easily identified on the bandpass filtered traces. It may well be that this event is an artificiality created by cross- correlation process during polarisation filtering.

From the final north-south model an average velocity-depth structure was created to generate true amplitude WKBJ seismograms. The resulting impulse response synthetic seismogramis given in Figure 5.9 (a). Figure 5.9(b) shows the result after convolution with an approximate source function. The dark lines are events picked from these calculated seismograms. Similar variation in amplitude of the predicted and observed arrivals are noted when Figure 5.9 is compared with Figure 5.6 .

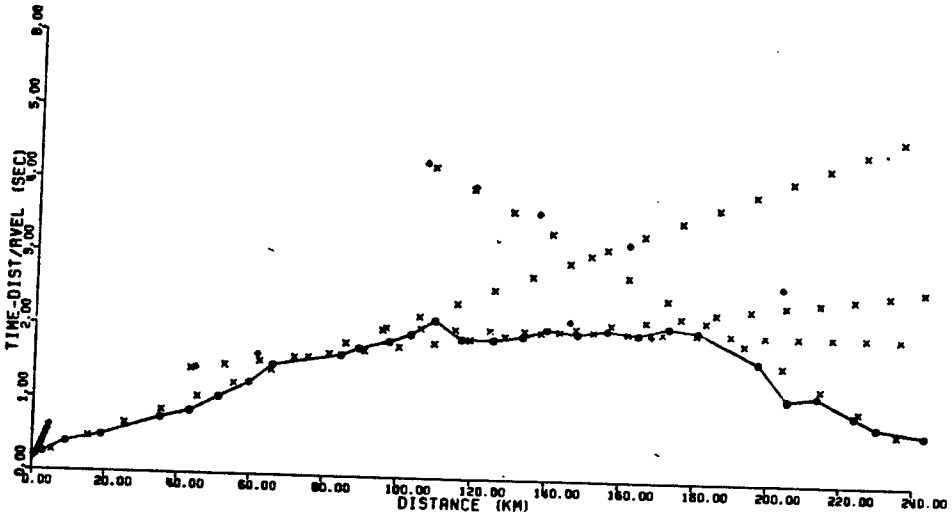

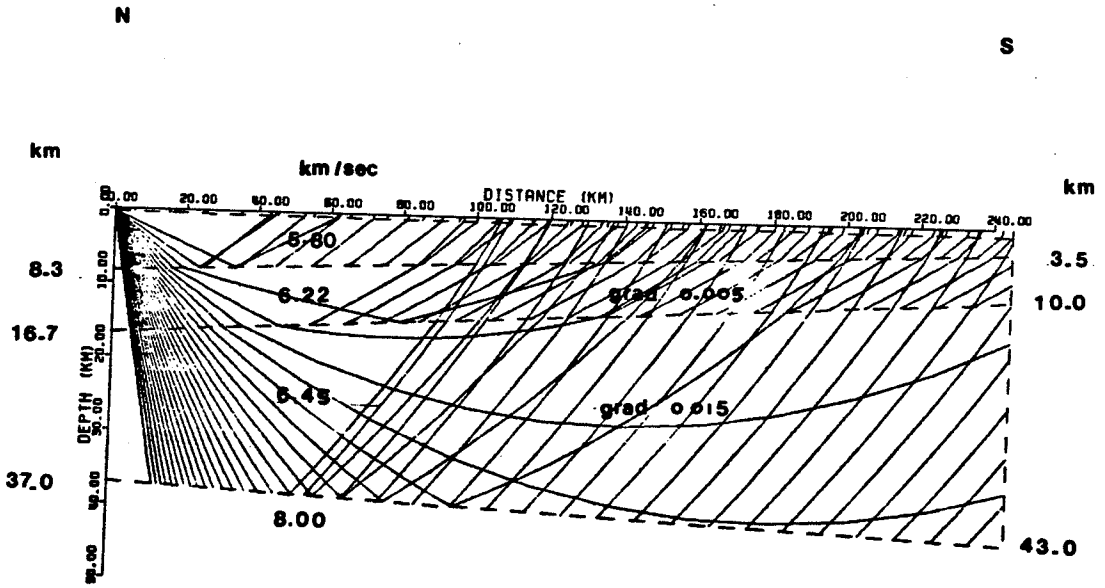

Figure 5.5 (a) - Ray tracing results for the final N/S model (north shot).

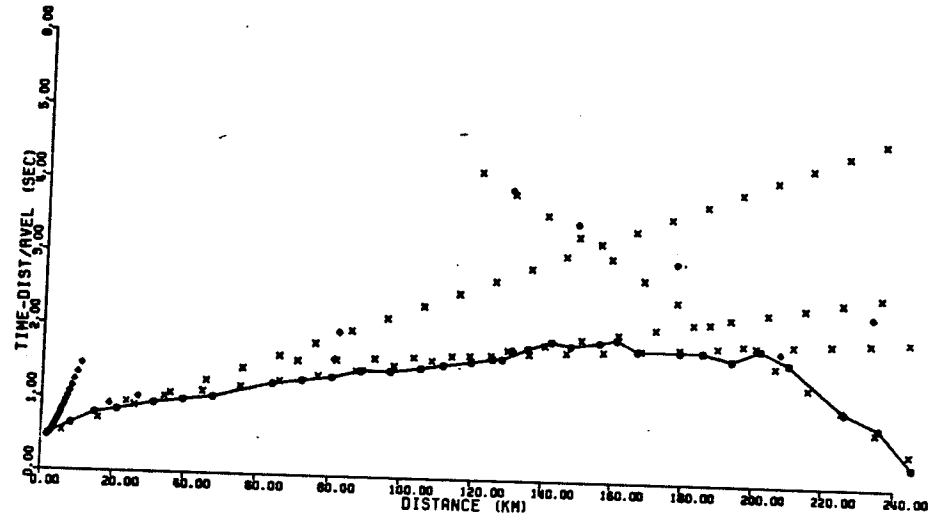

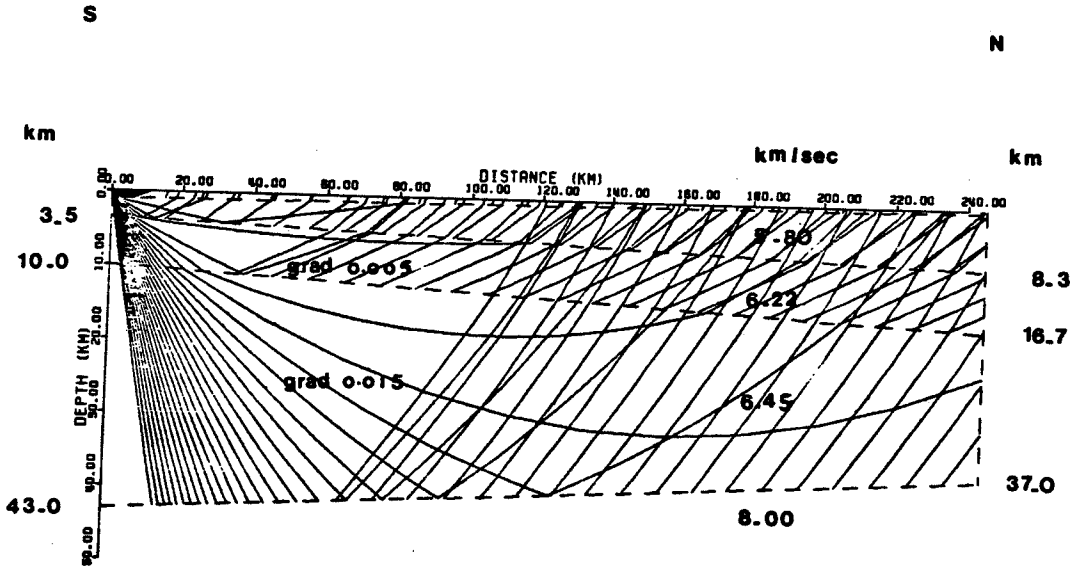

Figure 5.5 (b) - Ray tracing results for the final N/S model (south shot).

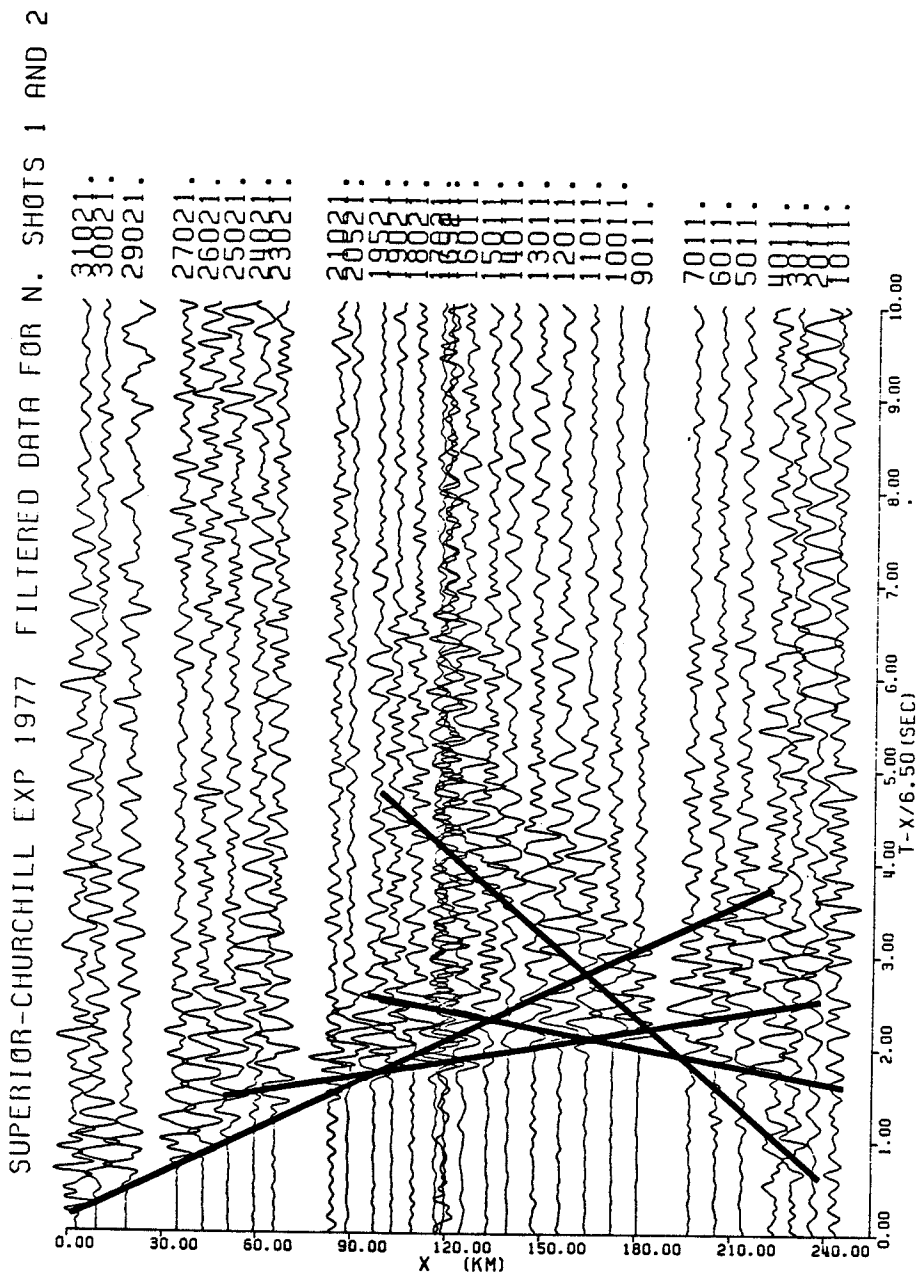

Figure 5.6 (a) - First and later arrivals for seismograms from the north shot.

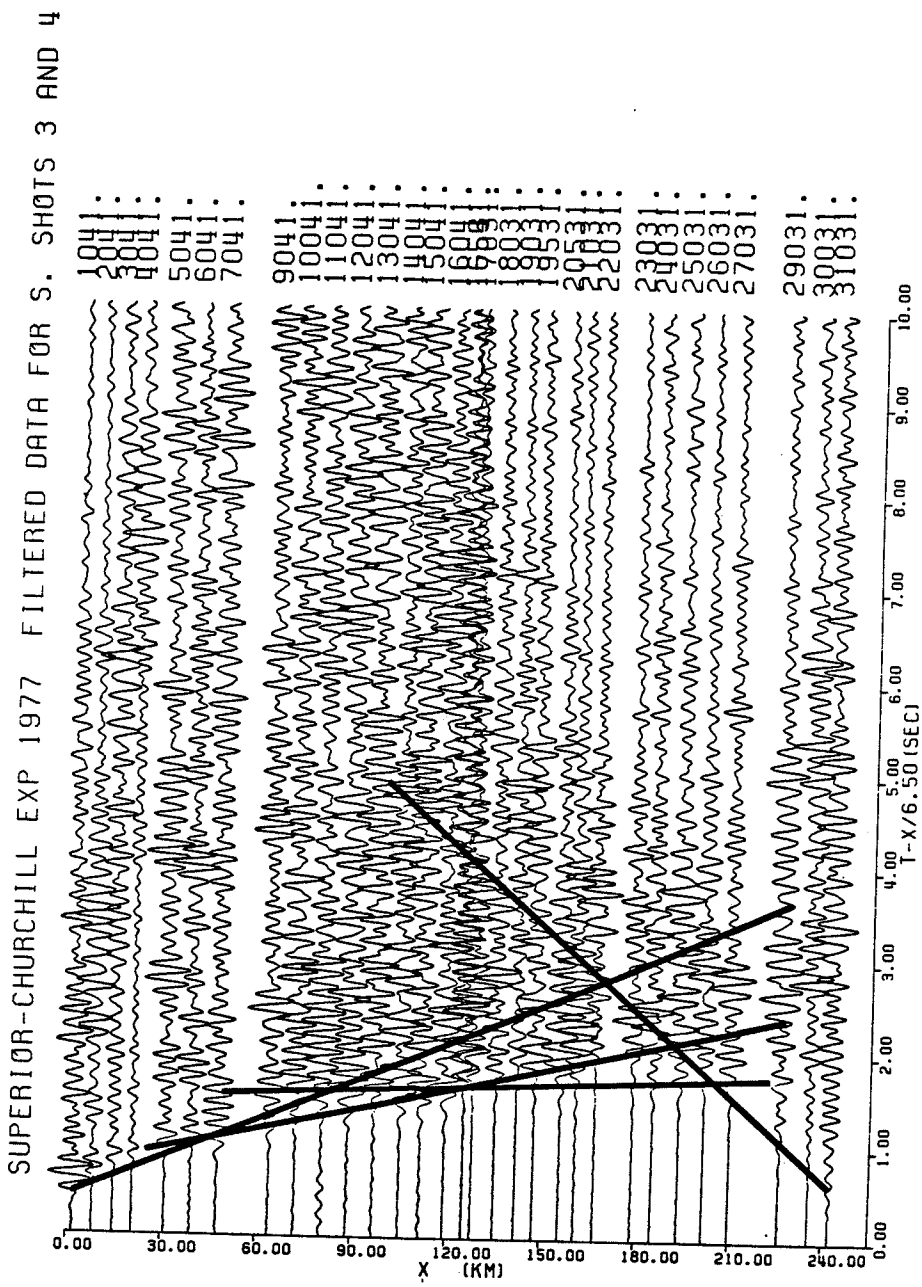

Figure 5.6 (b) - First and later arrivals for seismograms from the south shot.

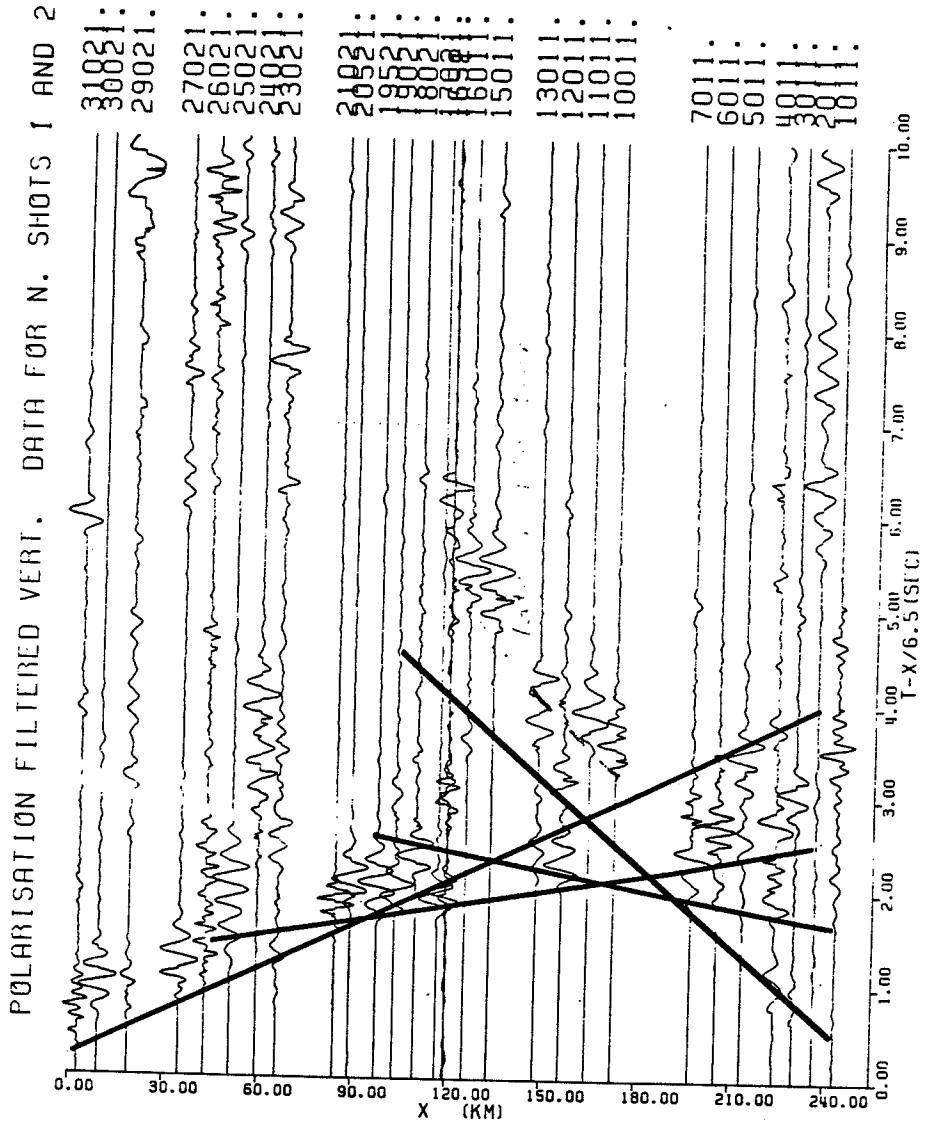

Figure 5.7 (a) - First and later arrivals from polarisation filtered traces for the north shot.

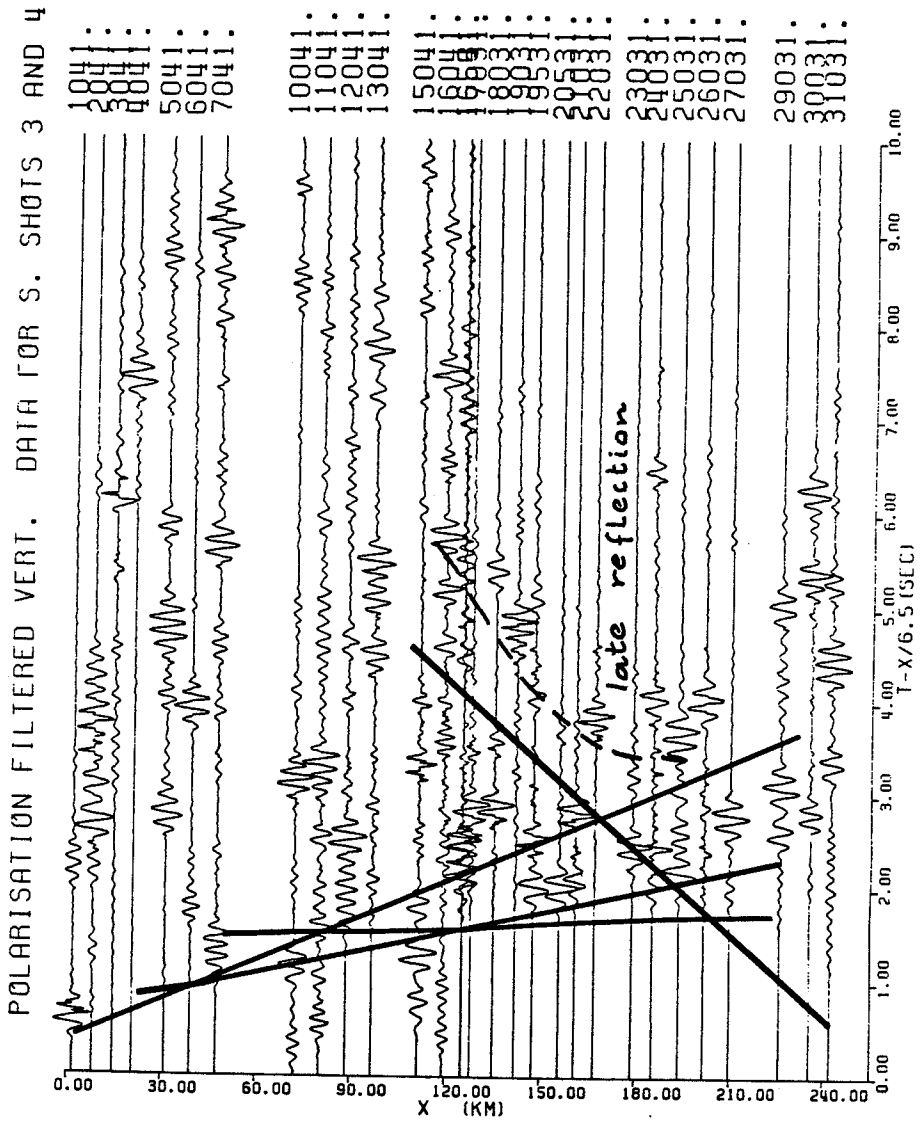

Figure 5.7 (b) - First and later arrivals from polarisation filtered traces for the south shot.

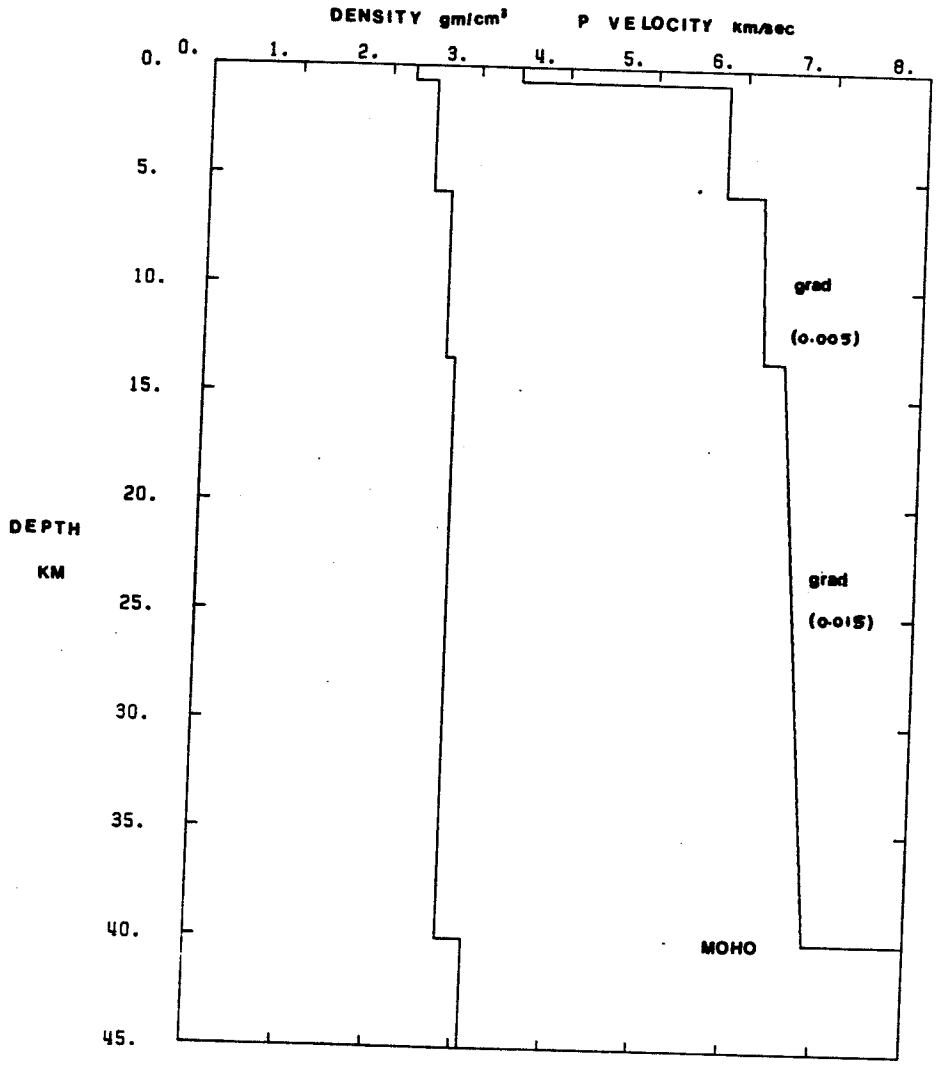

Figure 5.8 - Average velocity-depth structure.

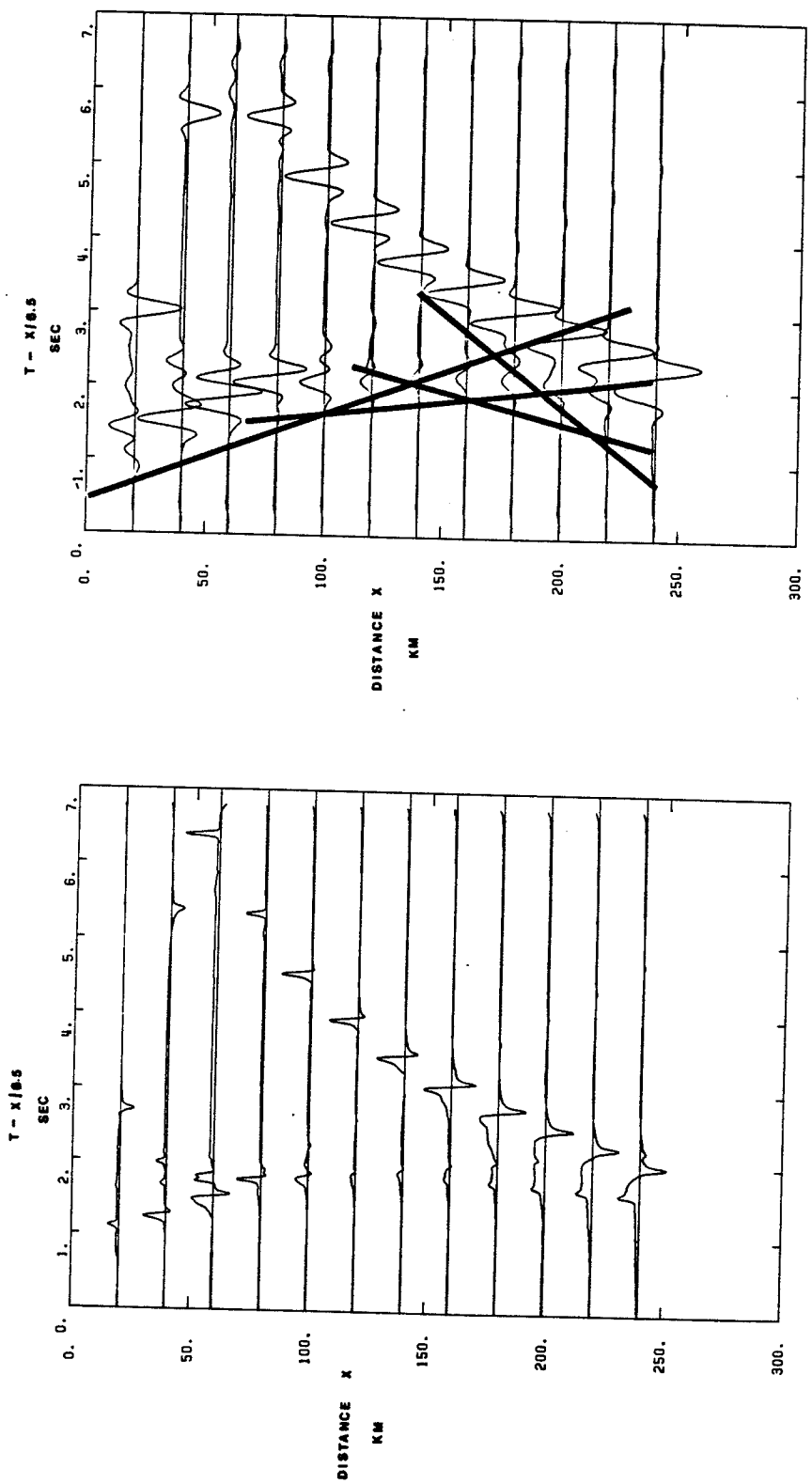

Figure 5.9 - WKBJ synthetic seismograms.

The small amplitude of the predicted Moho refraction is in agreement with that found in the observed data.

5.7 INTERPRETATION OF THE EAST-WEST LINE

With the velocities and depths found in the vicinity of the south shot as a control for the eastern side of the east/west profile, modelling of this line was attempted. Numerous velocity-depth distributions were tried in order to match the complicated travel-time curves. The final best-fit model obtained for the east-west line is shown in Figure 5.10 (a) and (b).

This final east/west model includes a thin surface low velocity layer (3.50 km/sec at a depth of 0.97 - 2.02 km from east to west). Underlying this layer is a layer of velocity 5.98 km/sec. To account for the 0.5 second (reduced time) difference in the arrivals for the east shot at a distance of 160 km, a fault was introduced at the second interface. The discontinuity between the lower and upper crust features a region of overlap. The overlap was required to model first arrivals from the western shot between 130 - 190 km and the eastern shot between 160 - 210 km . Beneath this discontinuity lies a heterogenous lower crust. The velocity and gradient in the eastern portion are higher than in the west. The increases in velocity from 6.49 km/sec in the west to 6.5 km/sec in the east down to 7.83 km/sec at the crust-mantle interface best fit the

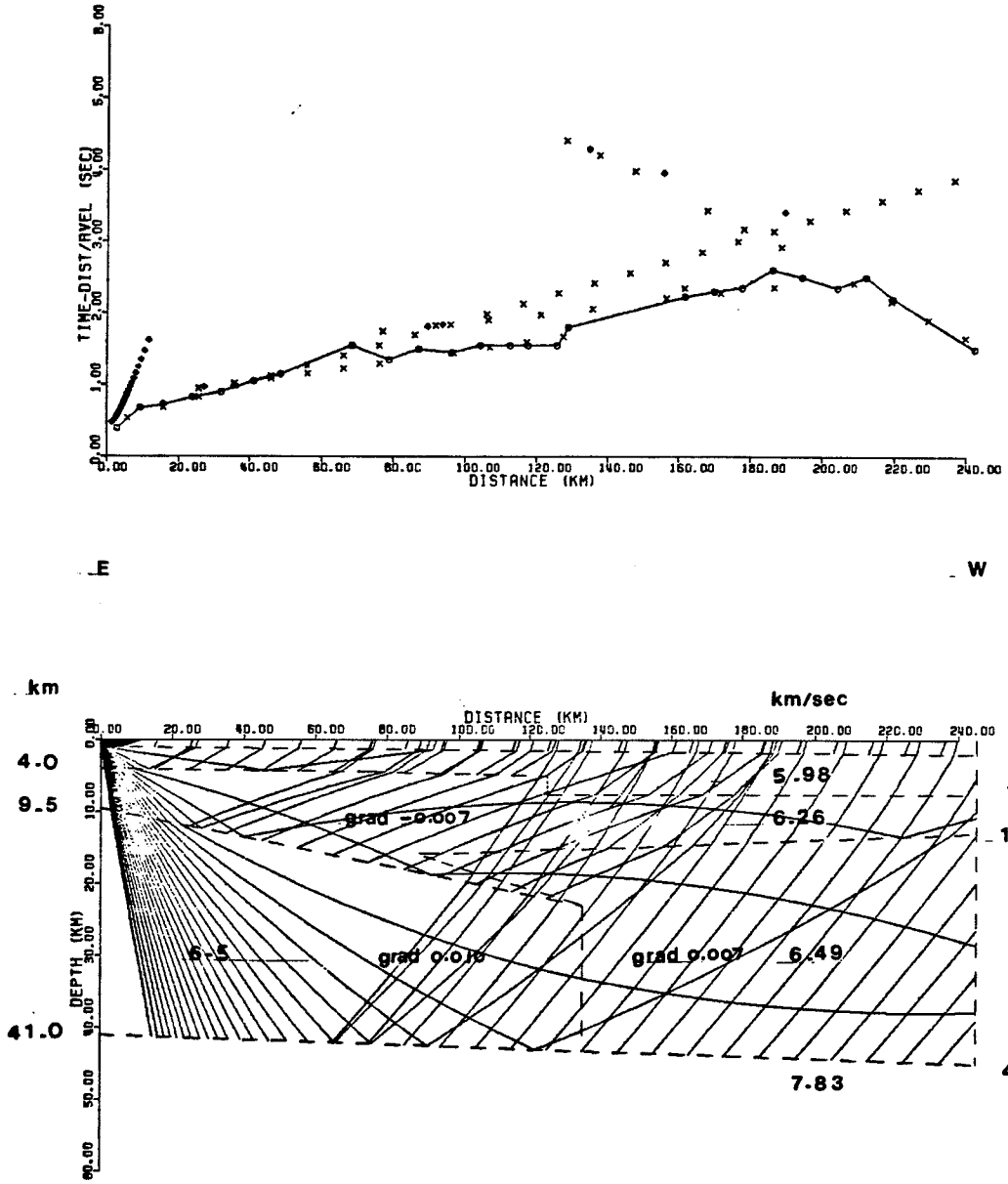

Figure 5.10 (a) - Ray tracing results for the final E/W model (east shot).

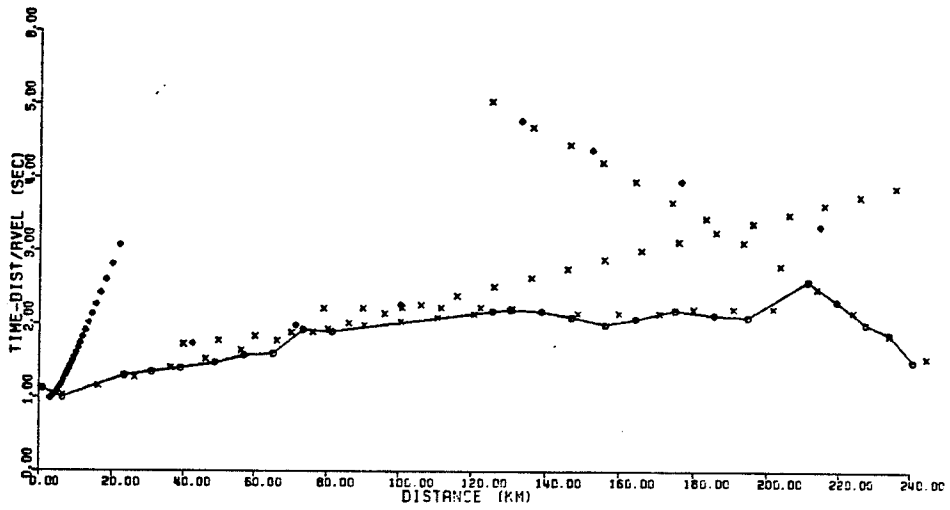

W E

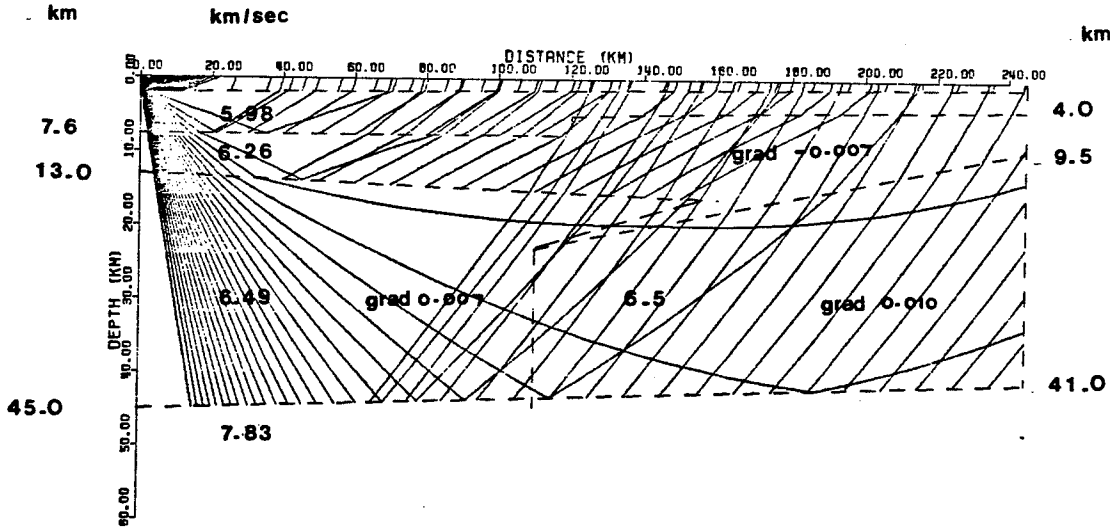

Figure 5.10 (b) - Ray tracing results for the final E/W model (west shot).

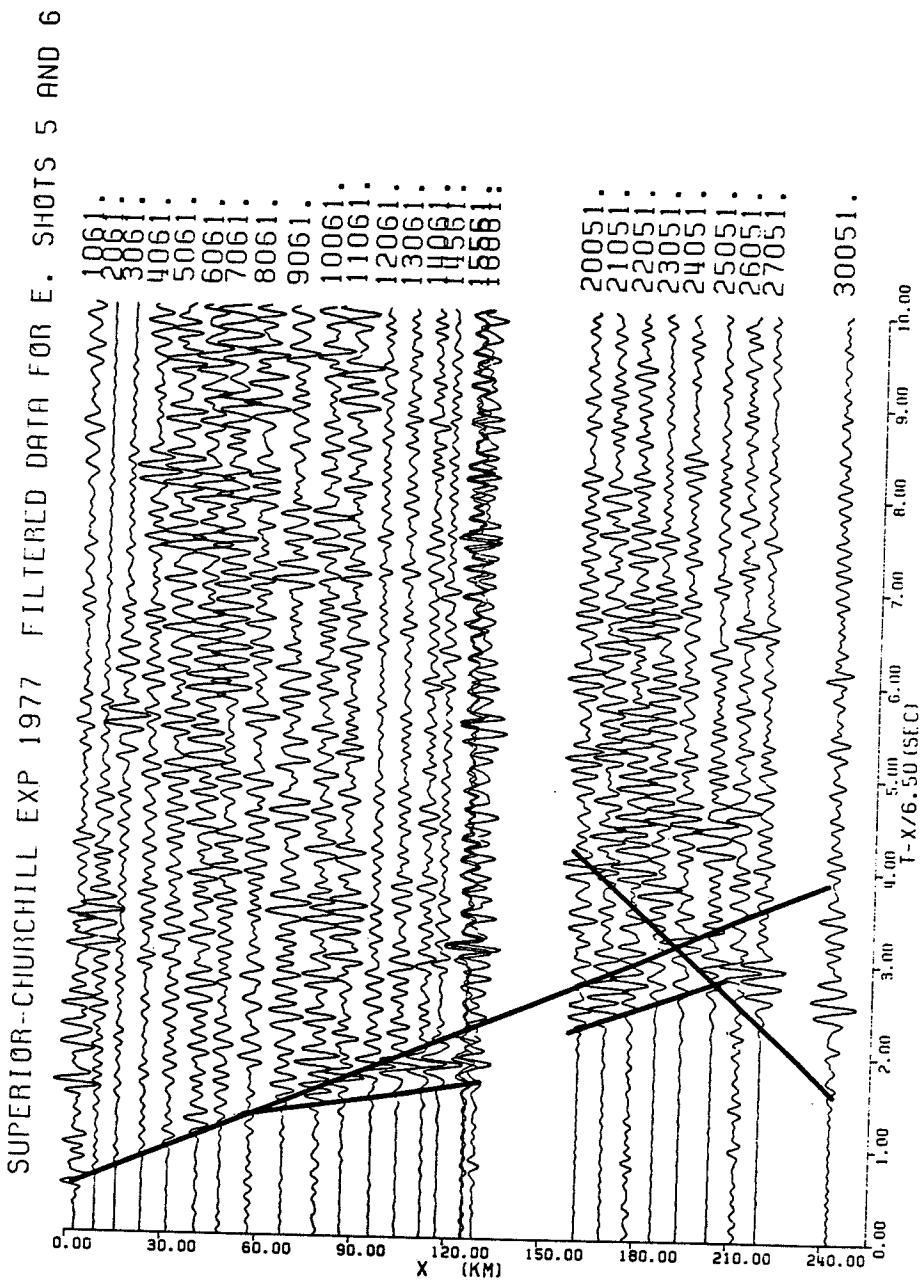

Figure 5.11 (a) - First and later arrivals for seismograms from the east shot.

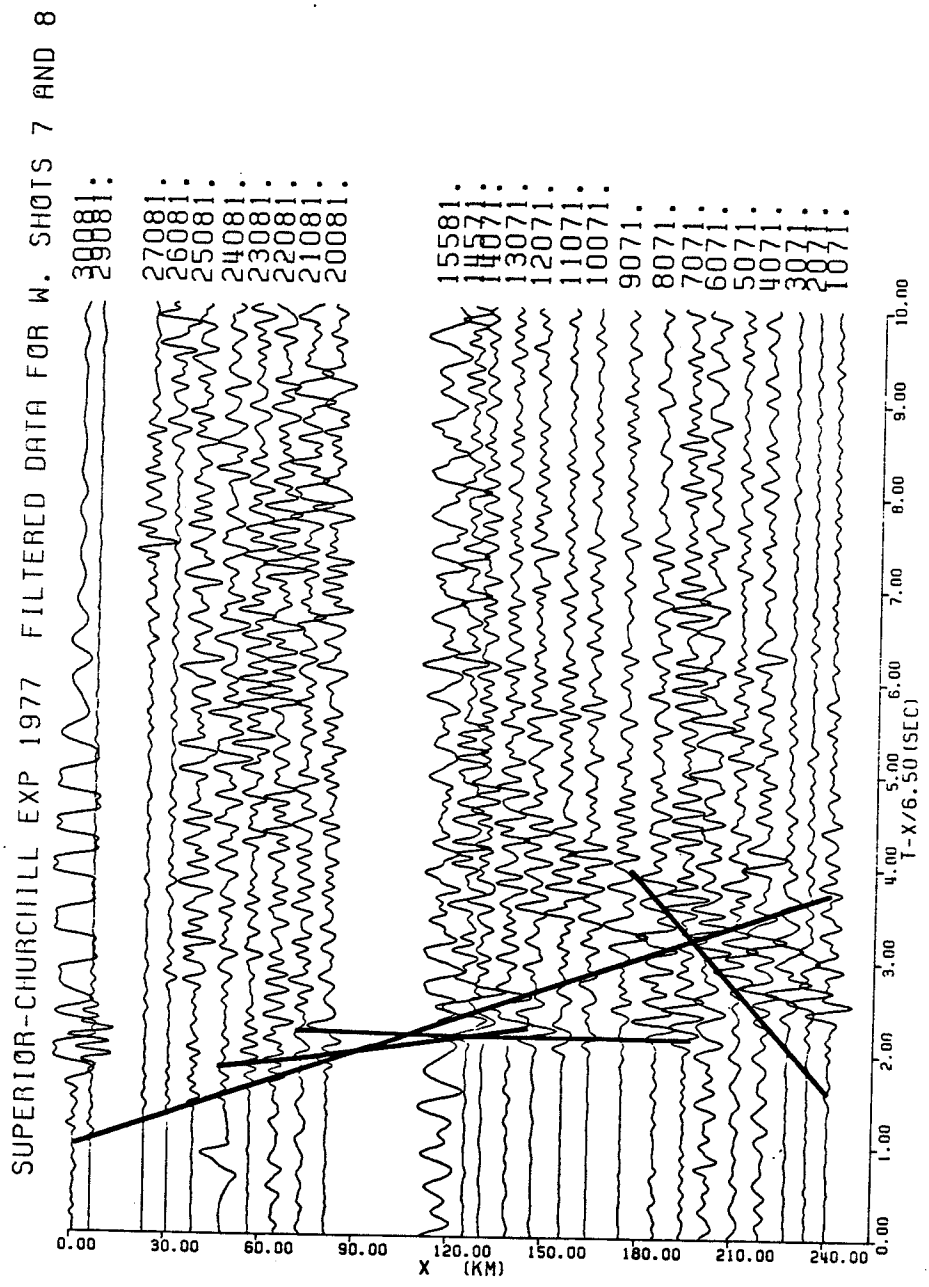

Figure 5.11 (b) - First and later arrivals for seismograms from the west shot.

observed data. The Moho discontinuity for this model is westerly dipping at a depth of 41 to 45 km .

The lack of traces at crucial positions along the east/west profile makes the similarities between the observed events (see Figure 5.11) and the predicted events less obvious than for the north/south line. Nonetheless a reasonably good fit was obtained.

WKBJ modelling on this profile was not attempted because of the complex nature of the mid-crustal interfaces.

Chapter VI

CONCLUSION

The final models derived from this seismic sounding survey are shown in Figures 6.1 and 6.2. In this chapter the salient features of each of the models will be described and compared to the results of other studies done in areas to the east in the Superior Province, to the west in the Churchill Province and in the boundary zone to the north. The geological significance of the east/west crustal structure in determining the position and nature of the boundary between the Churchill and Superior Provinces is also discussed.

6.1 THE NORTH/SOUTH MODEL

The most striking characteristics of the north/south crustal model (see Figure 6.1) are :

(a) a thin sedimentary layer of average velocity 3.46 km/sec,

(b) the lateral homogeneity exhibited in the layers,

(c) the gradual increase in velocity both within each layer and between layers,

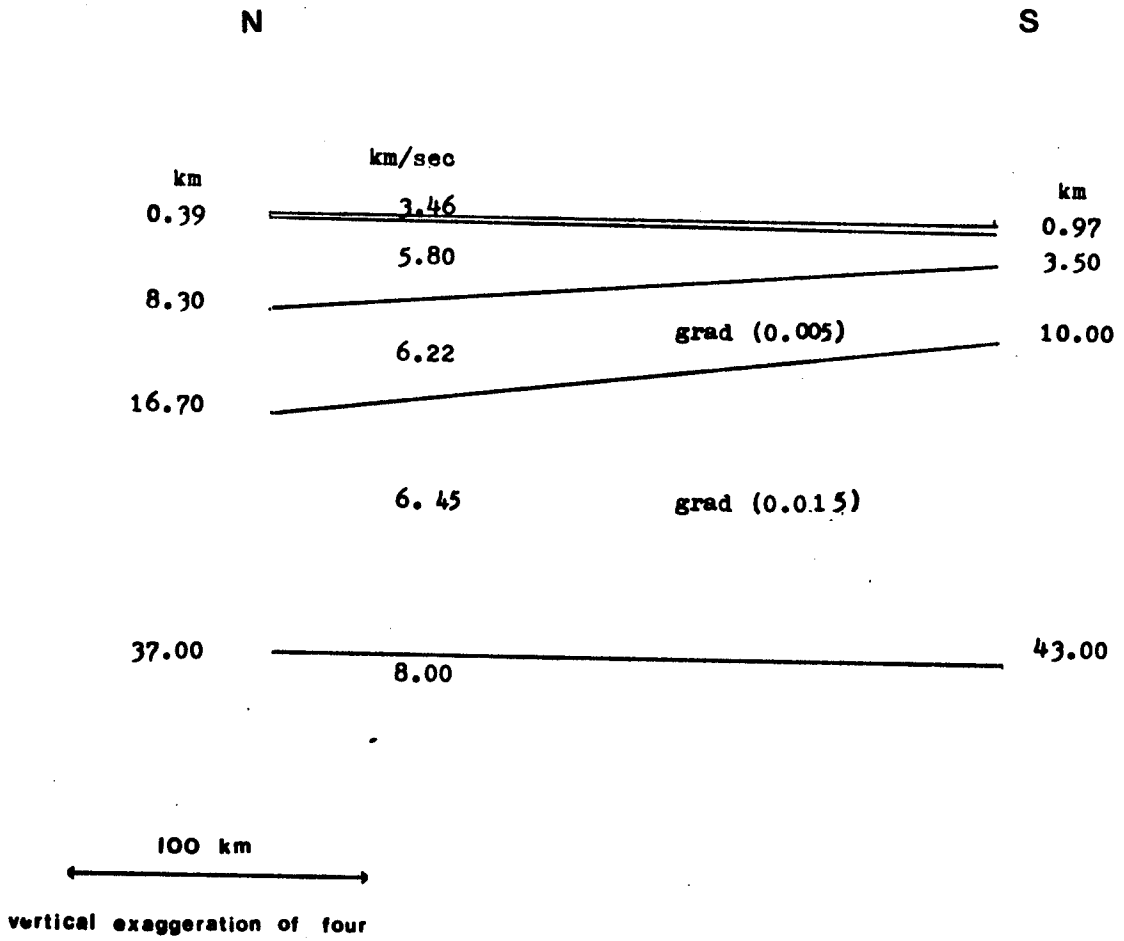

Figure 6.1 - Final north/south crustal model.

(d) the lack of differentiation into layers in the lower crust. Instead there is a gradual increase in velocity down to the Moho, and

(e) the depth to the Moho discontinuity is 37 km in the north and 43 km in the south.

In the publication by Green et al. (1979), an attempt was made to extend the Superior Subprovince belts westward from northwestern Ontario into Manitoba. According to their extension, the north/south survey area lies well within a single subprovince (the Granite-Greenstone Subprovince) of the Superior Province. The lateral homogeneity in the north/south crustal model with dips as shown corresponds to these models. The gradual increase in velocity with depth proposed by this research corresponds to the predictions of preliminary modelling done by Lewanski (1979) and Lau (1979) on the data. Lewnaski and Lau using reflectivity method and WKBJ modelling respectively, found that the gradually increasing velocity-depth structures were needed in order to duplicate the charateristics of the observed seismograms, even though they assumed a flat layered Earth.

As hinted in Green et al. (1980) from his preliminary interpretation of the north-south profile, there is no evidence for a distinct layer of 7.1 km/sec velocity in the lower crust.

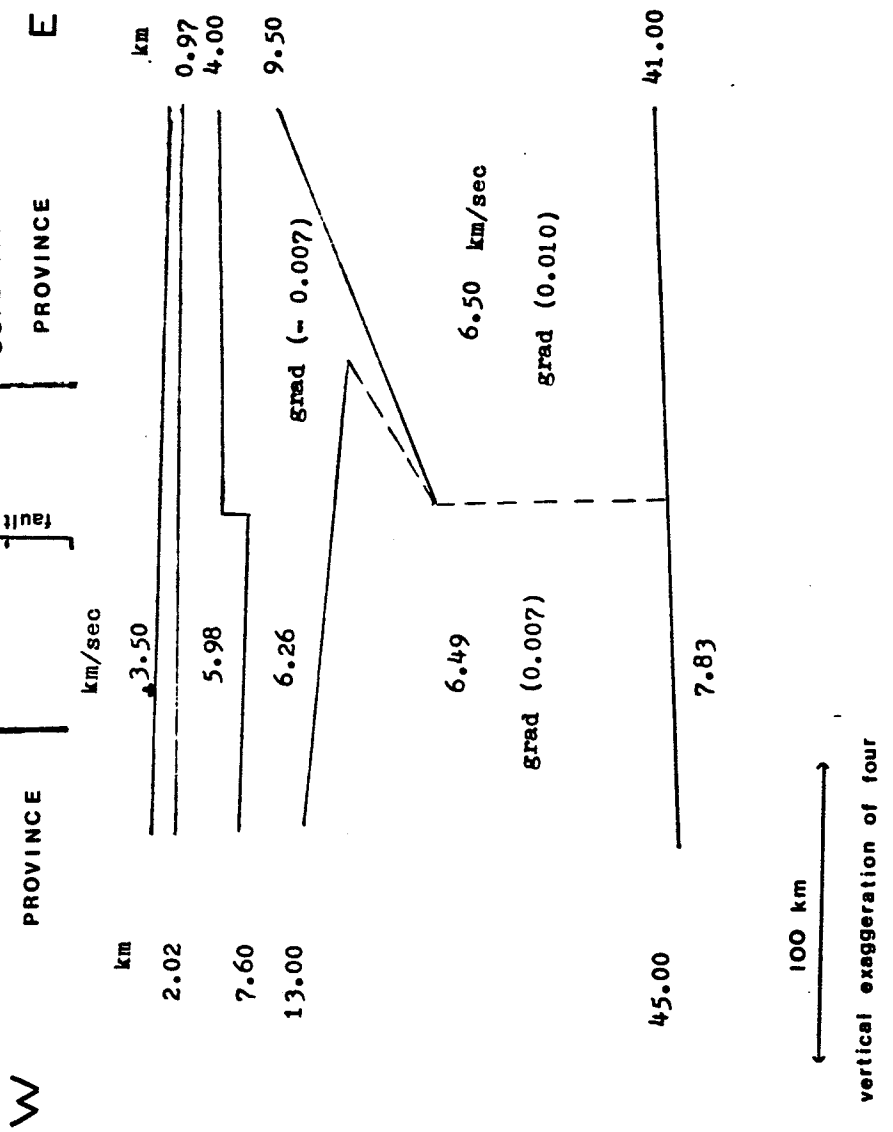

Figure 6.2 - Final east west crustal model.

Instead of differentiation into two distinct layers, there is an increase in velocity in the lower crust down to the Moho discontinuity. Similar velocity gradient in the lower crust was proposed by Hall and Hajnal (1973) and by Wright and West (1976) for the Superior Province in northwestern Ontario.

Mereu and Hunter (1968) deduced a depth of 30 - 35 km for the Moho discontinuity in the Superior Province, in northern Manitoba and Ontario. This is in close correspondence to the 37 to 43 km depth derived in the present analysis. Previous work done by Hall and Hajnal (1969) for a survey area within the Superior Province and some 500 km northeast of the present survey deduced a southward thickening of the lower crust. A similar lower crustal thickening is proposed from the present north- south model.

6.2 THE EAST/WEST MODEL

The major features of the east/west model are:

(a) a thin sedimentary layer of velocity 3.46 km/sec,

(b) the presence of lateral inhomogeneities in the second and third interfaces. These take the form of a fault with a vertical displacement of ~2 km down from east to west at a mean depth of 5 km and a 'thrust fault' type overlap feature which seems to indicate

lateral movement of the western over the eastern block at a depth ranging from 15 to to 20 km,

(c) the presence of a low-velocity zone in the upper crust between 4km and 23 km depth,

(d) a basin type depression at the base of the upper crust,

(e) lateral inhomogeneity in the lower crust and

(f) the depth to the Moho of 41 to 45 km from east to west.

It is interesting to note the close correspondence of the position of the fault structure on the second interface and the lower crustal velocity discontinuity to the position of the fault predicted by Green et al. (1979) from the magnetic anomaly map of the area. The positon of the margin of the overlap structure on the third interface is also spacially closely related to the previously proposed position of the boundary zone.

These two points strengthen the conviction that this east/west model may be truely representative of the crustal structure in the Churchill-Superior boundary and that it is further evidence which can be used in deducing the tectonic relationship which may have existed between the Churchill and Superior Provinces in the early history of the Earth.

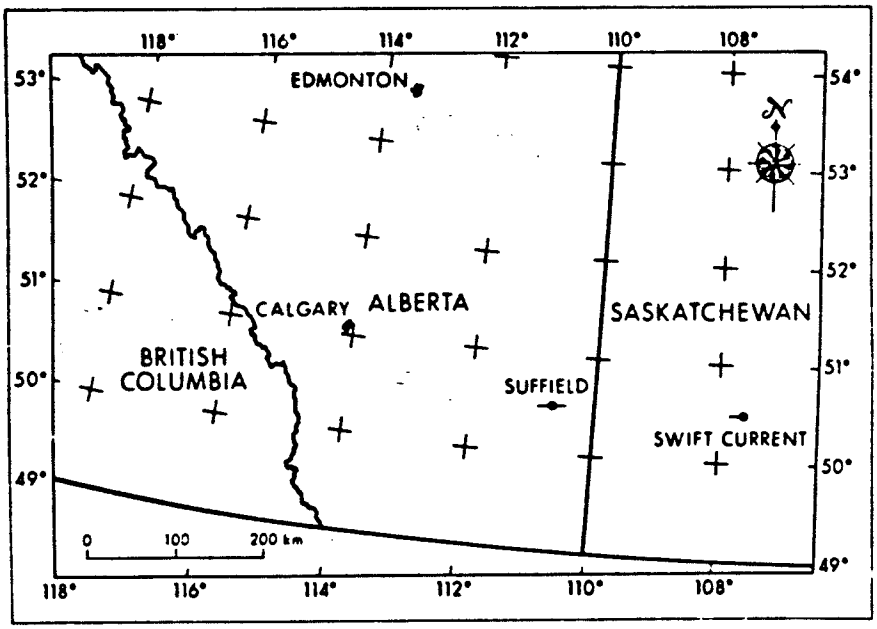

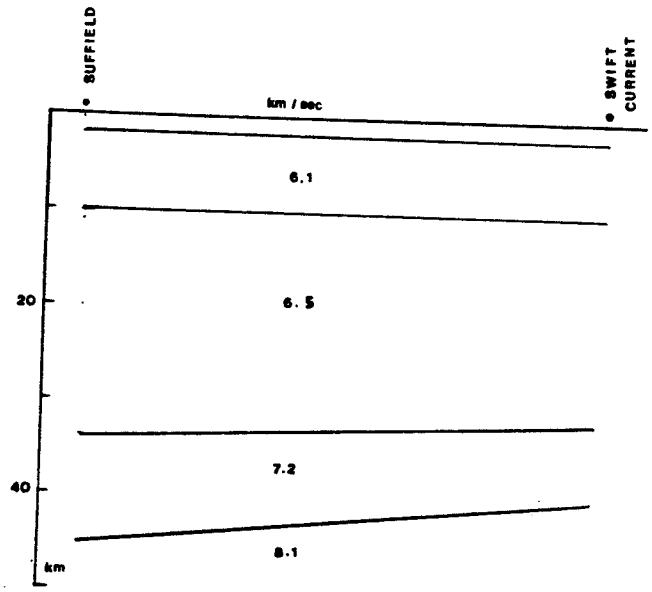

Figure 6.3 - 'Swift Current' model
(Chandra and Cumming, (1972)).

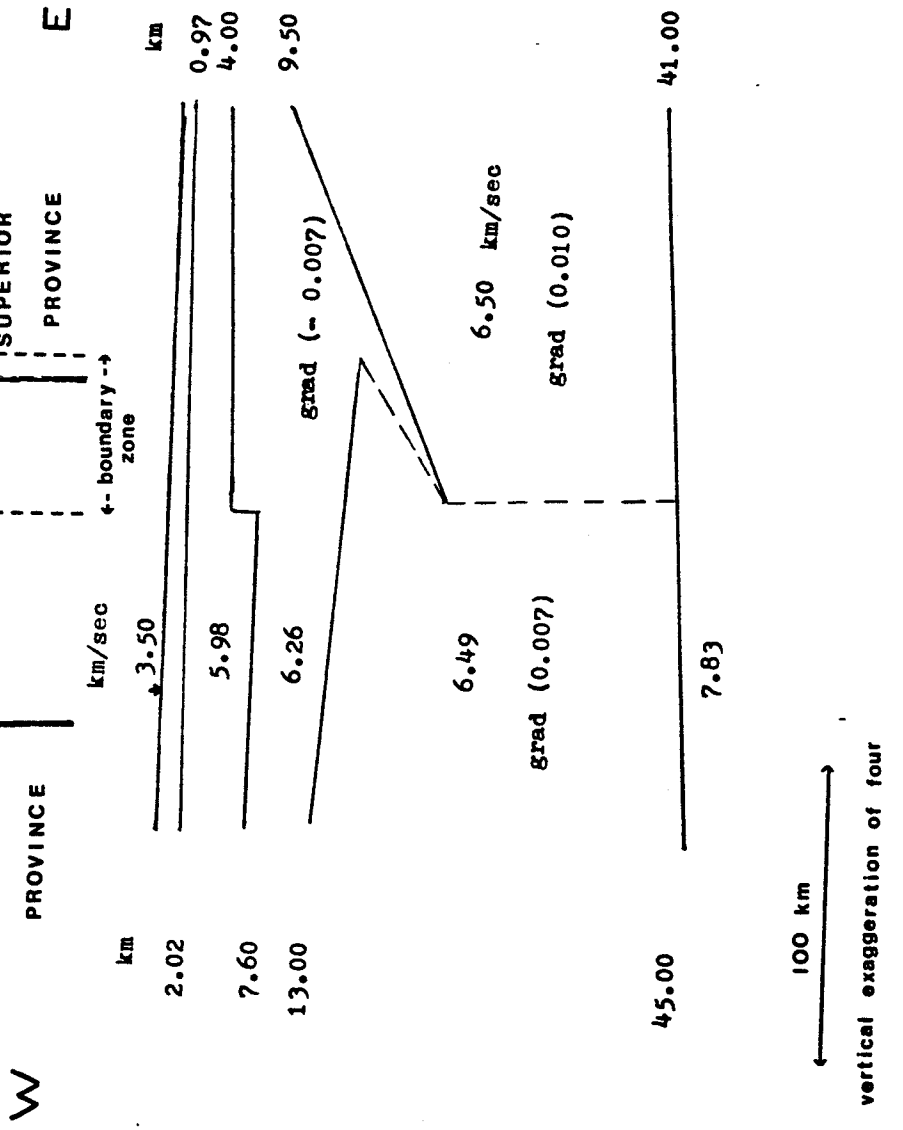

Figure 6.4 - Proposed position of the Churchill-Superior boundary from seismic interpretation.

Seismic measurements across the boundary area to the north show the crust thickens rapidly from 30 - 35 km in the Superior Province 40 - 45 km beneath the Churchill Province. A depth of 45 km for the Moho discontinuity was also deduced by Chandra and Cummings (1972) from seismic deep sounding beneath the Churchill province (see Figure 6.3).

The good comparision of the velocity-depth structure of the Swift Current model (see Figures 6.3, 6.4) with the western side of the east/west model as far east as the fault discontinuity, suggests that the eastern limit of the Churchill Province is in the vicinity of the fault. There is also good correspondence between the crustal structure derived for the southern end of the north/south profile and the eastern end of the east/west profile up to the overlap region. If this region of overlap is taken as marking the western limit of the Superior Province, the boundary area from this seismic analysis is less extensive than assumed by Green et al. (1979) and is shifted some 60 km east, toward the Superior Province. The boundary indicated from this interpretation is seen to be an area of finite lateral extent in which crustal deformation has taken place and is characterised by upper crustal discontinuities and lower crustal velocity changes.

BIBLIOGRAPHY

1. Basham, P.W. and Ellis, R.M., (1969) The composition of P codas using magnetic tape seismograms. Bulletin of Seismological Society of America, vol. 59, pp 473 -486.

2. Bell,C.K., (1971) Boundary Geology, Upper Nelson River Area, Manitoba and northwestern Ontario. The Geological Association of Canada Special Paper 9, pp 11 - 41.

3. Bohdan, A., Homeniuk, L.,(1970) Subsurface geology of the Precambrian of southwestern Manitoba. Bsc. Thesis, University of Manitoba.

4. Butterworth, S., (1930) On the theory of filter amplifiers. Wireless Engr 1.

5. Cerveny, V., Ravindra, R., (1971) Theory of seismic headwaves. University of Toronto Press.

6. Chapman, C.H., (1978) A new method of computing synthetic seismograms. Geophysical Journal of the Royal Astronomical Society, vol. 58, pp 490 - 503.

7. Chandra, N.N., Cumming, G.L., (1972) Seismic refraction studies in western Canada. Canadian Journal of Earth Sciences, vol. 9, pp 1099 - 1109.

8. Cummings, W.B., Clowes, R.M., Ellis, R.M., (1979) Crustal structure from seismic refraction profiles across Southern British Columbia. Canadian Journal of Earth Sciences, vol. 16, pp 1024 - 1040.

9. Dix, C.H., (1955) Seismic velocity from surface measurements. Geophysics, vol. 20, no. 1, pp 68 - 86.

10. Dobrin, M.B., (1976) Introduction to geophysical prospecting. Mc Graw and Hill, 3rd edit.

11. Gerver, M., Markushevich, V., (1966) Determination of seismic wave velocity from the travel-time curve. Geophysics Journal of the Royal Astronomical Society, vol. 11, pp 165 - 173.

12. Gerver, M., Markushevich, V., (1967) On characteristic properties of travel time curves. Geophysics Journal of the Royal Astronomical Society, vol. 13; pp 165 - 173.

13. Gibb, R.A., (1975) Collision Tectonics in the Canadian Shield Earth and Planetary Science Letters, no. 27, pp 378 - 382.

14. Golden, R.M., Kaiser, J.F., (1964) Design of wide-band sampled data filters. The Bell Telephone Technical Journal.

15. Grant, F.S., West, G.F., (1965) Interpretation theory in applied geophysics. McGraw and Hill, New York.

16. Green, A.G., Stephenson, O.G., Mann,G.D., Kanasewich, E.R., Cumming, G.L., Hajnal, Z., Mair, J.A., West, G.F., (1980) Cooperative seismic surveys across the Superior-Churchill boundary zone in southern Canada. Canadian Journal of Earth Sciences, vol. 17, pp 617 - 632.

17. Green, A.G., Cumming, G.L., Cedarwell, D., (1979) Extension of the Superior-Churchill Boundary into southern Canada Canadian Journal of Earth Sciences, vol. 16, pp 1691 - 1701.

18. Hall, D.H., (1968) Regional magnetic anomalies, magnetic units and crustal structure in the Kenora District of Ontario. Canadian Journal of Earth Sciences, vol. 5, pp 1277 - 1296.

19. Hall, D.H. (1971) Geophysical determination of the deep crustal structure in Manitoba. The Geological Association of Canada, Special Paper 9, pp 83 - 88.

20. Hall, D.H. and Hajnal, Z. (1969) Crustal structure of northwestern Ontario, refraction seismology. Canadian Journal of Earth Sciances, vol. 6, pp 81 - 99.

21. Hall, D.H. and Hajnal, Z. (1973) Deep seismic crustal studies in Manitoba. Bulletin of Seismological Society of America, vol. 63, pp 885 - 910.

22. Keilis-Borok, V.I. and Yanovskaja, T.B., (1967) Inverse Problems of seismology (structural review). Geophysics Journal of the Royal Astronomical Society, vol. 13, pp 223 - 234.

23. Kornik, L.J., (1971) Magnetic subdivisions of Precambrian rocks in Manitoba The Geological Association of Canada Special Paper 9, pp 51 - 61.

24. Kornik, L.J., (1969) An aeromagnetic study of the Moak Lake - Setting Lake structure in northern Manitoba. Canadian Journal of Earth Sciences, vol. 6, pp 373 - 381.

25. Kornik, L.J. and MacLaren, A.S., (1966) Aeromagnetic study of the Churchill-Superior boundary in northern Manitoba. Canadian Journal of Earth Sciences, vol. 3, pp 517 - 557.

26. Lau, C.S., (1979) Synthetic seismogram analysis of refraction data recorded in S. W. Manitoba. Thesis presented to the Association of Professional Engineers of Manitoba.

27. Lewanski, R. (1979) Synthetic seismogram study of crustal velocity models. Bsc. Thesis, University of Manitoba.

28. McCabe, H.R., (1963) Mississippian Oilfields of southwestern Manitoba. Mines Branch, Dept. of Mines and Natural Resources, Province of Manitoba. Publication 60, no. 5.

29. McCabe, H.R., (1971) Stratigraphy of Manitoba, an introduction and review. The Geological Association of Canada Special Paper 9, pp 167 - 188.

30. McMechan, G.A., (1979a) Low-velocity zone inversion by Weichert-Herglotz integral. Bulletin of Seismological Society of America, vol. 69, no. 2, pp 375 - 385.

31. McMechan, G.A., (1979b) Weichert-Herglotz inversion as integration on a closed contour. Bulletin of Seismological Society of America, vol. 69, no. 5, pp 1439 - 1444.

32. McMechan, G.A., (1972) Depth limits in body wave inversions. Geophysical Journal of the Royal Astronomical Society, vol. 28, pp 459 - 473.

33. Mereu, R.F., Hunter, J.A., (1969) Crustal and upper mantle structure under the Canadian Shield from Project Early Rise data. Bulletin of the Seismological Society of America, vol. 59, pp 147 - 165.

34. Meuhlberger, W.R., Denison, R.E. and Liliak, E.G. (1967) Basement rocks in the continental interior of the United States. Bulletin of The American Association of Petroleum Geologists, vol. 51, pp 2351.

35. Mota, L., (1954) Determination of dips and depths of geological layers by seismic refraction method. Geophysics, vol. 19, pp 242 - 254.

36. Steinhart, J.S., Meyer, R.P., (1961) Minimum statistical uncertainty of the seismic refraction profile. Geophysics, vol. 26, no. 5, pp 574 - 587.

37. Weber, W., Scoates, R.F.J., (1978) Archean and Proterozoic Metamorphism in the northwestern Superior Province and along the Churchill - Superior Boundary in Mannitoba. Geological Survey of Canada Paper 78, no. 10, pp 5 - 16.

38. Whittall, K.P., Clowes, R.M., (1980) A simple efficient method for calculation of traveltimes and ray paths in laterally inhomogeneous media. Journal of the Canadian Society of Exploration Geophysicists, vol. 15, pp 21.

39. Wilson, H.D.B., (1971) The Superior province of Manitoba. The Geological Association of Canada, Special Paper 9, pp 41 - 50.

40. Wilson, H.D.B. Brisbin, W.C., (1961) Regional Structure of the Thompson-Moak Lake nickel belt. Bulletin of the Canadian Institute of Mining and Metallurgy, vol 64, pp 470 - 477.

41. Wright, J., West, G.F., (1976) Seismic studies in the southern Geotraverse. University of Toronto, Geotraverse Workshop, Toronto, Ontario.